ULTRAVIOLET CORONA DETECTION SENSOR STUDY

by

R. J. SCHMITT AND J. P. MATHERN

MCDONNELL AIRCRAFT COMPANY

Saint Louis, Missouri

Contract NAS 9-14613

March 1976

Final Report for Period July - December 1975

prepared for

NATIONAL AERONAUTICS AND SPACE ADMINISTRATION

LYNDON B. JOHNSON SPACE CENTER

HOUSTON, TEXAS 77058

NASA CR
MDC A4054
COPY NO. 1

ULTRAVIOLET CORONA DETECTION SENSOR STUDY

by

R. J. SCHMITT AND J. P. MATHERN

MCDONNELL AIRCRAFT COMPANY
Saint Louis, Missouri

Contract NAS 9-14613
March 1976

Final Report for Period July - December 1975

prepared for

NATIONAL AERONAUTICS AND SPACE ADMINISTRATION
LYNDON B. JOHNSON SPACE CENTER
HOUSTON, TEXAS 77058

1 Report No	2 Government Accession No	3 Recipient's Catalog No

4 Title and Subtitle	5 Report Date
ULTRAVIOLET CORONA DETECTION SENSOR STUDY	31 March 1976
	6 Performing Organization Code
7. Author(s)	8 Performing Organization Report No
R. J. Schmitt and J. P. Mathern	MDC A4054
	10 Work Unit No
9. Performing Organization Name and Address McDonnell Aircraft Company P. O. Box 516 St. Louis, Missouri 63166	11 Contract or Grant No NAS9-14613
	13 Type of Report and Period Covered Contractor Report July 1975-December 1975
12. Sponsoring Agency Name and Address National Aeronautics and Space Administration Washington, D. C. 20546	14 Sponsoring Agency Code

15. Supplementary Notes

Contracting Officer Representative, L. E. Birdsong, NASA Johnson Space Center, Houston, Texas

16. Abstract

A program is described for evaluating the feasibility of detecting electrical corona discharge phenomena in a space simulation chamber via emission of ultraviolet light. A specially-designed computer-interfaced spectroradiometer, calibrated using National Bureau of Standards secondary spectral radiance standard lamps, was employed to measure the absolute spectral intensity distribution of corona glows in the 200 to 400 nanometer waveband. A corona simulator, with a hemispherically-capped point-to-plane electrode geometry, was used to generate corona glows over a wide range of pressure, voltage, current, electrode gap length and electrode point radius. Several candidate ultraviolet detectors, including a copper-cathode gas discharge tube and a UV-enhanced silicon photodiode detector, were evaluated in the course of the spectral intensity measurements. The performance of both silicon-target (S-T) vidicons and silicon-intensified-target (SIT) visicons was evaluated analytically using the data generated by the spectroradiometer scans and the performance data supplied by the manufacturers.

17. Key Words (Suggested by Author(s))	18. Distribution Statement
Corona Ultraviolet Emission Spectra Electrical Discharges Thermal Vacuum Testing Ultraviolet Detectors SIT Vidicons	Unclassified-Unlimited

19. Security Classif (of this report)	20. Security Classif. (of this page)	21. No. of Pages	22. Price*
Unclassified	Unclassified	83	

*For sale by the National Technical Information Service, Springfield, Virginia 22151

NASA — JSC

TABLE OF CONTENTS

LIST OF PAGES

Title Page
ii - v
1-1 - 1-4
2-1 - 2-9
3-1 - 3-25
4-1 - 4-18
5-1 - 5-15
6-1
7-1
A-1 - A-4

LIST OF FIGURES

LIST OF FIGURES (Continued)

LIST OF TABLES

1.0 INTRODUCTION

A persistent problem faced by practitioners of thermal vacuum testing of satellites and space vehicles arises from the appearance of electrical corona phenomena during the course of a test run. When powered electrical equipment is part of the test configuration, corona discharges are likely to occur as the pressure is varied or when voltages are altered in the test article. Frequently, corona processes will be activated during pumpdown when favorable conditions of pressure and voltage are established. The corona "turn on" at one pressure only to cease as the pressure falls in the chamber. Usually, it is possible to identify a potential source of corona discharge on a test article prior to actual thermal vacuum testing. For example, a microwave antenna, a vidicon-type television camera, a photomultiplier detector or a high voltage (several kV) power supply are obvious potential sources of corona if they are operated during a pump down procedure. Such equipment usually is specifically tested for corona prior to incorporation into satellite systems and appropriate measures devised (e.g. potting, heremetic enclosing) to prevent the occurrence of corona.

The corona problem arises when unexpected corona processes are revealed during a thermal vacuum test. The first indication of possible corona problems usually arises from observations of unexpected fluctuations in the normal electrical operating parameters of a specific satellite subsystem. Careful trouble-shooting procedures applied to the electrical systems often can successfully isolate the source of the corona and thus reveal design faults in a specific satellite subsystem.

Other instances of corona are extremely difficult to identify. For instance, a common problem arises when breaks occur in the insulation of wires and coaxial cables. Corona processes due to these faults are difficult to isolate, especially when large runs of cable are involved. In such cases, it is prudent to inquire as to the possibility of using some property of the corona process itself as a means of isolating the source of the corona. Attempts in this direction have included methods based on electromagnetic (radio and microwave) emissions, acoustic emissions and visible light emissions. The thrust of this program is to extend this inquiry to include methods of corona detection based on the emission of ultraviolet (UV) light.

It is well known that electrical discharge phenomena, of which corona is only one of numerous types of discharge, emit UV light. The common fluorescent lamp and the high power mercury and xenon arc lights are common examples of light sources which produce UV emission via electrical discharges. It is appropriate, at this point to consider the rich variety of emission modes exhibited by electrical discharges in a gas. Figure 1-1 shows the voltage-current characteristics of an electrical discharge for a parallel-plate electrode configuration together with an identification of the numerous regimes of electrical discharge phenomena. This type of curve is typical of discharges in a uniform electric field, such as that provided by the parallel plate electrode geometry. The corona is characterized by currents in the range 10^{-6} to 10^{-3} amps and is a self-sustained-type of discharge, i.e., it is independent of an external ionizing source. This is in contrast to regions A, B and C in which the current falls to zero as soon as the external ionizing source is removed. If the series resistance is sufficiently low, corona processes may not be observed at all. Rather, the discharge becomes an abnormal glow if the power supply can produce currents on the order of 10^{-2} to 10^{-1} amps. The current increases with increasing voltage in the abnormal glow region until a transition to an arc discharge occurs. This high energy discharge process shows a strong negative resistance characteristic (current increases with decreasing voltage).

The parallel plate electrode geometry, while useful for elucidating the various types of gaseous discharge phenomena, is not a particularly good model for typical corona processes, which are characterized by extremely non-uniform electrical fields. In fact, many corona phenomena arise in the vicinity of pointed electrodes, for instance, on sharp edges or points where high localized electric fields occur. The first task in this study, therefore, is to simulate actual corona discharge phenomena (nonuniform electric field) and to measure the UV emission spectra characteristic of such corona. Section 2 contains background material leading to the design of the corona simulator used in this study. The equipment employed to measure the UV corona emission spectra in an NBS-traceable manner is described in Section 3. Presentation of the spectral data and of data analysis is contained in Section 4.

The second task in this study involves an analysis of candidate optical designs which conceiveably can function as in-situ corona detection systems.

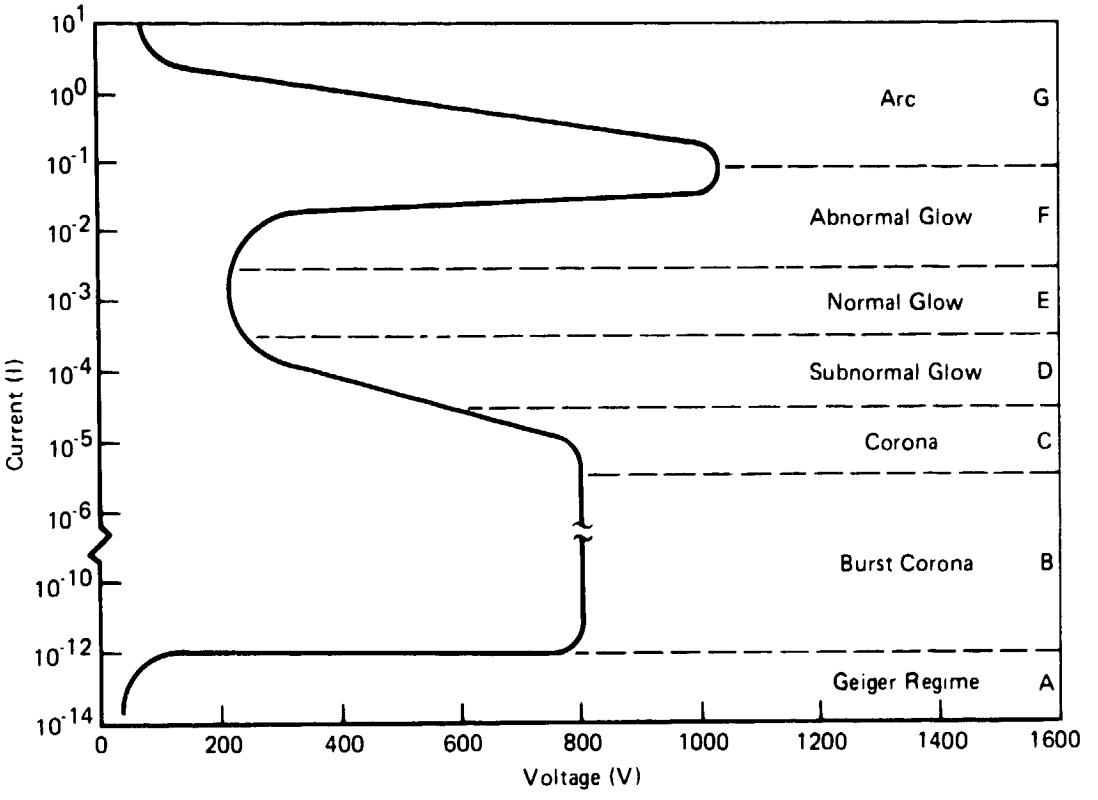

FIGURE 1-1 VOLTAGE-CURRENT CHARACTERISTICS - PARALLEL PLATE DISCHARGE

GP76 6183 21

The spectral UV emission data are used as representative inputs to such a system typical of real-life corona processes. Several breadboard UV detection systems were evaluated in the course of the spectral data acquistion phase of this study. The performance of these systems is detailed in Section 5. Other candidate detection systems were evaluated on paper, since it was not possible, within the time and budgetary constraints of this study, to assemble these systems into breadboards for evaluation during the spectral emission testing phase. Details of this system analysis are contained in Section 5.

The results of this study are presented in the form of conclusions and recommendations in Section 6. The most promising candidate UV corona section systems, in terms of both technical feasibility and cost, are identified.

The RFP-SOW requires that McDonnell Aircraft (MCAIR) quote a price for six (6) copies of one of the candidate UV corona detection system types identified in this study. This quotation has been forwarded to the NASA-JSC Contracting Officer under separate cover (MCAIR Report MDC A4176, 17 May 1976).

This study was managed and conducted by personnel of the MCAIR Applied Optics Laboratory (AOL), located in St. Louis, Missouri. The study commenced in July 1975 and was completed in December 1975.

2.0 BACKGROUND

An impetus for this study arose due to the lack of data on the UV emission spectrum of corona processes in the literature. In spite of an enormous literature on almost every conceiveable aspect of electrical discharge phenomena, it appears that little work has been devoted exclusively to the study of the absolute UV spectral intensity characteristics of corona processes. Loeb, in his encyclopedic work on electrical coronas[1], summerizes the spectra studies of corona phenomena performed up to 1965. A number of photographic studies have been reported for pulsed corona processes, but without yielding much spectral resolution or absolute intensity data. Loeb describes a study of time-resolved pulsed corona and spark spectra obtained by Byer and Davis in 1962. Photographic plates were used to obtain spectral data from 200 nm to 550 nm. The band spectra characteristic of the second positive group of N_2^+ were observed, but no absolute intensity data were obtained. The spark spectra showed lines characteristic of nitrogen and oxygen

Grum and Costa[2] studied high resolution spectra of corona discharges in air, nitrogen and helium. The corona were generated via a test coil operating at 20kV at a pressure of 1 lb/in^2 ($0.062 kgm/cm^2$ - 52 torr). The wavelengths and the relative intensities of the main lines in the corona emission spectra were reported in the 200 nm to 900 nm waveband. Absolute spectra intensity data were not obtained.

The literature search revealed no spectral intensity information which could be applied to the present study. Consequently, a series of tasks were accomplished to supply the necessary data upon which to base an assessment of candidate corona detection systems operating via the UV corona emissions.

2.1 TASK 1 - DESIGN OF THE CORONA SIMULATOR. A means for obtaining reproducible corona discharges is the first requirement. In addition, the simulator is required to produce corona which are representative of actual corona discharges likely to be encountered in thermal vacuum testing. The literature search revealed many electrode configurations which have been used in the study of corona emission phenomena. These include parallel plates, coaxial cylinders, spherical electrodes, and point-to-plane electrodes. The parallel plate geometry produces a uniform electric field for which both analytical and experimental approaches have been

successful in establishing a model of the corona discharge processes in this geometry. In general, actual corona processes are most likely to occur for geometries in which the electric field is highly non-uniform. The uniform field is characterized by a rapid transition to a high energy plasma channel (arc) once detectable ionization has occurred. Conversely, in the nonuniform electric field, numerous manifestations of locally confined ionization and excitation processes (coronas, glass) can be observed and measured long before an arc breakdown occurs.

The fact that coronas are most frequently observed in nonuniform electric fields weighs heavily on the choice of electrode geometry. The coaxial cylinder, double spherical and point-to-plane geometrics all yield nonuniform electric fields. However, in the first two geometries, both electrodes play important roles in determining the characteristics of the corona discharge process. The complexity introduced by two participating electrodes quickly led investigators to the point-to-plane geometry, because in this instance, only the pointed electrode has decisive influence on the corona processes. The plane electrode, if sufficiently large, functions as an effective infinite plane conductor (an infinite "ground" plane) and is essentially passive. A great number of studies have been conducted with a quasi-pointed electrode consisting of a cylindrical rod with a hemispherical tip. Thus, the hemispherical "point"-to-plane geometry has become an effectively "standard" electrode geometry for studying corona processes. Loeb[1] and Nasser[3] present detailed discussions of the vast literature which has accumulated from studies of corona processes in the standard geometry.

An important paper on the point-to-plane corona in dry air by H. W. Bandel appeared in 1951[4]. Although spectral emission data were not obtained by Bandel, he did provide comprehensive data on the DC current-voltage (I-V) characteristics of the point-to-plane corona. These results are useful in the present study since Bandel related the various electrical discharge phenomena of the standard geometry to the DC current drawn by the corona processes. Figure 2-1 is a reproduction of Bandel's data for a 0.5 mm dia hemispherical electrode separated from the plane electrode by a 4 cm gap. The constant current region at ~10 amp represents the Geiger plateau, this current due to the ions generated by external ionizing sources (radio-activity, cosmic rays, etc). As the voltage is increased, the free electrons start to acquire enough kinetic energy (due to the applied electric

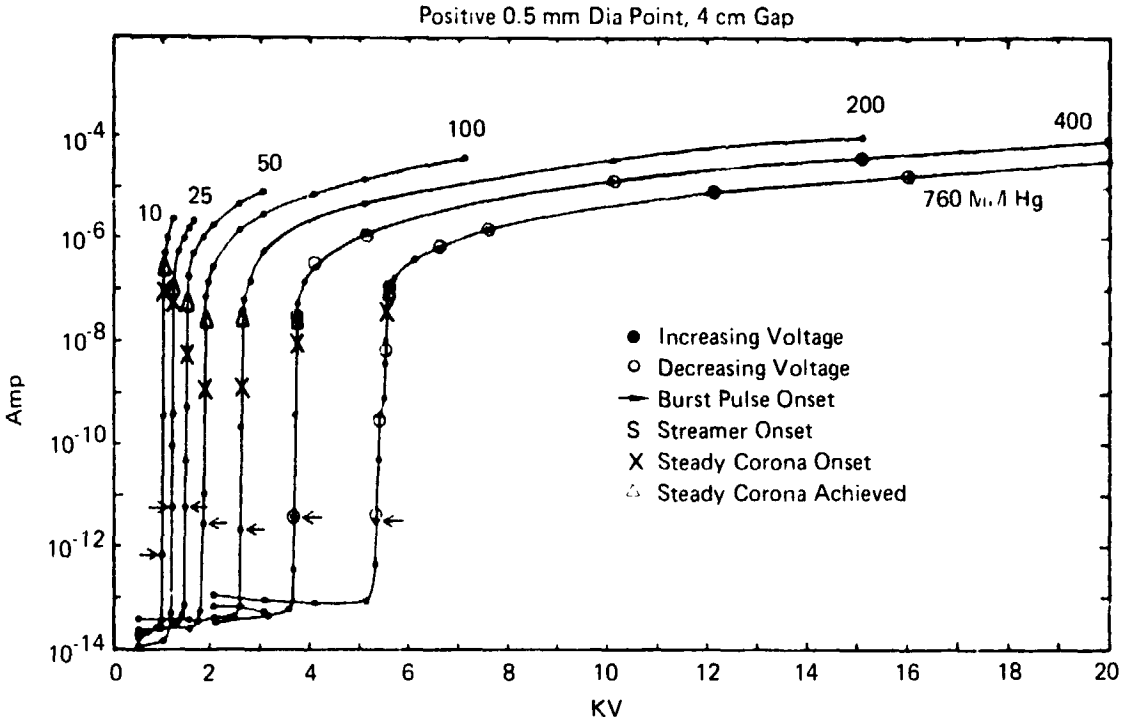

FIGURE 2-1 CURRENT-VOLTAGE CHARACTERISTICS - POSITIVE POINT CORONA - AFTER BANDEL (REF. 4)

GP76 6183 20

field) to ionize the gas. In this region the "burst pulse" phenomenon is observed. Bandel and others have conducted detailed studies of the burst pulses in order to gain insight into the physical processes occurring between the electrodes. Using oscilloscopes with increasing sweep rates, it has been found that the frequency or duration of the burst pulses increases as the applied voltage is raised. Bandel noted that a threshold for continuous discharge was somewhat difficult to define. He defined a "steady" corona as a discharge with a duration greater than 0.1 sec. It should be noted that the burst pulses emitted little, if any, visible radiation. Bandel indicated by the words "steady corona achieved" the point on the I-V curve at which the discharge is truly continuous and shows no pulse pattern on the oscilloscope. This threshold was observed to coincide roughly with the onset of visible light emission from the corona.

Further increases in the applied voltage causes a glow discharge to arise near the pointed electrode. The glow grows brighter and spreads over the pointed electrode as the voltage increases. As the threshold for arc (spark) breakdown is approached, low frequency oscillations are observed in the current. Increasing voltages causes both the amplitude and frequency of these current oscillations

to increase. Simultaneously, the glow becomes brighter and begins to move towards the plane electrode. The glow begins to show a streamer structure, the so-called "prebreakdown" streamers. These streamers start at random spots on the pointed electrode and appear to end at random locations in the electrode gap. Eventually, a voltage is reached at which one of the streamers terminates on the plane electrode. This causes the gap to breakdown into a spark discharge.

In spite of the seeming complexity of these discharge processes, Nasser has pointed out that in reality there are only two fundamental modes of positive DC corona, the intermittent streamer and the steady glow. There are two types of streamers, the intermittent streamers, which are called "burst pulses" by Bandel, and the "prebreakdown" streamers. Visible light emission is observed for the glows, the prebreakdown streamers and the sparks (at currents $\geq$10μa). Investigators, relying on visual observations, report that the onset streamers do not emit visible light. Using sensitive detectors, such as photomultiplier tubes, the visual threshold for light emission undoubtedly can be extended to currents lower than 10μa. Thus, there should be a more or less precisely defined light emission threshold for each type of detector. This discussion is continued below in the section on Task 3.

Bandel[4] has described the I-V characteristics of negative DC corona in his 1951 paper. Figure 2-2 shows Bandel's data for the 0.5 mm dia point with the 4 cm gap, this time with the point negative with respect to the plate electrode. Bandel studied a combination of gamma ray and ultraviolet triggering in order to supply a quantity of free electrons to initiate the burst pulses. Without triggering, the discharge processes in both the Geiger and the burst pulse regions are very difficult to control and observe. With the negative point, a Geiger plateau is observed similar to that seen for the positive point. However, the negative point produces burst pulses with a regular frequency and amplitude, whereas these pulses for the positive point are random both in frequency and amplitude. These regular pulses, called Trichel pulses, continue to be observed as the voltage is increased until a new mode of corona, a steady glow on the cathode (point), is initiated. The glow corona persists until spark breakdown occurs.

The comments on light emission for the positive point apply, in general, to the negative point-to-plane geometry. The Trichel pulses, like the pointed

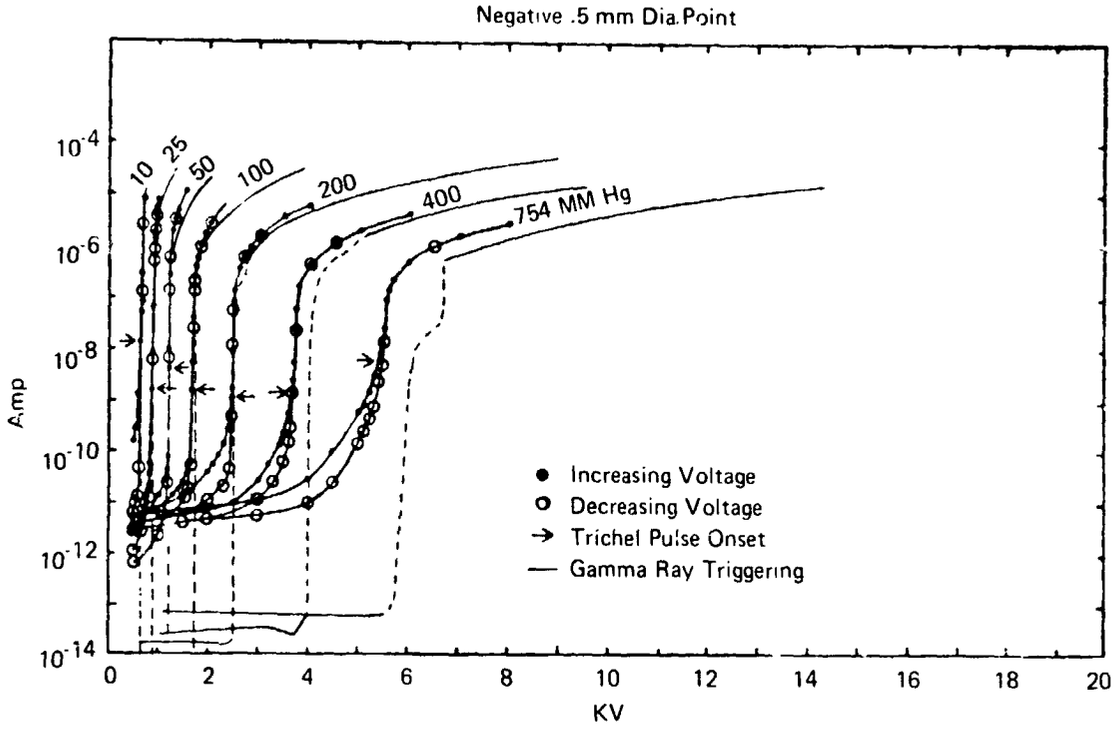

FIGURE 2-2 CURRENT-VOLTAGE CHARACTERISTICS - NEGATIVE POINT CORONA - AFTER BANDEL (REF. 4) GP76 6183 22

anode burst pulses, emit visible light which can be measured by sensitive detectors. The negative glow discharge can be observed visually and appears bluish to the eye. The principal differences between the two cases, arising from the regularity of the Trichel pulses, has stimulated much research in an attempt to gain understanding of the fundamental processes of the negative point discharge.

The work of Loeb, Nasser, Bandel, and others, while devoid of specific spectral intensity data required for this program, is valuable in selecting a design for the corona simulator. The extensive data already available on the I-V characteristics of the point-to-plane electrode geometry makes the selection of this geometry particularly attractive, since it eliminates the need for an extensive study of these characteristics in this program. Likewise, the experience gained from these studies in the operation of such corona simulators was found to be an invaluable guide in this program.

2.2 TASK 2 - DESIGN OF A CALIBRATED SPECTRORADIOMETER. The principal purpose of this study, to determine the performance of candidate UV corona detection systems, can be achieved only by measuring the absolute spectral ultraviolet intensity of

corona processes. The term "absolute" means NBS-traceable measurements; that is, measurements obtained by means of a spectroradiometer which has been calibrated using NBS secondary standards of spectral radiance and/or spectral irradiance. The design of the spectroradiometer used in this study, and the procedures for obtaining an NBS-traceable calibration, are detailed in Section 3.

One important aspect of the spectroradiometer design is the range of wavelengths over which the instrument has to function. The ultraviolet spectral region is divided into two parts, the near ultraviolet extending from 190 nm to 400 nm wavelength and the vacuum ultraviolet (VUV) ranging from approximately 100 nm to 190 nm wavelength. The ambient atmosphere is transparent to the near UV; however, the vacuum ultraviolet wavelengths are strongly absorbed by atmospheric oxygen (hence, VUV spectrometers must be evacuated to pressures below 1×10^{-3} torr).

The key issue, vis-a-vis the vacuum UV measurements, is the partial pressure of oxygen in the pressure-voltage regime in which the corona processes are expected to occur in actual thermal vacuum tests. Oxygen strongly absorbs vacuum UV radiation, a fact evident from Figure 2-3, which shows the spectral absorption coefficient for oxygen at room temperature and pressure (NTP). The transmission of a gas at pressure p (torr) and for a path length x (cm) is

$$T_{x,p} = \exp(-\alpha_p px) \qquad (2\text{-}1)$$

where α_p = absorption coefficient ($\text{torr}^{-1}\text{cm}^{-1}$).
and px = optical thickness (torr-cm).

To assess the effects of oxygen absorption at vacuum UV wavelengths, a path length of 300 cm was used to typify the distance between corona source and UV detection in space chamber corona detection applications. As corona processes occur over a wide range of pressures, the data of Loeb[1] presented in Figure 2-4 was used to establish a reasonable range of pressures over which corona processes are most likely to occur in space chamber situations. In Figure 2-4 the onset of corona in a point-to-plane electrode geometry is presented in terms of pressure-electrode separation (torr-cm) versus the electrode potential threshold. For space chamber work, potentials in the 0.5 to 5kv range are typical, implying that corona onset can be expected for the 20 to 400 torr-cm region. For a 0.1mm gap, the pressure range for corona onset will be $0.2 \leq p \leq 2$ torr.

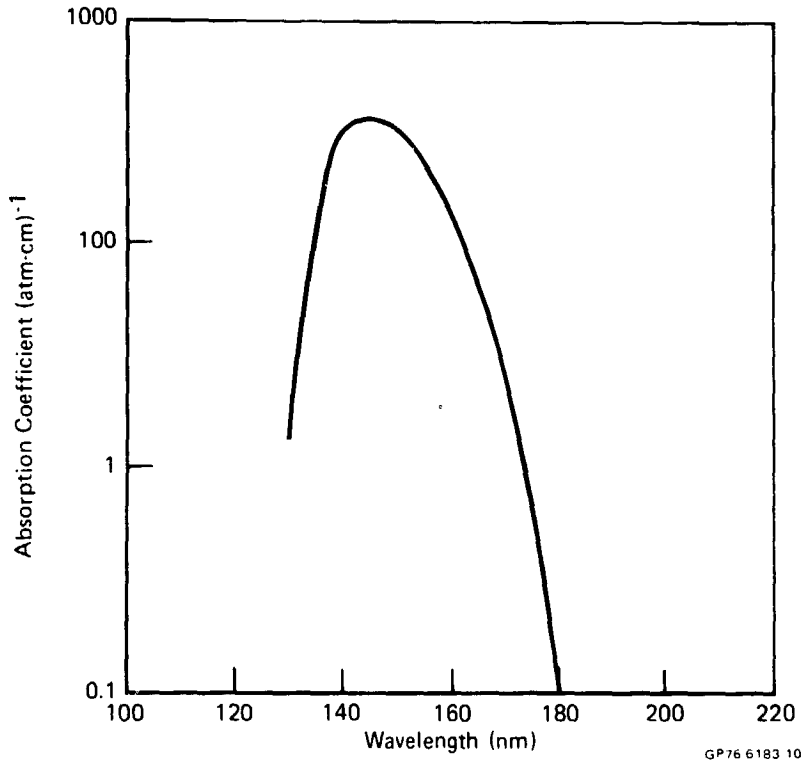

FIGURE 2-3 ABSORPTION COEFFICIENT OF OXYGEN

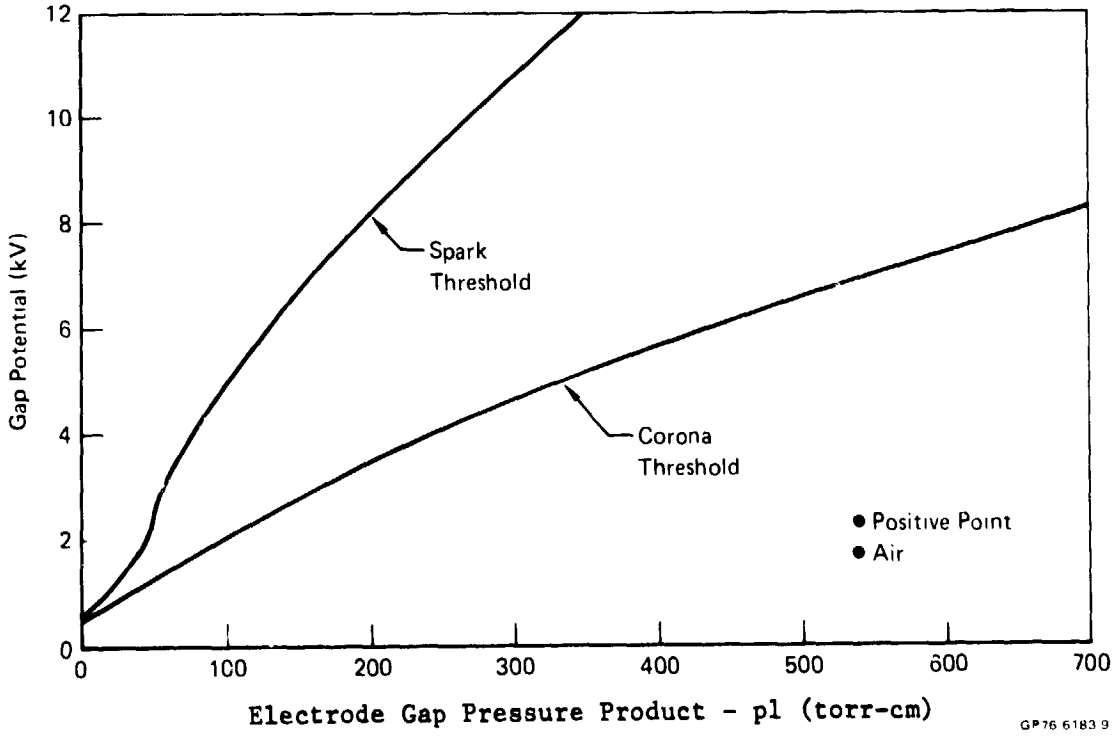

FIGURE 2-4 THRESHOLD POTENTIALS FOR CORONA AND SPARK - POINT-TO-PLANE ELECTRODE

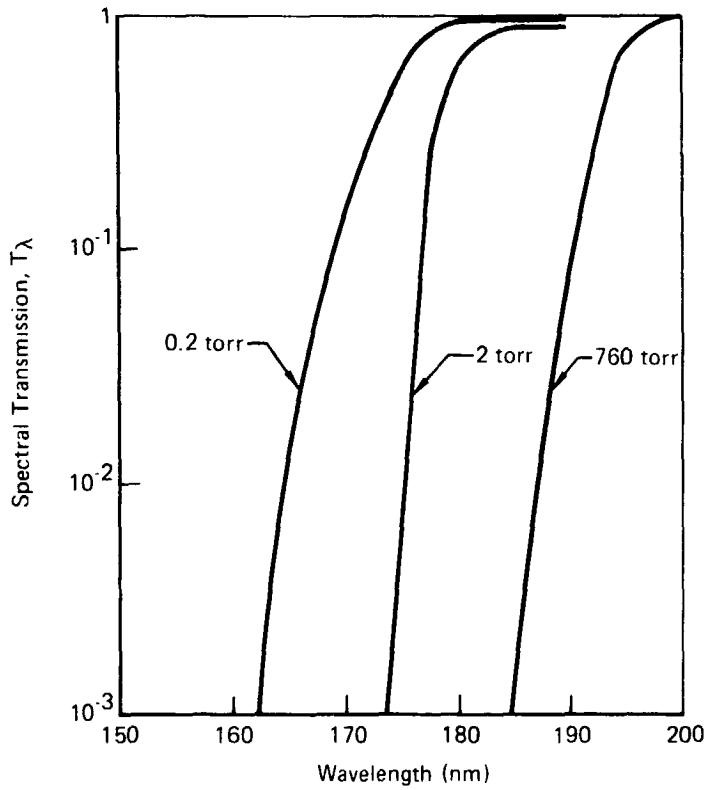

FIGURE 2-5 SPECTRAL TRANSMISSION OF OXYGEN FOR 300 cm PATH

Figure 2-5 shows the spectral transmission, T_λ, of a 3 meter thickness of oxygen at 0.2 torr, 2 torr, and 760 torr. T_λ falls below 1% at 165 nm at 0.2 torr and at 175 nm at 2 torr. At 760 torr T_λ is singificant at wavelenghths longer than 190 nm, which represents the practical lower wavelength limit for spectroscopy at atmospheric pressure. For wavelengths less than 190 nm the optical path of the spectrometer must be maintained at vacuum in order to conduct spectroscopic measurements.

These results show that only a small part of the vacuum UV spectral region (165-190 nm) is expected to be sufficiently transparent for possible use in corona detection.

Therefore, in this study the spectral intensity measurements were concentrated in the spectral range 190 to 400 nm by employing conventional, atmospheric pressure spectroscopy rather than vacuum UV spectroscopy. Considerable savings in time and effort were realized since the atmospheric measurements are relatively easy to perform.

2.3 TASK 3 - UV SPECTRAL INTENSITY MEASUREMENTS. The next task in this study, viz. UV spectral intensity measurements of corona discharges, is detailed in Section 4. . Included in these measurements are both spectral intensity data produced by the spectroradiometer and the outputs of various type. of candidate UV corona detection systems. The latter measurements were combined with the spectroradiometer scans in the interest of economy in this program. Two considerations were addressed in the course of these measurements: First, to provide the required data on UV spectral intensity for corona processes, the corona simulator was operated over wide ranges of current and pressure in order to obtain data for a variety of corona discharge types (burst pulses, steady glow, prebreakdown streamers, etc.). Second, to study the threshold sensitivity of the breadboarded UV corona detection systems, the corona simulator was operated at conditions near the burst pulses-to-steady glow transition.

2.4 TASK 4 - ANALYSIS OF UV CORONA DETECTION SYSTEM PERFORMANCE. Section 5 contains the system performance analysis of candidate UV corona detection systems. The UV spectral intensity data provides the basic input to this analysis, which encompasses both the breadboard systems tested in the previous task and conceptual systems not tested in this program. The latter analysis relies on manufacturer's data for the various components which comprise the conceptual systems. The principal result of this analysis was the determination of a range-intensity relationship for each candidate system, i.e. the minimum corona intensity which could be detected at a given separation between the corona discharge and the UV corona detection system. An additional extremely important consideration addressed in the analysis confirmed the effects of background light on the corona detection system. A practical system will be required to operate in the presence of light from tungsten filament lamps, quartz heater lamps, fluorescent lights and, possibly, a high fidelity solar simulator. These background light sources will impose a quasi-steady input to the UV corona detector system which possibly could completely obliterate the signal due to a weakly emitting corona discharge. These potentially serious effects are amenable to analysis, once the range-intensity relationship has been determined, since sufficient data are available on the spectral intensity characteristics of these background light sources.

3.0 EXPERIMENTAL APPROACH

This section contains a description of the spectroradiometer system, the procedures required to obtain an NBS-traceable calibration and the data acquisition system used in this program.

3.1 UV SPECTRORADIOMETER SYSTEM. The UV spectroradiometer is shown schemetically in Figure 3-1. This system was built around a Jarrell-Ash 0.5 meter grating spectrometer optimized for the 190-400 nm waveband. The 1180 line/mm grating provided 1.6 nm (=16Å) per mm dispersion at the spectrometer exit slit. The entrance slit and the exits slit both were set at maximum (2 mm) during this program to maximize the throughput (light gathering capacity) of the spectrometer. Spectral resolution was traded for maximum throughput since the main purpose of the spectroradiometric measurements was to obtain spectral intensity data from extremely weak corona emissions.

The detector, an EMI Model 9558QC photomultiplier tube (PMT) with an S-20 photocathode, was positoned at the spectrometer exit slit. The PMT operating voltages were provided by a Fluke Model 408B DC power supply (cf. Figure 3-2a). The 9558QC PMT was selected for its good quantum efficiency in the 190 nm to 400 nm range, and for its high intrinsic overall gain due to the 11-stage internal amplification.

A plane flip mirror permitted light from either the standard lamp or the corona to be directed through the spectrometer entrance slit. Focussing optics were not used to image the lamp or the corona onto the entrance slit since it was required that the PMT detector view the entire corona discharge. Thus the corona, confined to the gap region between the electrodes, only partially filled the spectrometer field of view. The spectrometer viewed the corona through a Suprasil window (synthetic fused silica) mounted on the corona simulator vacuum chamber.

A similar Suprasil window was positioned between the flip mirror and the standard lamp system to compensate for the effects of the vacuum chamber window. The standard lamp was a General Electric Model E-25 30A/3.5V tungsten strip lamp issued by the NBS as a secondary spectral radiance standard. A permanent optical transfer system, consisting of two 4 inch dia by 36 in.F.L. off-axis paraboloidal mirrors, was used to form an image of the tungsten strip filament

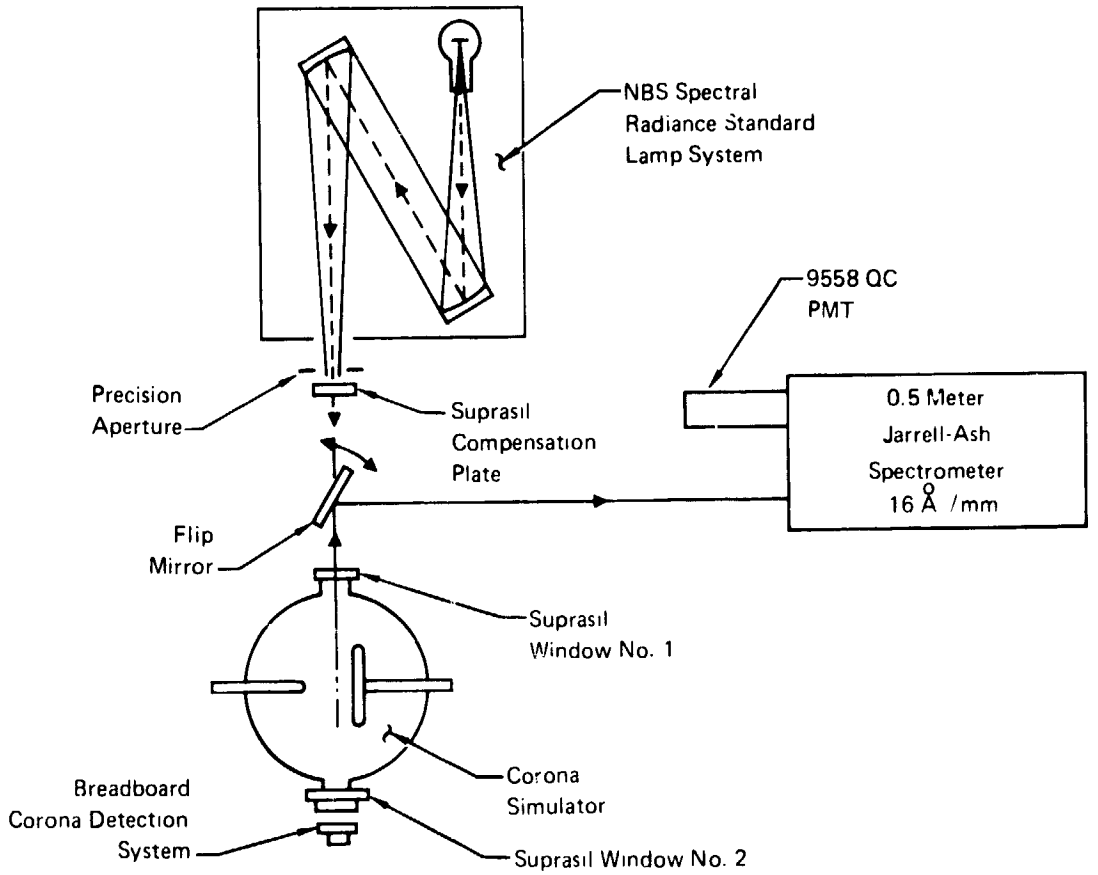

FIGURE 3-1 UV SPECTRORADIOMETER SYSTEM - OPTICAL LAYOUT

GP76 6183 14

on a precision circular aperture. The standard lamp was powered by a NJE 36V/50A DC power supply and the lamp current was set at 39.00 amps by use of a precision 1 millivolt current shunt and a Data Technology Corp. Model 350 4-1/2 digit voltmeter.

The two-mirror imaging system formed a convenient image of the strip lamp which permitted easy adjustment of the effective spectral radiance of the standard lamp by varying the size of the precision aperture. However, to use the lamp/mirror system as a spectral radiance standard, a cross calibration with another NBS standard lamp is required to account for the effects of the two parabloidal mirrors. This calibration procedure is discussed in Section 3.2.

Schematics of the data acquisition circuit and the corona simulator circuit are shown in Figures 3-2a and 3-2b, respectively. DC power to the 9558QC PMT was provided by a Fluke Model 408A DC Power Supply. The PMT anode current was measured by a Kin-Tel Model 203 Microvolt-Ammeter, operated on the current

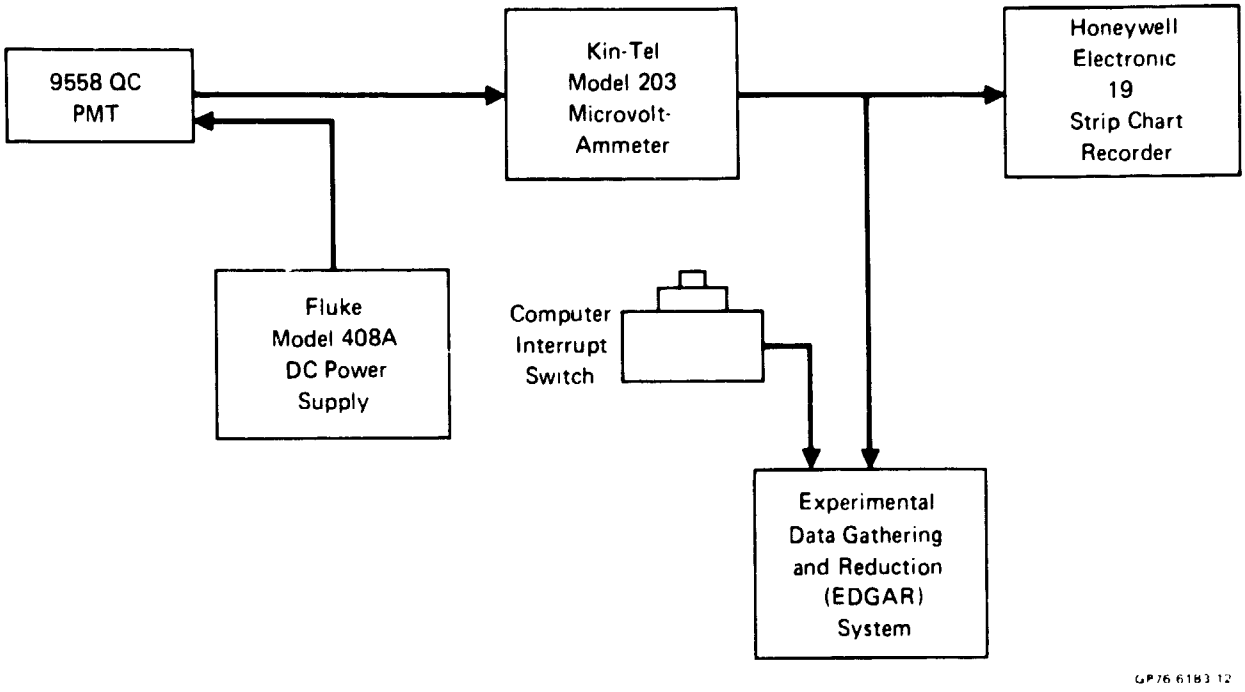

FIGURE 3-2a UV SPECTRORADIOMETER DATA ACQUISITION SYSTEM

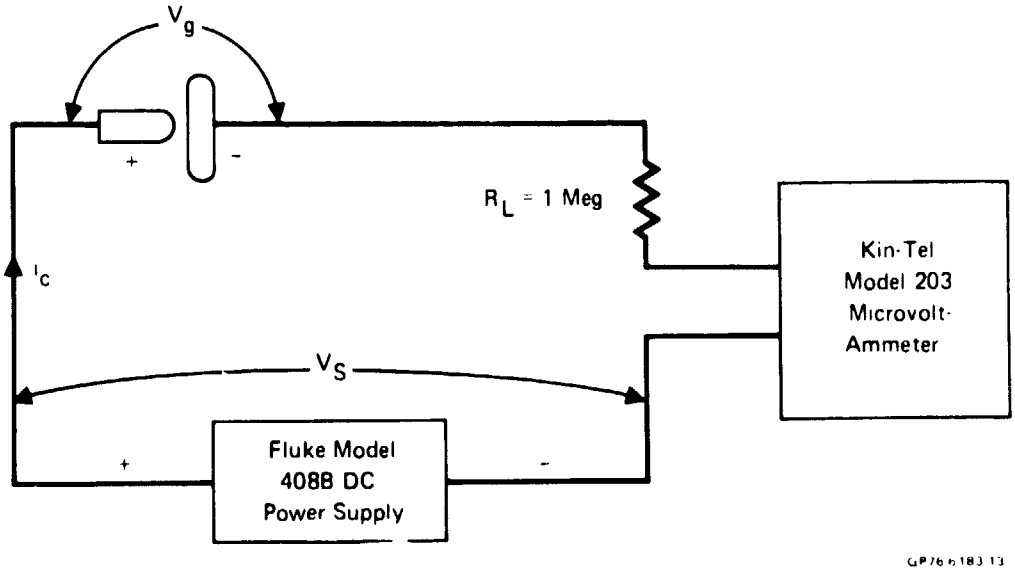

FIGURE 3-2b CORONA SIMULATOR CIRCUIT

ranges. The Kin-Tel produced an amplified voltage at the RECORDER output proportional to the PMT anode current. This signal was monitored by a Honeywell Electronik 19 strip chart recorder and was directed into the Applied Optics Laboratory Experimental Data Gathering and Reduction (EDGAR) System. Details of the EDGAR System are presented in Section 3.3. A computer interrupt switch allowed the oeprator to cue EDGAR at the start of a spectroradiometer scan.

Another Kin-Tel Model 203 Microvolt-Ammeter was used to measure the current in the corona simulator circuit (Figure 3-2b). The power for the corona simulator was provided by a Fluke Model 408B DC Power Supply (0-6kV, 0-20ma). A 1 Meg load resistor was used in series with the corona simulator to limit the current drawn by the corona discharge. The load resistor reduced the sensitivity of the corona to changes in applied voltage and permitted stable operation of the corona simulator from the pre-onset burst pulse region to the spark breakdown threshold. The voltage drop across the load resistor ($i_L R_L$) was subtracted from the DC power supply voltage (V_S) to yield the voltage drop across the electrode gap (V_g).

The corona simulator vacuum chamber is shown in Figure 3.3. The chamber was pumped via a 15 cfm rotary pump through a series molecular sieve trap and a LN_2 cold finger. Chamber pressure above 5 torr was monitored by a Wallace and Tiernan dial gauge (0-800 torr full scale, ±1 torr accuracy). Below 5 torr, pressure was measured via a NRC Alphatron Gauge (±5% full scale accuracy). The pressure level in the corona simulator was established dynamically by balancing the flow of bleed gas through a Granville-Phillips micrometer valve and the pumping speed via a throttle valve in the line to the rotary pump.

A view of the corona simulator through the glass top plate is shown in Figure 3-4. The plane electrode was a 6 in. diameter stainless steel plate with rods which, in turn, are carried by two linear motion vacuum passthrus. The pointed electrodes were also fabricated from stainless steel. The electrodes are supported by plexiglas rods. The electrode gap can be adjusted to ±0.2 mm accuracy by means of a micrometer feed screw attached to the hemispherical electrode holder. The electrodes are electrically isolated from the vacuum chamber via the plexiglas supports and via high voltage vacuum feedthrus.

Suprasil window #2 (cf. Figure 3-1) is visible in Figure 3-3 along with a

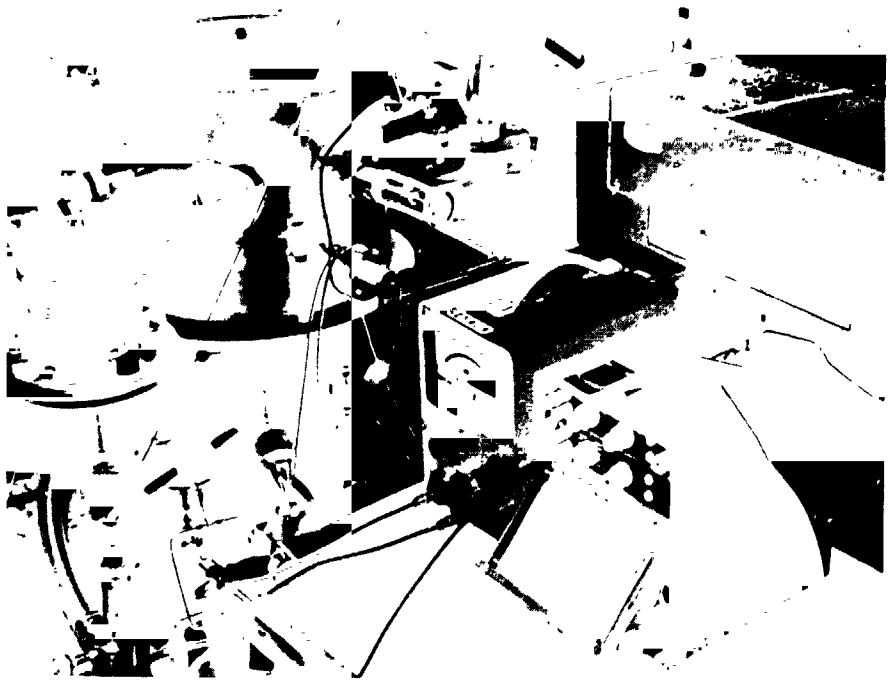

FIGURE 3-3 CORONA SIMULATOR VACUUM CHAMBER

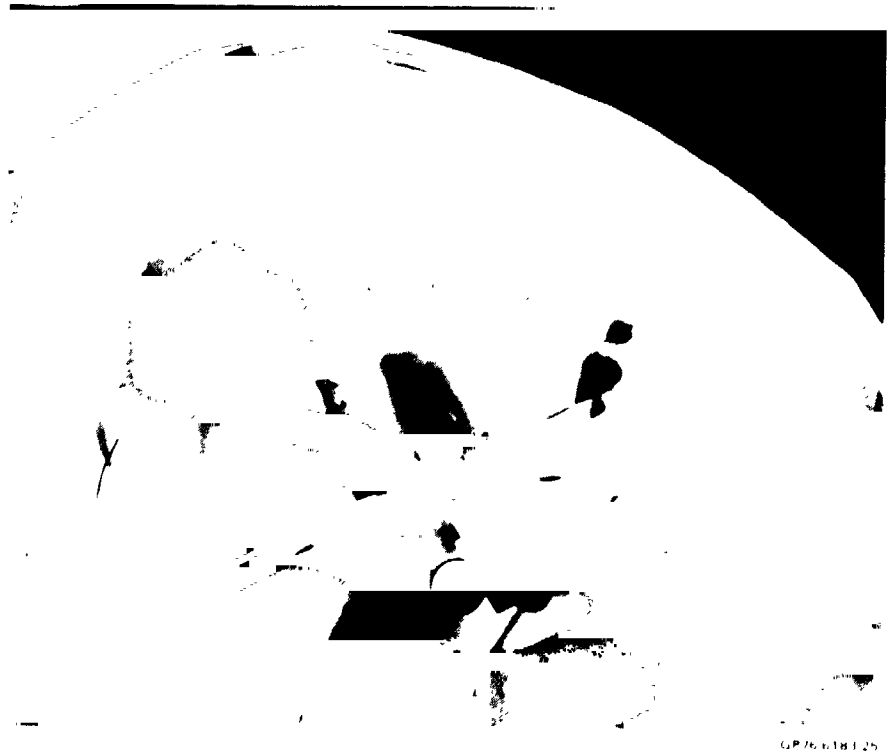

FIGURE 3-4 CORONA SIMULATOR - TOP VIEW

Honeywell UV gas tube detector. The Honeywell detector was used to monitor the UV corona emissions for most of the spectral data runs since it is a candidate sensor for a possible UV corona detection system. Four candidate detectors were breadboarded and positioned at various distances from window #2 during several spectroradiometer runs to determine their response to different corona simulator operating conditions. By adjusting the separation between the corona simulator and the detector breadboards, the intensity-distance relationship for the detector systems could be determined.

3.2 SPECTRORADIOMETER CALIBRATION. Due to the presence of the two paraboloidal transfer mirrors in the standard lamp system, it was necessary to establish the calibration of the complete lamp-mirror system by comparison with other NBS secondary lamp standards. Two cross-checks were used: a) comparison to another NBS secondary spectral radiance standard lamp without interferring transfer optics; and b) comparison to an NBS secondary standard of spectral irradiance. Method (a) was accomplished via the McDonnell Douglas Bureau of Standards using a Cary 14 spectrometer, and a 9558QC PMT to effect the transfer of calibration. The solid line of Figure 3-5 shows the calibration curve for the spectroradiometer standard lamp system obtained by method (a). To check method (a) the UV spectroradiometer system itself was used to compare the spectral radiance lamp-mirror system to an NBS spectral irradiance standard (Serial No. 1325). The spectral irradiance at the UV spectroradiometer entrance slit due to the spectral irradiance standard lamp is given by

$$H_\lambda(1) = H_\lambda(s)\left(\frac{D_s}{D_1}\right)^2 \qquad (3\text{-}1)$$

where $H_\lambda(1)$ = spectral irradiance at the entrance slit ($Wcm^{-2}\ nm^{-1}$)

$H_\lambda(s)$ = spectral irradiance at 50 cm for the spectral irradiance standard (#1325) ($Wcm^{-2}nm^{-1}$)

D_s = standard distance = 50 cm

D_1 = lamp-to-entrance slit distance (cm).

Similarly the spectral irradiance at the entrance slit due to the standard spectral radiance system with the paraboloidal mirrors is given by

$$H_\lambda(R) = H_\lambda(1) \cdot R \qquad (3\text{-}2)$$

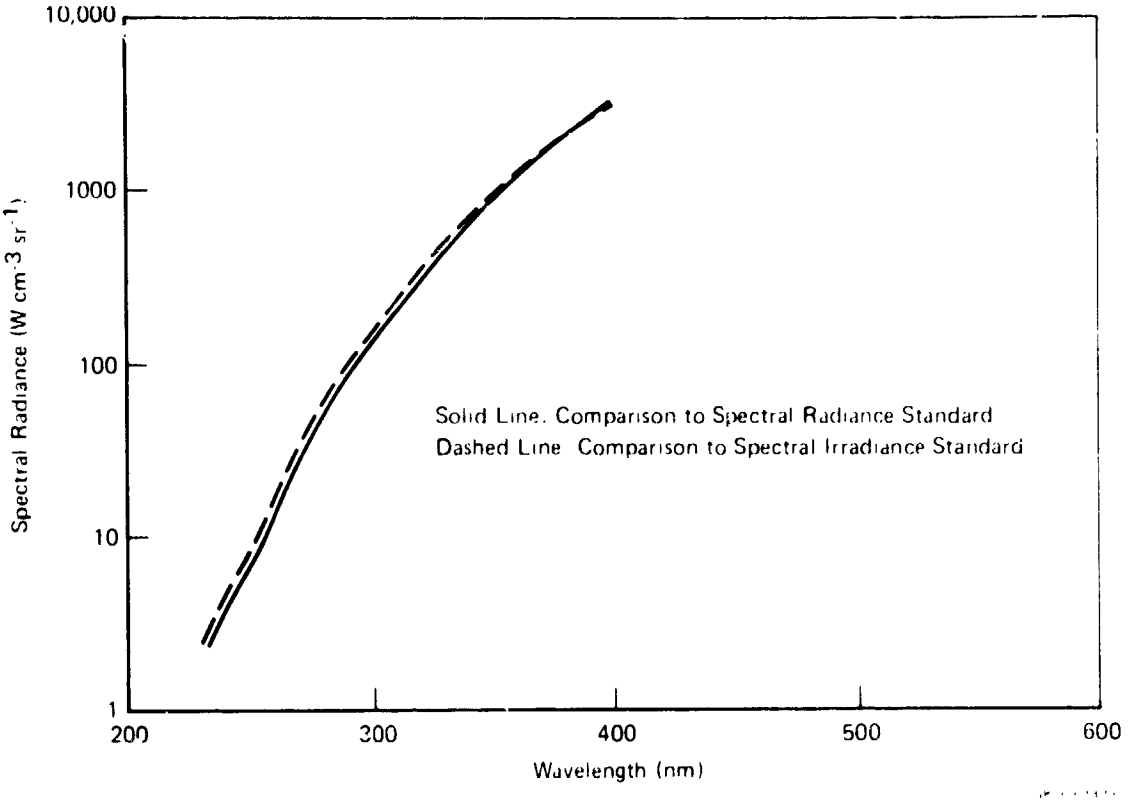

FIGURE 3-5 INTERCOMPARISON OF STANDARD LAMPS

where $H_\lambda(R)$ = spectral irradiance at the entrance slit due to the standard spectral radiance system

R = ratio of the PMT anode current for $H_\lambda(1)$ and $H_\lambda(R)$ $(=i[H_\lambda(1)]/i[H_\lambda(R)]$

The spectral radiance of the lamp-mirror system can be calculated from

$$N_\lambda(R) = H_\lambda(R)/\Omega$$

$$= H_\lambda(R)/(A_2/D_2{}^2) \qquad (3\text{-}3)$$

where $N_\lambda(R)$ = spectral radiance of the lamp-mirror system $(W\ cm^{-2} sr^{-1} nm^{-1})$,

Ω = solid angle subtended by the precision aperture of the lamp-mirror system viewed from the spectrometer entrance slit,

A_2 = area of the precision aperture (cf. Figure 3-1) (cm^2),

D_2 = distance from the entrance slit to the precision aperture (cm).

The dashed curve in Figure 3-5 represents the results of applying Eq. (3-3)

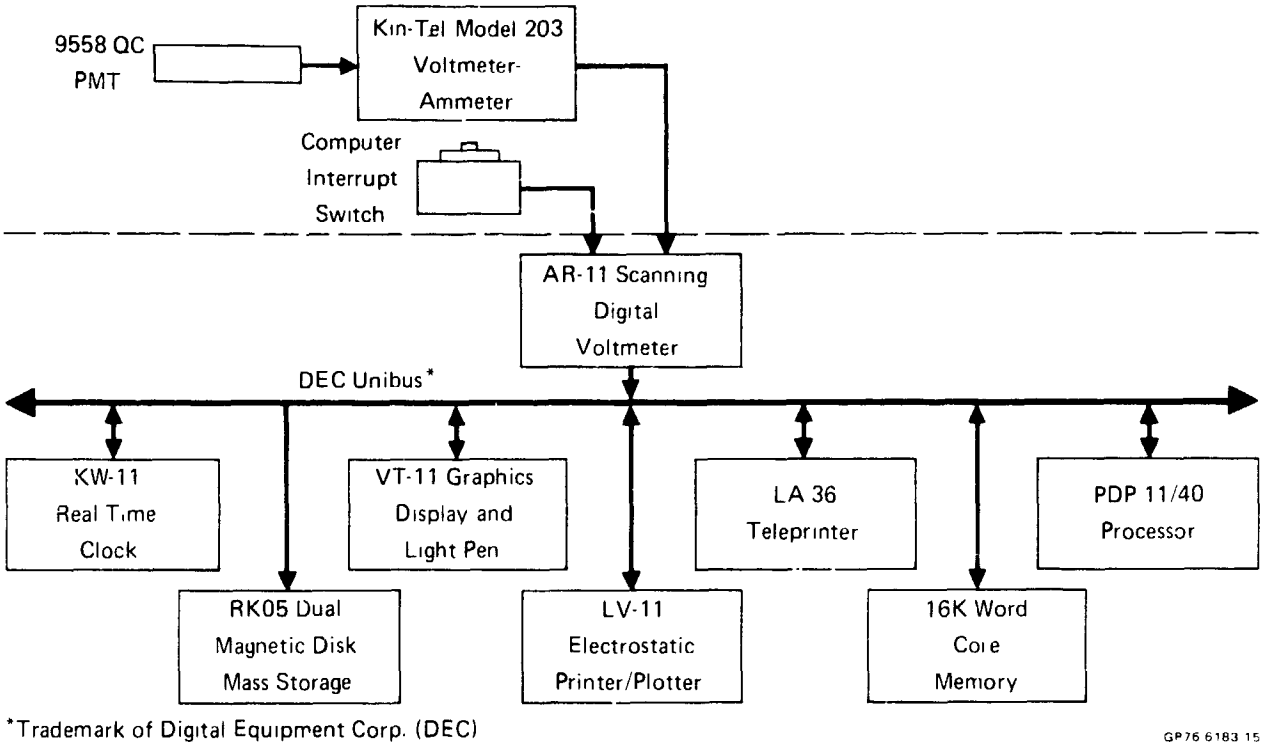

FIGURE 3-6 EDGAR SYSTEM BLOCK DIAGRAM

to the intercomparison data. Agreement between the two lamps is approximately ±10% over the 250 to 400 nm waveband. Periodic checks were made during the course of the spectral data scans to detect any deviations between the two lamps. No significant out of tolerance (±10%) conditions were noted.

3.3 DATA ACQUISITION AND ANALYSIS. The spectral intensity ($Wcm^{-2}nm^{-1}$) of the corona simulator discharges under a variety of operating conditions (voltage, gap length, pressure, gas species) comprises the principal output of the data acquisition and analysis procedures. The methods used for these procedures are detailed in this section.

The EDGAR system enabled large quantities of spectral data to be accumulated and analyzed with minimum operator intervention. Figure 3-6 shows the key elements in the EDGAR system and the functional interrelations. The anode current signal from the PMT was connected to an equivalent voltage by the Kin-Tel ammeter and input to one of the 16 channels of the AR-11 scanning digital voltmeter (10 bit resolution). A computer interrupt switch allowed the operator to synchronize the EDGAR hardware and data acquisition software with the start of the spectrometer scan. The UV corona spectra were stored on the magnetic disks in labeled files

FIGURE 3-7 EDGAR SYSTEM

which were subsequently recalled by the operator during the data analysis sessions at the teleprinter terminal. Both raw spectral data and processed spectra were displayed on the graphics terminal during the data reduction procedure. Hardcopy of the UV corona emission spectra were produced via the electrostatic printer/plotter (c.f. Figure 3-7).

The UV corona emission spectra were scanned in two wavebands, 200 nm to 265 nm and 265 nm to 400 nm. In each of these intervals, 220 spectral data points were obtained, i.e. there were $\frac{220 \cdot 1.6}{65} = 5.4$ samples per 1.6 nm resolution element in the lower interval and $\frac{220 \cdot 1.6}{135} = 2.6$ samples per 1.6 nm resolution element in the upper interval. The spectrometer scanning speed was 12.5 nm/min in the lower interval and 25 nm/min in the upper interval. This subdivision of the waveband was necessitated since the PMT DC voltage had to be changed at $\lambda = 265$ nm to increase the overall system gain in the 200 nm to 265 nm region.

The first step in the data analysis procedure involved the development of an equation describing the spectral radiance of the standard lamp-mirror system.

TABLE 3-1 - CALIBRATION DATA FOR SPECTRAL RADIANCE STANDARD LAMP

Wavelength (microns)	Spectral Radiance ($W\text{-}CM^{-3} - SR^{-1}$)	Radiance Equivalent Blackbody Temperature Kelvins (IPTS-68)
0.300	1.292×10^{2}	2428
0.325	3.675×10^{2}	2418
0.360	1.182×10^{3}	2403
0.400	3.282×10^{3}	2385
0.450	8.222×10^{3}	2356
0.500	1.634×10^{4}	2328
0.550	2.671×10^{4}	2296
0.600	3.853×10^{4}	2264
0.650	5.096×10^{4}	2234
0.700	6.234×10^{4}	2201
0.750	6.968×10^{4}	2160
0.800	7.608×10^{4}	2123
1.00	1.059×10^{5}	2048
1.20	1.036×10^{5}	1954
1.50	7.690×10^{4}	1802
1.75	5.617×10^{4}	1687
2.00	3.941×10^{4}	1578
2.35	2.481×10^{4}	1451
2.50	2.040×10^{4}	1401

The calibration data of Table 3-1 were approximated by a polynominal relating blackbody temperature T to wavelength λ,

$$T = A_1 + A_2\lambda + A_3\lambda^2 + A_4\lambda^3 \ (^\circ K) \qquad (3\text{-}4)$$

where $A_1 = 2747.36$
$A_2 = -2217.31$
$A_3 = 5540.93$
$A_4 = -5658.01$

TABLE 3-2 - EXTRAPOLATED RADIANCE STANDARD CALIBRATION DATA

Wavelength (nm)	Radiance Equivalent Blackbody Temperature (°K) (IPTS-68)
200	2480.27
225	2464.53
250	2450.93
275	2438.96
300	2428.08
325	2417.77
350	2407.48
375	2396.69
400	2384.87
425	2371.49

The data of Table 3-1, extrapolated down to λ = 200 nm using equation (3-4), are shown in Table 3-2. The validity of this extrapolation was established using the NBS secondary spectral irradiance standard. Equation (3-4) and Planck's Equation were used to obtain values of the spectral radiance of the standard lamp-mirror system,

$$N_\lambda(R) = \frac{1.1909 \times 10^{-12}}{\lambda^5} \quad \frac{1}{\exp(1.4380/\lambda T)-1} \qquad (3\text{-}5)$$

where $N_\lambda(R)$ = standard lamp system spectral radiance ($Wcm^{-3}sr^{-1}$)
λ = wavelength (cm)
T = temperature (°K)

The next step in the calibration procedure is to determine the overall sensitivity of the UV spectroradiometer by measuring the transfer function, S,

$$S = \frac{OUTPUT}{INPUT} = \frac{^iA}{N_\lambda(R)} \qquad (3\text{-}6)$$

where ^iA = PMT anode current (μa)

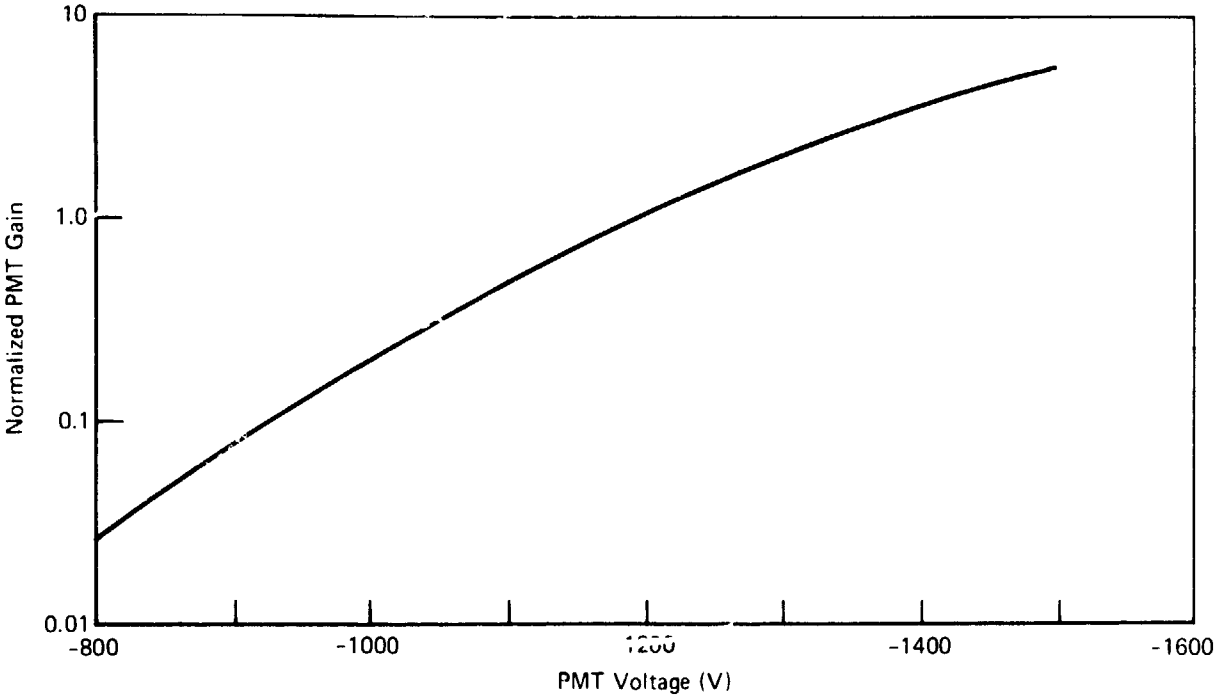

FIGURE 3-8 NORMALIZED PMT GAIN vs PMT VOLTAGE

GP76 0183 5

S = transfer function of the UV spectroradiometer
$(\mu a/Wcm^{-3}sr^{-1})$

The transfer function, S, depends on the DC operating voltage of the PMT, which was set at -1200 volts for the calibration runs. At times during the corona test runs it was necessary to vary the PMT voltages to obtain optimum system gain for a given set of corona simulator operating conditions. The dependency of system gain on PMT voltage was determined in a separate set of data runs, the results of which are shown in Figure 3-8. The relative PMT anode current $i_{rel}=i_{PMT}/i(-1200)$, plotted as a function of overall PMT voltage, V_{PMT} in Figure 3-8, is independent of wavelength in the 200 nm to 400 nm waveband. Using the PMT factor i_{rel}, an effective transfer function for the UV spectroradiometer can be defined as,

$$S' = \frac{S}{i_{rel}} \quad (\mu a/Wcm^{-3}sr^{-1}) \qquad (3\text{-}7)$$

Thus, S' represents the transfer function for PMT voltage V_{PMT} not necessarily equal to -1200V.

TABLE 3-3 - IDENTIFICATION OF FORTRAN VARIABLES

FORTRAN Variable	Corresponding Variable Of Section 3-3	Meaning
STD(I)	$N_\lambda(R)$	Radiance of the standard lamp-mirror system ($Wcm^{-3}sr^{-1}$)
PMT1	V_{PMT}	Overall PMT voltage used for the corona scan in the 265 to 400 nm waveband (V)
PMT2	V_{PMT}	Overall PMT voltage used for the corona scan in the 200 to 265 nm waveband (V)
FACT1	D	Scaling factor for the spectroradiometer transfer function due to PMT1
FACT2	D	Scaling factor for the spectroradiometer transfer function due to PMT2
FS1	N/A	Full-scale microamp range of the Kin-Tel microammeter in the 265 to 400 nm waveband (μa)
FS2	N/A	Full-scale microamp range of the Kin-Tel microammeter in the 200 to 265μm waveband (μa)
DAT(I)	N/A	Digital output of the AR-11 due to the PMT anode current, i_c, ranges from -2048 to +2048. The currents FS1 and FS2 produce a value DAT(I) = +2048.
AREA	A	Area of the precision aperture (cf. Figure 3-1) (cm^2)
CAL(I)	$\dot{i}(1200)$	PMT anode current due to the standard lamp-mirror system for V_{PMT}=-1200V(μa).

The spectral intensity of the corona discharge was calculated according to

$$J_\lambda = i_{Corona} \cdot S' \cdot A \cdot F \qquad (3\text{-}3)$$

where J_λ = spectral intensity ($Wsr^{-1}nm^{-1}$)
A = area of the precision aperture (cf. Figure 3-1) (cm^2)
$F = 10^{-7}$ = conversion factor from centimeters to nanometers.

The FORTRAN computer code CORDAR (CORona DAta Reduction) used in this program

to generate the corona spectral intensity data is listed in Appendix A. To facilitate cross-reference between the analysis of this section and the FORTRAN variables used in the code, the identifications of Table 3-3 are used.

The FORTRAN equivalent to Eq. (3-8) in the computer program for the 265 to 400 nm waveband is

$$\text{INTENS(I)=DAT(I)*FS1)*}\frac{\text{STD(I)}}{\text{CAL(I)*FACT1}}\text{*AREA} \qquad (3\text{-}9)$$

The corresponding equation for the 200 to 265 nm is obtained by replacing FS1 by FS2 and FACT1 by FACT2 in Eq (3-9).

A complete tabulation of the raw data and processed results for a single spectroradiometer scan is presented in Table 3-4. The data entitled "Calibration Data-Averaged" is the PMT anode current for the standard lamp-mirror system at v_{PMT}=-1200V (called CAL(I) in the FORTRAN program). Similarly the data entitled "Sensitivity" is the reciprocal of the spectroradiometer transfer function defined by Eq (3-7). Finally the "Corrected Corona Data" are the quantities calculated from the relations

$$\frac{\text{DAT(I)*FS1}}{\text{FACT1}} \quad \text{and} \quad \frac{\text{DAT(I)*FS2}}{\text{FACT2}} \ .$$

The sheer volume of similar data operated for the several hundred spectroradiometer scans obtained in this study makes it impossible to include all of it in this report. For the purposes of the system analyses presented in the following sections, computer-generated plots of the spectral intensity of the corona discharge versus wavelength are presented in Section 4.1 as appropriate. However, tabular data such as that shown in Table 3-4 remain stored in magnetic disk files of the EDGAR system.

UV CORONA DATA REDUCTION LISTING

DATA FROM FILES: JOE040 & JOE041

TABLE 3-4 - DATA ANALYSIS COMPUTER PROGRAM OUTPUT

WAVELENGTH (NANOMETERS)	STANDARD LAMP RADIANCE (WATTS/CM^3-SR)	CALIBRATION DATA-AVERAGED (MICROAMPS)	SENSITIVITY (WATTS/NM-SR PER MICROAMP)	CORRECTED CORONA DATA (MICROAMPS)	CORONA INTENSITY (WATTS/NM-SR)
400.000	0.330379E-03	81.7057	0.227246E-07	4.52899	0.102919E-06
399.375	0.325852E-03	80.4036	0.227762E-07	4.38745	0.999296E-07
398.750	0.321367E-03	79.9154	0.225999E-07	4.38745	0.991562E-07
398.125	0.316925E-03	78.7760	0.226099E-07	4.10439	0.927999E-07
397.500	0.312524E-03	78.4505	0.223885E-07	3.96286	0.887224E-07
396.875	0.308165E-03	77.4740	0.223544E-07	3.67980	0.822599E-07
396.250	0.303848E-03	76.6602	0.222752E-07	3.39674	0.756632E-07
395.625	0.299572E-03	75.8464	0.221974E-07	3.53827	0.785405E-07
395.000	0.295337E-03	75.1953	0.220731E-07	3.96286	0.874726E-07
394.375	0.291144E-03	74.5443	0.219498E-07	4.10439	0.900904E-07
393.750	0.286992E-03	73.4049	0.219725E-07	4.24592	0.932937E-07
393.125	0.282880E-03	72.9167	0.218028E-07	4.38745	0.956587E-07
392.500	0.278810E-03	72.4284	0.216340E-07	4.38745	0.949180E-07
391.875	0.274780E-03	71.7773	0.215146E-07	4.52899	0.974395E-07
391.250	0.270790E-03	70.6380	0.215442E-07	4.24592	0.914752E-07
390.625	0.266842E-03	69.8242	0.214775E-07	4.24592	0.911920E-07
390.000	0.262933E-03	69.4987	0.212621E-07	4.10439	0.872679E-07
389.375	0.259065E-03	68.3594	0.212984E-07	3.82133	0.813883E-07
388.750	0.255237E-03	67.8711	0.211346E-07	3.39674	0.717888E-07
388.125	0.251448E-03	67.0573	0.210736E-07	2.54755	0.536860E-07
387.500	0.247699E-03	66.0807	0.210662E-07	2.12296	0.447227E-07
386.875	0.243989E-03	65.5924	0.209051E-07	1.69837	0.355046E-07
386.250	0.240319E-03	64.6159	0.209019E-07	1.41531	0.295826E-07
385.625	0.236688E-03	63.9648	0.207956E-07	1.13225	0.235457E-07
385.000	0.233096E-03	63.1510	0.207439E-07	1.41531	0.293590E-07
384.375	0.229543E-03	62.3372	0.206944E-07	3.53827	0.732222E-07
383.750	0.226028E-03	61.0352	0.208122E-07	4.38745	0.913127E-07
383.125	0.222552E-03	60.5469	0.206574E-07	4.95358	0.102328E-06
382.500	0.219114E-03	59.2448	0.207853E-07	5.51970	0.114728E-06
381.875	0.215714E-03	58.2682	0.208057E-07	5.94429	0.123675E-06
381.250	0.212352E-03	57.1289	0.208899E-07	6.22736	0.130089E-06
380.625	0.209027E-03	55.9896	0.209813E-07	6.36889	0.133627E-06
380.000	0.205741E-03	55.0130	0.210180E-07	6.08582	0.127912E-06
379.375	0.202491E-03	54.0365	0.210599E-07	5.94429	0.125186E-06
378.750	0.199279E-03	52.7344	0.212375E-07	5.80276	0.123236E-06
378.125	0.196104E-03	51.7578	0.212934E-07	5.80276	0.123561E-06
377.500	0.192965E-03	50.6185	0.214242E-07	5.51970	0.118255E-06
376.875	0.189863E-03	49.6419	0.214945E-07	5.51970	0.118643E-06
376.250	0.186796E-03	48.8281	0.214998E-07	5.51970	0.118673E-06
375.625	0.183767E-03	47.8516	0.215828E-07	5.66123	0.122185E-06

(cont'd)

TABLE 3-4 - (cont'd)

WAVELENGTH (NANOMETERS)	STANDARD LAMP RADIANCE (WATTS/CM^3-SR)	CALIBRATION DATA-AVERAGED (MICROAMPS)	SENSITIVITY (WATTS/NM-SR PER MICROAMP)	CORRECTED CORONA DATA (MICROAMPS)	CORONA INTENSITY (WATTS/NM-SR)
375.000	0.180773E-03	46.3750	0.216735E-07	5.37817	0.116564E-06
374.375	0.177815E-03	45.7357	0.218499E-07	5.09511	0.111328E-06
373.750	0.174892E-03	44.7591	0.219597E-07	4.95358	0.108779E-06
373.125	0.172005E-03	43.9453	0.219971E-07	4.52899	0.996245E-07
372.500	0.169153E-03	43.1315	0.220405E-07	4.38745	0.967018E-07
371.875	0.166335E-03	42.4805	0.220055E-07	4.10439	0.903194E-07
371.250	0.163553E-03	41.8367	0.220600E-07	3.82133	0.842985E-07
370.625	0.160805E-03	40.5273	0.222991E-07	3.67980	0.820561E-07
370.000	0.158090E-03	40.0391	0.221900E-07	3.53827	0.785144E-07
369.375	0.155410E-03	39.0625	0.223592E-07	3.25521	0.727838E-07
368.750	0.152764E-03	38.8997	0.220704E-07	2.83062	0.624728E-07
368.125	0.150151E-03	38.0859	0.221564E-07	2.40602	0.533088E-07
367.500	0.147571E-03	37.4349	0.221544E-07	1.98143	0.438975E-07
366.875	0.145024E-03	36.6211	0.222559E-07	1.69837	0.377988E-07
366.250	0.142511E-03	36.2956	0.220663E-07	1.83990	0.405998E-07
365.625	0.140030E-03	35.6445	0.220782E-07	1.83990	0.406216E-07
365.000	0.137581E-03	35.1562	0.219933E-07	1.69837	0.373528E-07
364.375	0.135164E-03	34.3424	0.221190E-07	1.55684	0.344357E-07
363.750	0.132779E-03	33.8542	0.220422E-07	1.55684	0.343161E-07
363.125	0.130426E-03	33.2031	0.220760E-07	1.27378	0.281199E-07
362.500	0.128104E-03	33.0404	0.217899E-07	1.13225	0.246715E-07
361.875	0.125813E-03	32.3893	0.218304E-07	3.67980	0.803315E-07
361.250	0.123554E-03	32.0638	0.216560E-07	5.09511	0.110340E-06
360.625	0.121325E-03	31.5755	0.215941E-07	6.08582	0.131418E-06
360.000	0.119127E-03	30.9245	0.216493E-07	7.07654	0.153202E-06
359.375	0.116958E-03	30.5990	0.214813E-07	7.92572	0.170255E-06
358.750	0.114820E-03	30.1107	0.214306E-07	8.49185	0.181985E-06
358.125	0.112712E-03	29.7852	0.212670E-07	9.05797	0.192636E-06
357.500	0.110633E-03	28.9714	0.214611E-07	9.05797	0.194394E-06
356.875	0.108583E-03	28.4831	0.214245E-07	8.63338	0.184966E-06
356.250	0.106562E-03	27.9948	0.213925E-07	8.20879	0.175607E-06
355.625	0.104570E-03	27.6693	0.212397E-07	7.50113	0.159322E-06
355.000	0.102607E-03	27.1810	0.212152E-07	6.93501	0.147128E-06
354.375	0.100672E-03	26.5299	0.213259E-07	6.36889	0.135822E-06
353.750	0.987643E-04	26.3672	0.210510E-07	5.94429	0.125133E-06
353.125	0.968850E-04	25.7161	0.211732E-07	6.93501	0.146836E-06
352.500	0.950332E-04	25.3906	0.210348E-07	6.51042	0.136945E-06
351.875	0.932084E-04	25.0651	0.208988E-07	6.08582	0.127187E-06
351.250	0.914110E-04	24.4141	0.210424E-07	5.51970	0.116148E-06
350.625	0.896402E-04	24.0885	0.209136E-07	4.95358	0.103597E-06

TABLE 3-4 - (cont'd)

WAVELENGTH (NANOMETERS)	STANDARD LAMP RADIANCE (WATTS/CM^3-SR)	CALIBRATION DATA-AVERAGED (MICROAMPS)	SENSITIVITY (WATTS/NM-SR PER MICROAMP)	CORRECTED CORONA DATA (MICROAMPS)	CORONA INTENSITY (WATTS/NM-SR)
350.000	0.878958E-04	23.4375	0.210762E-07	4.24592	0.894881E-07
349.375	0.861779E-04	23.4375	0.206643E-07	3.39674	0.701913E-07
348.750	0.844857E-04	22.7865	0.208374E-07	2.68909	0.560334E-07
348.125	0.828196E-04	21.9727	0.211830E-07	2.26449	0.479687E-07
347.500	0.811789E-04	22.1354	0.206107E-07	1.83990	0.379216E-07
346.875	0.795637E-04	21.6471	0.206562E-07	1.41531	0.292349E-07
346.250	0.779734E-04	21.3216	0.205524E-07	1.55684	0.319968E-07
345.625	0.764078E-04	20.8333	0.206118E-07	1.69837	0.350064E-07
345.000	0.748666E-04	20.5078	0.205166E-07	1.83990	0.377485E-07
344.375	0.733500E-04	20.1823	0.204252E-07	1.98143	0.404711E-07
343.750	0.718573E-04	20.0195	0.201722E-07	1.83990	0.371148E-07
343.125	0.703884E-04	19.6940	0.200865E-07	2.12296	0.426428E-07
342.500	0.689431E-04	19.3685	0.200047E-07	1.69837	0.339753E-07
341.875	0.675212E-04	18.8802	0.200988E-07	1.98143	0.398243E-07
341.250	0.661221E-04	18.5547	0.200276E-07	5.66123	0.113381E-06
340.625	0.647459E-04	18.3919	0.197843E-07	7.64266	0.151205E-06
340.000	0.633923E-04	17.9036	0.198990E-07	9.34103	0.185877E-06
339.375	0.620610E-04	17.7409	0.196598E-07	10.8979	0.214250E-06
338.750	0.607516E-04	17.4154	0.196048E-07	12.1716	0.238622E-06
338.125	0.594643E-04	16.7643	0.199346E-07	13.5870	0.270850E-06
337.500	0.581984E-04	16.4389	0.198965E-07	14.0115	0.278781E-06
336.875	0.569539E-04	16.4388	0.194711E-07	13.3039	0.259041E-06
336.250	0.557305E-04	15.7878	0.198385E-07	12.3132	0.244275E-06
335.625	0.545279E-04	15.7878	0.194104E-07	10.8979	0.211532E-06
335.000	0.533460E-04	15.2995	0.195957E-07	9.19950	0.180271E-06
334.375	0.521845E-04	15.1367	0.193752E-07	7.78419	0.150820E-06
333.750	0.510430E-04	14.6484	0.195831E-07	5.94429	0.116408E-06
333.125	0.499214E-04	14.3229	0.195881E-07	4.81205	0.942587E-07
332.500	0.488195E-04	13.9974	0.196012E-07	4.38745	0.859994E-07
331.875	0.477371E-04	13.8346	0.193921E-07	4.10439	0.795927E-07
331.250	0.466738E-04	13.5091	0.194170E-07	3.82133	0.741989E-07
330.625	0.456294E-04	13.3464	0.192140E-07	3.53827	0.679844E-07
330.000	0.446038E-04	12.8581	0.194954E-07	3.25521	0.634616E-07
329.375	0.435966E-04	12.5326	0.195501E-07	3.53827	0.691735E-07
328.750	0.426077E-04	12.3698	0.193581E-07	3.25521	0.630145E-07
328.125	0.416367E-04	12.0443	0.194282E-07	2.83062	0.549937E-07
327.500	0.406836E-04	11.8815	0.192435E-07	2.54755	0.490239E-07
326.875	0.397480E-04	11.7187	0.190621E-07	2.12296	0.404681E-07
326.250	0.388298E-04	11.3932	0.191538E-07	1.69837	0.325302E-07
325.625	0.379287E-04	11.0677	0.192596E-07	1.27378	0.245324E-07

TABLE 3-4 - (cont'd)

WAVELENGTH (NANOMETERS)	STANDARD LAMP RADIANCE (WATTS/CM^3-SR)	CALIBRATION DATA-AVERAGED (MICROAMPS)	SENSITIVITY (WATTS/NM-SR PER MICROAMP)	CORRECTED CORONA DATA (MICROAMPS)	CORONA INTENSITY (WATTS/NM-SR)
325.000	0.370443E-04	10.9049	0.190912E-07	1.13225	0.216160E-07
324.375	0.361767E-04	10.7422	0.189266E-07	1.27378	0.241083E-07
323.750	0.353255E-04	10.5794	0.187656E-07	1.27378	0.239032E-07
323.125	0.344905E-04	9.92839	0.195235E-07	1.27378	0.248685E-07
322.500	0.336715E-04	9.76562	0.193775E-07	1.41531	0.274252E-07
321.875	0.328682E-04	9.70052	0.190422E-07	1.55684	0.296456E-07
321.250	0.320804E-04	9.27734	0.194336E-07	1.41531	0.275045E-07
320.625	0.313080E-04	8.91927	0.197270E-07	2.12296	0.418798E-07
320.000	0.305507E-04	8.70768	0.197176E-07	5.09511	0.100464E-06
319.375	0.298084E-04	8.47982	0.197555E-07	6.22736	0.123025E-06
318.750	0.290806E-04	8.21940	0.198838E-07	7.21807	0.143523E-06
318.125	0.283674E-04	8.10547	0.196688E-07	8.20879	0.161457E-06
317.500	0.276684E-04	7.91016	0.196579E-07	8.91644	0.175278E-06
316.875	0.269836E-04	7.82878	0.193705E-07	10.0487	0.194648E-06
316.250	0.263125E-04	7.56836	0.195387E-07	10.1902	0.199104E-06
315.625	0.256551E-04	7.42187	0.194266E-07	10.0487	0.195211E-06
315.000	0.250111E-04	7.25911	0.193636E-07	9.48256	0.183616E-06
314.375	0.243803E-04	7.12891	0.192200E-07	9.05797	0.174094E-06
313.750	0.237626E-04	6.94987	0.192156E-07	8.35032	0.160456E-06
313.125	0.231578E-04	6.80339	0.191297E-07	7.64266	0.146202E-06
312.500	0.225656E-04	6.67318	0.190042E-07	6.93501	0.131795E-06
311.875	0.219858E-04	6.51042	0.189789E-07	6.22736	0.118188E-06
311.250	0.214183E-04	6.38021	0.188663E-07	5.80276	0.109477E-06
310.625	0.208628E-04	6.25000	0.187599E-07	5.37817	0.100894E-06
310.000	0.203192E-04	6.13607	0.186103E-07	4.95358	0.921876E-07
309.375	0.197872E-04	6.00586	0.185160E-07	4.24592	0.786174E-07
308.750	0.192668E-04	5.87565	0.184285E-07	3.25521	0.599887E-07
308.125	0.187577E-04	5.76172	0.182963E-07	2.40602	0.440214E-07
307.500	0.182597E-04	5.59896	0.183283E-07	1.98143	0.363163E-07
306.875	0.177726E-04	5.46875	0.182641E-07	1.55684	0.284343E-07
306.250	0.172963E-04	5.38737	0.180432E-07	1.27378	0.229830E-07
305.625	0.168305E-04	5.24089	0.180480E-07	1.13225	0.204348E-07
305.000	0.163752E-04	5.14323	0.178931E-07	0.849185	0.151946E-07
304.375	0.159300E-04	4.99674	0.179170E-07	0.849185	0.152149E-07
303.750	0.154949E-04	4.89909	0.177750E-07	0.849185	0.150943E-07
303.125	0.150697E-04	4.78516	0.176988E-07	0.849185	0.150296E-07
302.500	0.146542E-04	4.67122	0.176306E-07	0.849185	0.149716E-07
301.875	0.142482E-04	4.55729	0.175707E-07	1.41531	0.248679E-07
301.250	0.138515E-04	4.47591	0.173921E-07	2.40602	0.418459E-07
300.625	0.134641E-04	4.36198	0.173472E-07	3.67980	0.638344E-07

TABLE 3-4 - (cont'd)

WAVELENGTH (NANOMETERS)	STANDARD LAMP RADIANCE (WATTS/CM^3-SR)	CALIBRATION DATA-AVERAGED (MICROAMPS)	SENSITIVITY (WATTS/NM-SR PER MICROAMP)	CORRECTED CORONA DATA (MICROAMPS)	CORONA INTENSITY (WATTS/NM-SR)
300.000	0.130857E-04	4.24805	0.173119E-07	4.24592	0.735051E-07
299.375	0.127162E-04	4.16667	0.171516E-07	4.52899	0.776795E-07
298.750	0.123554E-04	4.10156	0.169295E-07	4.95358	0.838616E-07
298.125	0.120032E-04	4.00391	0.168480E-07	5.23664	0.882269E-07
297.500	0.116593E-04	3.90625	0.167745E-07	5.09511	0.854680E-07
296.875	0.113237E-04	3.80859	0.167094E-07	4.95358	0.827715E-07
296.250	0.109962E-04	3.77604	0.163660E-07	4.67052	0.764376E-07
295.625	0.106767E-04	3.62956	0.165317E-07	4.52899	0.748719E-07
295.000	0.103649E-04	3.56445	0.163421E-07	4.10439	0.670743E-07
294.375	0.100607E-04	3.46680	0.163094E-07	3.39674	0.553987E-07
293.750	0.976409E-05	3.36914	0.162873E-07	2.26449	0.368825E-07
293.125	0.947480E-05	3.30404	0.161162E-07	1.41531	0.228093E-07
292.500	0.919271E-05	3.19010	0.161948E-07	0.990716	0.160444E-07
291.875	0.891769E-05	3.14128	0.159545E-07	0.707654	0.112902E-07
291.250	0.864962E-05	3.04362	0.159714E-07	0.707654	0.113022E-07
290.625	0.838933E-05	3.01107	0.156564E-07	0.707654	0.110793E-07
290.000	0.813670E-05	2.96224	0.154314E-07	0.707654	0.109201E-07
289.375	0.788558E-05	2.89714	0.152968E-07	0.707654	0.108249E-07
288.750	0.764386E-05	2.81576	0.152565E-07	0.707654	0.107963E-07
288.125	0.740843E-05	2.76693	0.150475E-07	0.707654	0.106484E-07
287.500	0.717909E-05	2.71810	0.148436E-07	0.707654	0.105042E-07
286.875	0.695579E-05	2.70182	0.144686E-07	0.707654	0.102387E-07
286.250	0.673834E-05	2.62044	0.144516E-07	0.849185	0.122720E-07
285.625	0.652669E-05	2.60417	0.140851E-07	0.990716	0.139543E-07
285.000	0.632065E-05	2.58789	0.137263E-07	1.27378	0.174842E-07
284.375	0.612014E-05	2.49023	0.138120E-07	1.41531	0.195483E-07
283.750	0.592501E-05	2.45768	0.135488E-07	1.55684	0.210932E-07
283.125	0.573520E-05	2.44141	0.132022E-07	1.55684	0.205536E-07
282.500	0.555054E-05	2.39258	0.130378E-07	1.41531	0.184526E-07
281.875	0.537094E-05	2.36003	0.127900E-07	1.41531	0.181018E-07
281.250	0.519629E-05	2.31120	0.126355E-07	1.27378	0.160948E-07
280.625	0.502648E-05	2.29492	0.123093E-07	1.13225	0.139371E-07
280.000	0.486138E-05	2.21354	0.123427E-07	0.990716	0.122281E-07
279.375	0.470094E-05	2.19727	0.120237E-07	0.707654	0.850862E-08
278.750	0.454499E-05	2.16471	0.117997E-07	0.707654	0.835007E-08
278.125	0.439348E-05	2.09961	0.117600E-07	0.707654	0.832199E-08
277.500	0.424627E-05	2.08333	0.114547E-07	0.707654	0.810599E-08
276.875	0.410329E-05	2.06706	0.111562E-07	0.424592	0.473684E-08
276.250	0.396442E-05	2.03451	0.109511E-07	0.566123	0.619967E-08
275.625	0.382959E-05	1.96940	0.109283E-07	0.566123	0.618678E-08

TABLE 3-4 - (cont'd)

WAVELENGTH (NANOMETERS)	STANDARD LAMP RADIANCE (WATTS/CM**3-SR)	CALIBRATION DATA-AVERAGED (MICROAMPS)	SENSITIVITY (WATTS/NM-SR PER MICROAMP)	CORRECTED CORONA DATA (MICROAMPS)	CORONA INTENSITY (WATTS/NM-SR)
275.000	0.369867E-05	1.93685	0.107321E-07	0.566123	0.607571E-08
274.375	0.357159E-05	1.93685	0.103634E-07	0.707654	0.733369E-08
273.750	0.344826E-05	1.87174	0.100819E-07	0.707654	0.732674E-08
273.125	0.332857E-05	1.85547	0.973016E-08	0.849185	0.856136E-08
272.500	0.321246E-05	1.85547	0.955669E-08	0.707654	0.688558E-08
271.875	0.309983E-05	1.82292	0.938756E-08	0.707654	0.676283E-08
271.250	0.299060E-05	1.79036	0.930894E-08	0.849185	0.797177E-08
270.625	0.288467E-05	1.74154	0.889443E-08	0.707654	0.656751E-08
270.000	0.278198E-05	1.75781	0.865631E-08	0.566123	0.503534E-08
269.375	0.268243E-05	1.74154	0.826773E-08	0.707654	0.612567E-08
268.750	0.258596E-05	1.75781	0.811918E-08	0.849185	0.689469E-08
268.125	0.249247E-05	1.72526	0.767929E-08	0.707654	0.543428E-08
267.500	0.240191E-05	1.75781	0.739880E-08	0.849185	0.628295E-08
266.875	0.231418E-05	1.75781	0.726167E-08	0.707654	0.513875E-08
266.250	0.222923E-05	1.72526	0.712818E-08	0.707654	0.504429E-08
265.625	0.214696E-05	1.69271	0.728401E-08	0.283062	0.206182E-08
265.000	0.206733E-05	1.50505	0.746977E-08	0.424592	0.317161E-08
264.375	0.199025E-05	1.49740	0.760300E-08	0.283062	0.215212E-08
263.750	0.191565E-05	1.41602	0.776271E-08	0.424592	0.329599E-08
263.125	0.184349E-05	1.33464	0.735910E-08	0.438745	0.322877E-08
265.000	0.206733E-05	1.57878	0.753136E-08	0.396286	0.298457E-08
264.688	0.202847E-05	1.51367	0.763576E-08	0.396286	0.302595E-08
264.375	0.199025E-05	1.46484	0.783955E-08	0.367980	0.288494E-08
264.063	0.195265E-05	1.39974	0.816618E-08	0.382133	0.312057E-08
263.750	0.191565E-05	1.31836	0.821390E-08	0.367980	0.302255E-08
263.438	0.187927E-05	1.28581	0.837536E-08	0.353827	0.296350E-08
263.125	0.184349E-05	1.23698	0.867205E-08	0.353827	0.306841E-08
262.813	0.180829E-05	1.17187	0.887587E-08	0.367980	0.326614E-08
262.500	0.177367E-05	1.12305	0.938565E-08	0.367980	0.345373E-08
262.188	0.173963E-05	1.04167	0.101050E-07	0.382133	0.386145E-08
261.875	0.170615E-05	0.948893	0.106597E-07	0.396286	0.422429E-08
261.563	0.167323E-05	0.882161	0.115364E-07	0.438745	0.508350E-08
261.250	0.164086E-05	0.795698	0.125415E-07	0.452899	0.568002E-08
260.938	0.160904E-05	0.721029	0.133525E-07	0.481205	0.642529E-08
260.625	0.157774E-05	0.664062	0.143591E-07	0.509511	0.731612E-08
263.313	0.154697E-05	0.605469	0.154946E-07	0.537817	0.833324E-08
260.000	0.151673E-05	0.558130	0.161972E-07	0.566123	0.916959E-08
259.688	0.148700E-05	0.515951	0.167786E-07	0.594429	0.997369E-08
259.375	0.145777E-05	0.488281	0.171930E-07	0.608582	0.104633E-07
259.063	0.142904E-05	0.467122			

TABLE 3-4 - (cont'd)

WAVELENGTH (NANOMETERS)	STANDARD LAMP RADIANCE (WATTS/CM^3-SR)	CALIBRATION DATA-AVERAGED (MICROAMPS)	SENSITIVITY (WATTS/NM-SR PER MICROAMP)	CORRECTED CORONA DATA (MICROAMPS)	CORONA INTENSITY (WATTS/NM-SR)
258.750	0.140081E-05	0.449219	0.175249E-07	0.608582	0.106654E-07
258.438	0.137305E-05	0.431315	0.178908E-07	0.636889	0.113944E-07
258.125	0.134578E-05	0.421549	0.179416E-07	0.636889	0.114268E-07
257.812	0.131897E-05	0.415039	0.178600E-07	0.651042	0.116276E-07
257.500	0.129263E-05	0.411784	0.176417E-07	0.665195	0.117352E-07
257.188	0.126674E-05	0.398763	0.178530E-07	0.651042	0.116230E-07
256.875	0.124131E-05	0.392253	0.177849E-07	0.651042	0.115787E-07
256.563	0.121632E-05	0.382487	0.178718E-07	0.636889	0.113824E-07
256.250	0.119177E-05	0.379272	0.176613E-07	0.636889	0.112483E-07
255.938	0.116765E-05	0.372121	0.176061E-07	0.622736	0.109639E-07
255.625	0.114395E-05	0.372121	0.172488E-07	0.622736	0.107415E-07
255.313	0.112067E-05	0.359701	0.175095E-07	0.594429	0.104082E-07
255.000	0.109781E-05	0.361328	0.170750E-07	0.594429	0.101499E-07
254.688	0.107535E-05	0.351562	0.171903E-07	0.551970	0.948852E-08
254.375	0.105329E-05	0.351562	0.168377E-07	0.537817	0.905558E-08
254.062	0.103163E-05	0.346680	0.167236E-07	0.495358	0.828417E-08
253.750	0.101035E-05	0.343424	0.165339E-07	0.481205	0.795620E-08
253.438	0.989453E-06	0.340169	0.163469E-07	0.467052	0.763486E-08
253.125	0.968936E-06	0.338542	0.160849E-07	0.438745	0.705719E-08
252.813	0.948708E-06	0.330404	0.161384E-07	0.424592	0.685225E-08
252.500	0.929008E-06	0.332031	0.157245E-07	0.367980	0.578631E-08
252.188	0.909589E-06	0.325521	0.157037E-07	0.353827	0.555640E-08
251.875	0.890522E-06	0.327148	0.152981E-07	0.339674	0.519635E-08
251.563	0.871803E-06	0.319010	0.153585E-07	0.325521	0.499952E-08
251.250	0.853430E-06	0.319010	0.150349E-07	0.353827	0.531974E-08
250.938	0.835393E-06	0.307617	0.152622E-07	0.367980	0.561617E-08
250.625	0.817690E-06	0.312500	0.147053E-07	0.367980	0.541127E-08
250.313	0.800315E-06	0.305990	0.146991E-07	0.396286	0.582505E-08
250.000	0.783265E-06	0.304362	0.144629E-07	0.452899	0.655022E-08
249.688	0.766529E-06	0.302734	0.142299E-07	0.481205	0.684751E-08
249.375	0.750108E-06	0.304362	0.138506E-07	0.509511	0.705705E-08
249.063	0.733994E-06	0.294596	0.140024E-07	0.566123	0.792707E-08
248.750	0.718184E-06	0.296224	0.136255E-07	0.608582	0.829223E-08
248.438	0.702670E-06	0.289714	0.136307E-07	0.665195	0.906709E-08
248.125	0.687452E-06	0.289714	0.133355E-07	0.721807	0.962567E-08
247.813	0.672520E-06	0.286458	0.131941E-07	0.792572	0.104573E-07
247.500	0.657874E-06	0.280086	0.128338E-07	0.835032	0.107167E-07
247.188	0.643507E-06	0.283203	0.127700E-07	0.877491	0.112056E-07
246.875	0.629415E-06	0.281703	0.124904E-07	0.891644	0.111370E-07
246.563	0.615593E-06	0.281703	0.122161E-07	0.891644	0.108924E-07

TABLE 3-4 - (cont'd)

WAVELENGTH (NANOMETERS)	STANDARD LAMP RADIANCE (WATTS/CM^3-SR)	CALIBRATION DATA-AVERAGED (MICROAMPS)	SENSITIVITY (WATTS/NM-SR PER MICROAMP)	CORRECTED CORONA DATA (MICROAMPS)	CORONA INTENSITY (WATTS/NM-SR)
246.250	0.602039E-06	0.2[illegible]7	0.123738E-07	0.[illegible]	0.108579E-07
245.938	0.588744E-06	0.2[illegible]3	0.119582E-07	0.[illegible]	0.101547E-07
245.625	0.575709E-06	0.2[illegible]5	0.120478E-07	0.[illegible]	0.107423E-07
245.313	0.562925E-06	0.2[illegible]4	0.120726E-07	0.[illegible]	0.102521E-07
245.000	0.550394E-06	0.2[illegible]9	0.116593E-07	0.[illegible]	0.973590E-08
244.688	0.538104E-06	0.2[illegible]7	0.116127E-07	0.[illegible]	0.920392E-08
244.375	0.526057E-06	0.2[illegible]2	0.112126E-07	0.[illegible]	0.825201E-08
244.063	0.514247E-06	0.2[illegible]6	0.113824E-07	0.[illegible]	0.773263E-08
243.750	0.502668E-06	0.2[illegible]1	0.109853E-07	0.[illegible]	0.668546E-08
243.438	0.491320E-06	0.2[illegible]9	0.106698E-07	0.[illegible]	0.588939E-08
243.125	0.480198E-06	0.2[illegible]1	0.104942E-07	0.[illegible]	0.564397E-08
242.813	0.469296E-06	0.2[illegible]6	0.106608E-07	0.[illegible]	0.497916E-08
242.500	0.458611E-06	0.2[illegible]3	0.103500E-07	0.[illegible]	0.468750E-08
242.187	0.448142E-06	0.2[illegible]1	0.100481E-07	0.[illegible]	0.426633E-08
241.875	0.437881E-06	0.2[illegible]8	0.100131E-07	0.[illegible]	0.382632E-08
241.563	0.427828E-06	0.2[illegible]3	0.965530E-08	0.[illegible]	0.341631E-08
241.250	0.417978E-06	0.2[illegible]1	0.962166E-08	0.[illegible]	0.326823E-08
240.938	0.408328E-06	0.2[illegible].3	0.946261E-08	0.[illegible]	0.308028E-08
240.625	0.398874E-06	0.2[illegible].3	0.924351E-08	0.[illegible]	0.300896E-08
240.313	0.389615E-06	0.2[illegible]5	0.908994E-08	0.[illegible]	0.347357E-08
240.000	0.380544E-06	0.2[illegible]3	0.906200E-08	0.[illegible]	0.397591E-08
239.688	0.371657E-06	0.23[illegible]3	0.885038E-08	0.[illegible]	0.425885E-08
239.375	0.362955E-06	0.239258	0.852556E-08	0.[illegible]	0.470585E-08
239.063	0.354433E-06	0.229492	0.867964E-08	0.[illegible]	0.540512E-08
238.750	0.346087E-06	0.229492	0.847526E-08	0.[illegible]	0.599756E-08
238.438	0.337914E-06	0.227865	0.833423E-08	0.[illegible]	0.648753E-08
238.125	0.329912E-06	0.231120	0.802226E-08	0.863338	0.692592E-08
237.813	0.322077E-06	0.224609	0.805876E-08	0.919950	0.741366E-08
237.500	0.314407E-06	0.227865	0.775446E-08	1.03317	0.801171E-08
237.188	0.306898E-06	0.226237	0.762372E-08	1.07563	0.820033E-08
236.875	0.299546E-06	0.226237	0.744110E-08	1.13225	0.842515E-08
236.563	0.292352E-06	0.226237	0.726237E-08	1.16055	0.842836E-08
236.250	0.285309E-06	0.221354	0.724376E-08	1.16055	0.840677E-08
235.938	0.278417E-06	0.219727	0.712114E-08	1.17471	0.836524E-08
235.625	0.271672E-06	0.222982	0.684717E-08	1.13225	0.775269E-08
235.313	0.265071E-06	0.216471	0.688175E-08	1.07563	0.740224E-08
235.000	0.258613E-06	0.219727	0.661461E-08	1.03317	0.683404E-08
234.688	0.252293E-06	0.219727	0.645296E-08	0.962409	0.621039E-08
234.375	0.246110E-06	0.216471	0.638949E-08	0.849185	0.542585E-08
234.063	0.240062E-06	0.214844	0.627967E-08	0.778419	0.488822E-08

TABLE 3-4 - (cont'd)

WAVELENGTH (NANOMETERS)	STANDARD LAMP RADIANCE (WATTS/CM^3-SR)	CALIBRATION DATA-AVERAGED (MICROAMPS)	SENSITIVITY (WATTS/NM-SR PER MICROAMP)	CORRECTED CORONA DATA (MICROAMPS)	CORONA INTENSITY (WATTS/NM-SR)
233.750	1.234145E-06	0.211589	0.621912E-08	0.693501	0.431296E-08
233.438	0.228357E-06	0.211589	0.606538E-08	0.622736	0.377713E-08
233.125	0.222696E-06	0.211589	0.591503E-08	0.566123	0.334864E-08
232.813	0.217160E-06	0.211589	0.576798E-08	0.467052	0.269394E-08
232.500	0.211745E-06	0.211589	0.562416E-08	0.438745	0.246758E-08
232.188	0.206450E-06	0.208333	0.556919E-08	0.396286	0.220699E-08
231.875	0.201273E-06	0.209961	0.538745E-08	0.353827	0.190623E-08
231.563	0.196211E-06	0.209961	0.525196E-08	0.325521	0.170962E-08
231.250	0.191262E-06	0.211589	0.508810E-08	0.325521	0.165368E-08
230.938	0.186423E-06	0.208333	0.502894E-08	0.297215	0.149467E-08
230.625	0.181694E-06	0.209961	0.486337E-08	0.297215	0.144547E-08
230.313	0.177070E-06	0.208333	0.477665E-08	0.325521	0.155490E-08
230.000	0.172551E-06	0.206706	0.469140E-08	0.396286	0.185914E-08
229.688	0.168135E-06	0.203451	0.464447E-08	0.424592	0.197201E-08
229.375	0.163819E-06	0.201823	0.456174E-08	0.467052	0.213057E-08
229.063	0.159602E-06	0.201823	0.444431E-08	0.523664	0.232732E-08
228.750	0.155481E-06	0.205078	0.426084E-08	0.566123	0.241216E-08
228.438	0.151455E-06	0.203451	0.418370E-08	0.594429	0.248691E-08
228.125	0.147522E-06	0.201823	0.410792E-08	0.651042	0.267443E-08
227.813	0.143679E-06	0.200195	0.403343E-08	0.707654	0.285437E-08
227.500	0.139925E-06	0.203451	0.386522E-08	0.764266	0.295405E-08
227.188	0.136259E-06	0.200195	0.382513E-08	0.778419	0.297756E-08
226.875	0.132678E-06	0.203451	0.366503E-08	0.820879	0.300854E-08
226.562	0.129181E-06	0.195312	0.371711E-08	0.835032	0.310390E-08
226.250	0.125766E-06	0.200195	0.353059E-08	0.835032	0.294815E-08
225.938	0.122432E-06	0.198568	0.346516E-08	0.820879	0.284447E-08
225.625	0.119176E-06	0.198568	0.337301E-08	0.792572	0.267336E-08
225.313	0.115997E-06	0.198568	0.328304E-08	0.764266	0.250912E-08
225.000	0.112895E-06	0.195312	0.324848E-08	0.735960	0.239075E-08
224.688	0.109866E-06	0.193685	0.318789E-08	0.707654	0.225592E-08
224.375	0.106909E-06	0.198568	0.302581E-08	0.651042	0.196993E-08
224.063	0.104024E-06	0.195312	0.299322E-08	0.608582	0.182162E-08
223.750	0.101208E-06	0.198568	0.286446E-08	0.551970	0.158109E-08
223.438	0.984559E-07	0.195312	0.283313E-08	0.495358	0.140341E-08
223.125	0.957785E-07	0.195312	0.275597E-08	0.467052	0.128718E-08
222.813	0.931624E-07	0.196940	0.265854E-08	0.382133	0.101592E-08
222.500	0.906101E-07	0.192057	0.265144E-08	0.382133	0.101320E-08
222.188	0.881203E-07	0.200195	0.247376E-08	0.840273E-09	0.840273E-09
221.875	0.856916E-07	0.200195	0.240559E-08	0.339674	0.817114E-09
221.563	0.833225E-07	0.201823	0.232021E-08	0.311368	0.722440E-09

TABLE 3-4 - (cont'd)

WAVELENGTH (NANOMETERS)	STANDARD LAMP RADIANCE (WATTS/CM^3-SR)	CALIBRATION DATA-AVERAGED (MICROAMPS)	SENSITIVITY (WATTS/NM-SR PER MICROAMP)	CORRECTED CORONA DATA (MICROAMPS)	CORONA INTENSITY (WATTS/NM-SR)
221.250	0.810123E-07	0.1	0.233177E-08	0.297215	0.[illegible]E-09
220.938	0.787594E-07	0.1	0.2266[illegible]E-08	0.297215	0.[illegible]E-09
220.625	0.765623E-07	0.1	0.2203[illegible]E-08	0.254755	0.[illegible]E-09
220.313	0.744201E-07	0.2	0.2072[illegible]E-08	0.268909	0.[illegible]E-09
220.000	0.723315E-07	0.1	0.2098[illegible]E-08	0.268909	0.[illegible]E-09
219.688	0.702953E-07	0.1	0.2022[illegible]E-08	0.268909	0.[illegible]E-09
219.375	0.683104E-07	0.1	0.2015[illegible]E-08	0.254755	0.[illegible]E-09
219.063	0.663758E-07	0.1	0.1909[illegible]E-08	0.283062	0.[illegible]E-09
218.750	0.644903E-07	0.1	0.1903[illegible]E-08	0.297215	0.[illegible]E-09
218.438	0.626526E-07	0.1	0.1817[illegible]E-08	0.311368	0.[illegible]E-09
218.125	0.608619E-07	0.1	0.1722[illegible]E-08	0.311368	0.[illegible]E-09
217.813	0.591171E-07	0.1	0.1720[illegible]E-08	0.353827	0.[illegible]E-09
217.500	0.574172E-07	0.1	0.1694[illegible]E-08	0.339674	0.[illegible]E-09
217.188	0.557609E-07	0.1	0.1578[illegible]E-08	0.367980	0.[illegible]E-09
216.875	0.541477E-07	0.1	0.1571[illegible]E-08	0.410439	0.[illegible]E-09
216.563	0.525762E-07	0.1	0.1565[illegible]E-08	0.424592	0.[illegible]E-09
216.250	0.510458E-07	0.1	0.1481[illegible]E-08	0.424592	0.[illegible]E-09
215.938	0.495551E-07	0.1	0.1425[illegible]E-08	0.438745	0.[illegible]E-09
215.625	0.481037E-07	0.1	0.1407[illegible]E-08	0.438745	0.[illegible]E-09
215.313	0.466902E-07	0.1	0.1366[illegible]E-08	0.452899	0.[illegible]E-09
215.000	0.453141E-07	0.1	0.1303[illegible]E-08	0.424592	0.[illegible]E-09
214.688	0.439746E-07	0.1	0.1297[illegible]E-08	0.438745	0.[illegible]E-09
214.375	0.426706E-07	0.1	0.1270[illegible]E-08	0.410439	0.[illegible]E-09
214.063	0.414013E-07	0.1	0.1221[illegible]E-08	0.396286	0.[illegible]E-09
213.750	0.401660E-07	0.1	0.1[illegible]E-08	0.367980	0.[illegible]E-09
213.438	0.389638E-07	0.1	0.1[illegible]E-08	0.353827	0.[illegible]E-09
213.125	0.377939E-07	0.1	0.1[illegible]E-08	0.339674	0.[illegible]E-09
212.813	0.366557E-07	0.1	0.1[illegible]E-08	0.311368	0.[illegible]E-09
212.500	0.355481E-07	0.1	0.1[illegible]E-08	0.297215	0.[illegible]E-09
212.188	0.344707E-07	0.1	0.1[illegible]E-08	0.283062	0.[illegible]E-09
211.875	0.334229E-07	0.1	0.9[illegible]E-09	0.268909	0.[illegible]E-09
211.563	0.324037E-07	0.1	0.9[illegible]E-09	0.240602	0.[illegible]E-09
211.250	0.314123E-07	0.1	0.9[illegible]E-09	0.240602	0.[illegible]E-09
210.937	0.304483E-07	0.1	0.8[illegible]E-09	0.240602	0.[illegible]E-09
210.625	0.295109E-07	0.1	0.8[illegible]E-09	0.212296	0.[illegible]E-09
210.313	0.285995E-07	0.1	0.8[illegible]E-09	0.212296	0.[illegible]E-09
210.000	0.277136E-07	0.1	0.8[illegible]E-09	0.212296	0.[illegible]E-09
209.688	0.268523E-07	0.1	0.7[illegible]E-09	0.212296	0.[illegible]E-09
209.375	0.260152E-07	0.1	0.7[illegible]E-09	0.212296	0.[illegible]E-09
209.063	0.252017E-07	0.1	0.7[illegible]E-09	0.183990	0.[illegible]E-09

TABLE 3-4 - (cont'd)

WAVELENGTH (NANOMETERS)	STANDARD LAMP RADIANCE (WATTS/CM^3-SR)	CALIBRATION DATA-AVERAGED (MICROAMPS)	SENSITIVITY (WATTS/NM-SR PER MICROAMP)	CORRECTED CORONA DATA (MICROAMPS)	CORONA INTENSITY (WATTS/NM-SR)
208.750	0.244110E-07	0.192057	0.7143[illegible]-09	0.198143	0.141537E-09
208.438	0.236427E-07	0.190430	0.6977[illegible]-09	0.212296	0.148129E-09
208.125	0.228963E-07	0.193685	0.6643[illegible]-09	0.212296	0.141042E-09
207.813	0.221710E-07	0.185547	0.6715[illegible]-09	0.212296	0.142564E-09
207.500	0.214666E-07	0.190430	0.6335 -09	0.212296	0.134495E-09
207.188	0.207824E-07	0.190430	0.6133 -09	0.226445	0.138889E-09
206.875	0.201178E-07	0.190430	0.5937 -09	0.212296	0.126045E-09
206.563	0.194725E-07	0.192057	0.5698 -09	0.226445	0.129053E-09
206.250	0.188458E-07	0.192057	0.5514 -09	0.240602	0.132685E-09
205.938	0.182373E-07	0.187174	0.5475 -09	0.240602	0.131750E-09
205.625	0.176467E-07	0.188802	0.5252 -09	0.254755	0.133818E-09
205.313	0.170733E-07	0.190430	0.5038 -09	0.240602	0.121232E-09
205.000	0.165167E-07	0.188802	0.4916 -09	0.240602	0.118292E-09
204.688	0.159766E-07	0.187174	0.4797 -09	0.240602	0.115418E-09
204.375	0.154525E-07	0.187174	0.4639 -09	0.226445	0.105065E-09
204.063	0.149439E-07	0.192057	0.4372 -09	0.240602	0.105213E-09
203.750	0.144504E-07	0.192057	0.4228 -09	0.226449	0.957[illegible]E-10
203.438	0.139717E-07	0.187174	0.4195 -09	0.212296	0.890[illegible]E-10
203.125	0.135073E-07	0.190430	0. -09	0.212296	0.846[illegible]E-10
202.813	0.130570E-07	0.190430	0. -09	0.212296	0.818[illegible]E-10
202.500	0.126202E-07	0.190430	0. -09	0.212296	0.790[illegible]E-10
202.188	0.121967E-07	0.193685	0. -09	0.198143	0.701[illegible]E-10
201.875	0.117860E-07	0.185547	0. -09	0.198143	0.707[illegible]E-10
201.563	0.113879E-07	0.182292	0. -09	0.169837	0.596[illegible]E-10
201.250	0.110019E-07	0.183919	0. -09	0.169837	0.570[illegible]E-10
200.938	0.106279E-07	0.188802	0. -09	0.169837	0.537[illegible]E-10
200.625	0.102653E-07	0.187174	0. -09	0.155684	0.479650E-10
200.313	0.991397E-08	0.187174	0. -09	0.155684	0.463427E-10
200.000	0.957357E-08	0.190430	0. -09	0.424592E-01	0.119963E-10
199.688	0.924378E-08	0.183919	0. -09	0.424592E-01	0.[illegible]E-10
199.375	0.892435E-08	0.190430	0. -09	0.[illegible]E-01	0.[illegible]E-10
199.063	0.861478E-08	0.188802	0. -09	0.566123E-01	0.145173E-10
198.750	0.831503E-08	0.188802	0.4475 -09	0.424592E-01	0.105091E-10
198.438	0.802477E-08	0.188802	0.2388 -09	0.424592E-01	0.101423E-10
198.125	0.774372E-08	0.183919	0.2266 -09	0.424592E-01	0.100469E-10
197.813	0.747158E-08	0.188802	0.2224 -09	0.424592E-01	0.944309E-11
197.500	0.720818E-08				

4.0 UV CORONA EMISSION MEASUREMENTS.

In this section the spectral intensity data are presented for corona discharge processes operating over a wide range of pressure, electrode gaps and voltage. Data are presented for corona discharges principally in air, since most coronas encountered in thermal vacuum testing are air coronas. Data obtained from a limited number of runs in helium are included, mainly to point out significant differences between these corona spectra and those obtained in air. The overwhelming majority of the corona spectra were measured for a positive point and negative plane electrode with applied DC voltages. No AC corona data were obtained due to scheduling constraints. A few spectral runs were made with reversed DC polarity to uncover any differences in these intensity spectra when compared to the positive-point corona data. The 304 stainless steel electrodes were used for all spectral scans obtained in this study. The surface condition of the steel electrodes was monitored visually in the course of this study to insure that obvious surface damage did not occur. Similarly, operation of the corona simulator in the spark breakdown regime was avoided to minimize heating of the electrodes. The effects of electrode surface conditioning and of corona triggering via external sources such as UV photons or gamma radiation were not part of this study.

In the next two sections, the data obtained from approximately fifty spectroradiometer scans are presented in a condensed format. Section 4.2 concentrates on the spectral characteristics of corona discharges operating at the extremes of current, voltage, pressure, gap length and anode radius. Section 4.3 presents tabular and graphical condensations of the complete range of spectral intensity data.

4.1 UV CORONA SPECTRAL INTENSITY PLOTS. The spectral features of the air corona intensity scans showed little significant variation due to changes in the operating parameters of the corona simulator. The relatively low spectral resolution due to the 2mm spectrometer entrance slit revealed a combined band structure due to overlapping oxygen and nitrogen emission spectra. However, as expected, the spectral intensity showed pronounced dependence on the corona simulator operating conditions. To eliminate needless repetition of spectral scans showing essentially the same band structure, a selected few corona

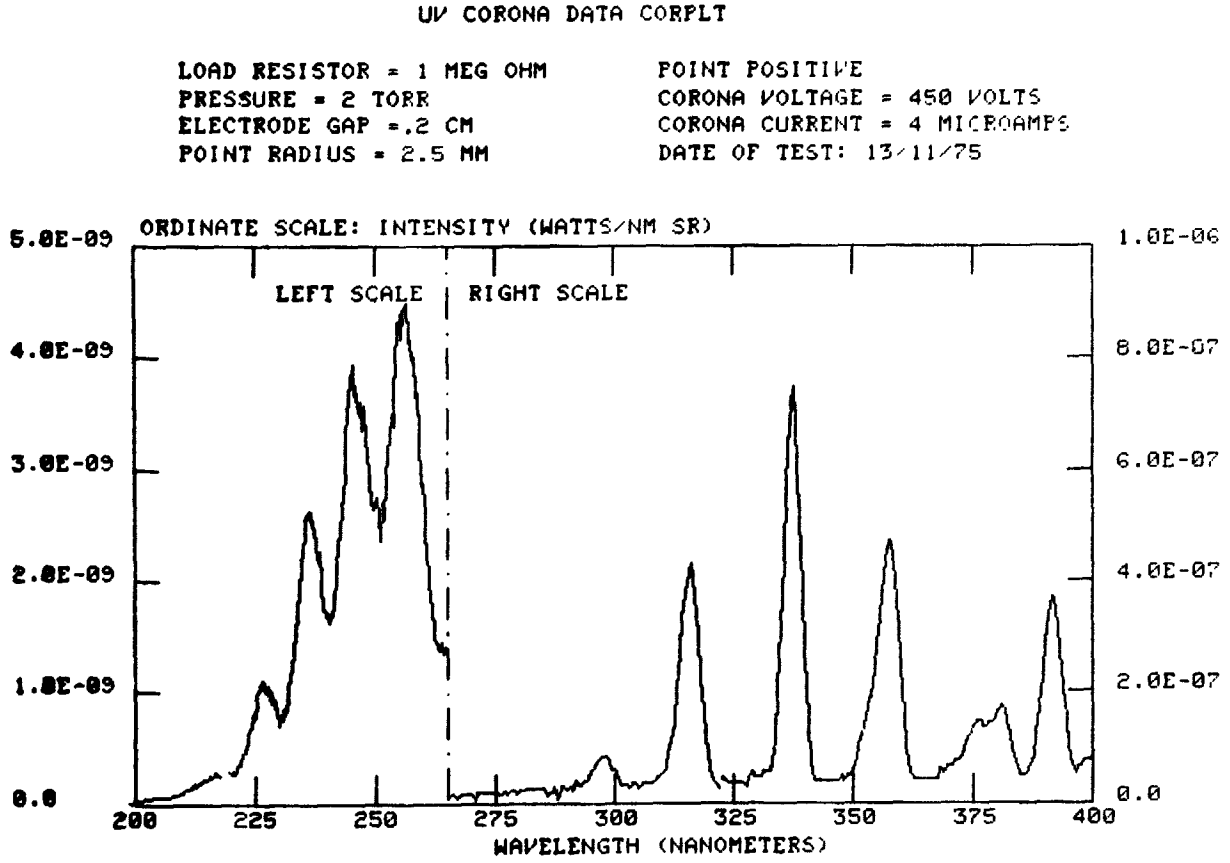

FIGURE 4-1 CORONA SPECTRAL INTENSITY - CURRENT = 4μa

intensity spectra are included in this section. These spectra were chosen to display the data obtained at the extremes of the operating conditions of the corona simulator used in this study. As such, these spectra typify those due both to threshold corona conditions prior to onset of the steady glow and to conditions immediately prior to the formation of a spark discharge.

Figures 4.1 and 4.2 show data taken at extremes of corona current, i.e. 4μa and 375μa, respectively. The significant difference lies in the approximately factor of ten increase in spectral intensity due to the increase in corona current. Intuitively, spectral intensity is expected to be strongly correlated with the current since the UV emission phenomenon arises mainly due to ionization and excitation processes from electron-gas molecule collisions. Similarly, increased UV photon emission results in photoionization processes in the gas, thus increasing the current (electrons) in the corona discharge. The photo-

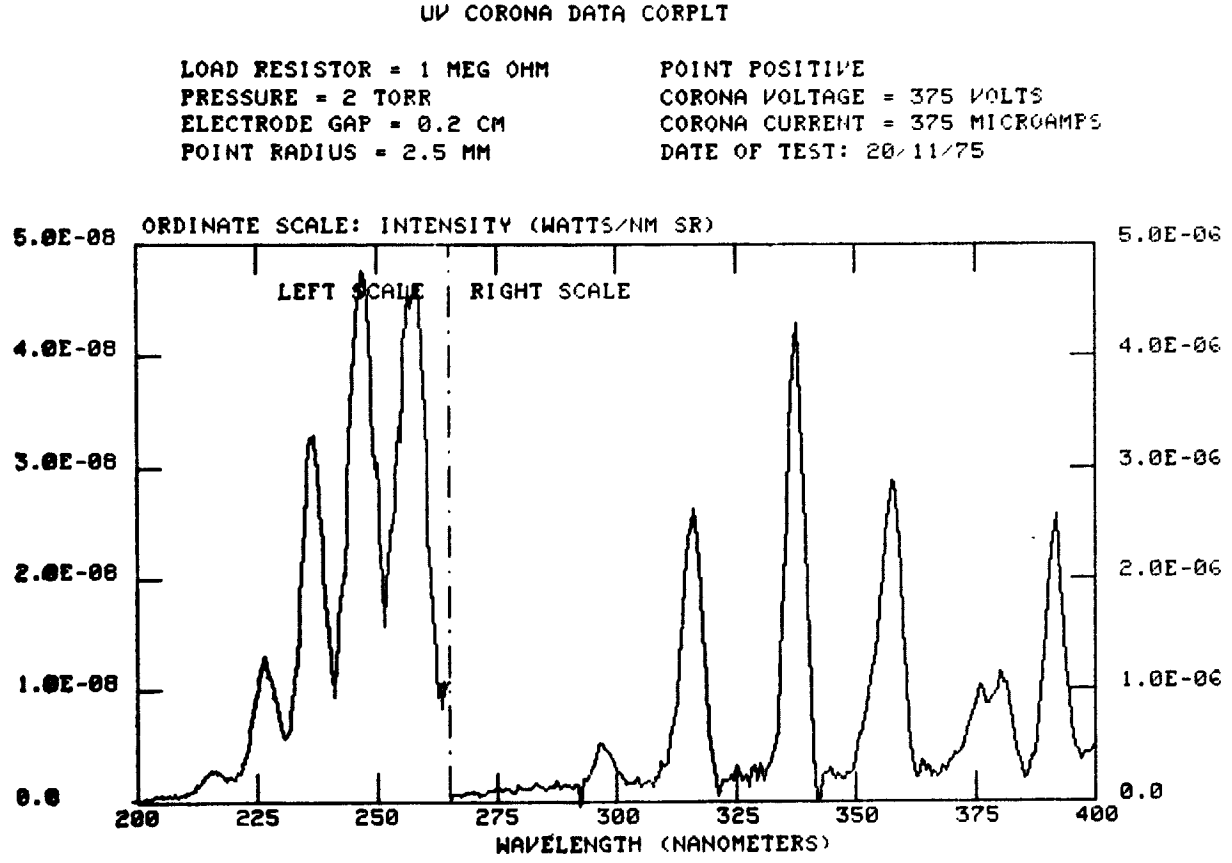

FIGURE 4-2 CORONA SPECTRAL INTENSITY - CURRENT 375μa

ionization process is enchanced by the presence of readily photoionized species, such as water vapor (which is certainly present in the bleed air admitted into the corona simulator). The corona of Run 28A (4μa current) was typical of an unsteady glow and required a slow spectroradiometer scan to smooth the fluctuations in the recorded spectrum due to the unsteady emission process.

The spectra of Figures 4.3 and 4.4 show characterics due to extremes in electrode gap length, i.e. 2mm and 6mm, respectively. As the other parameters were held constant, the intensity in the 200-400nm waveband decreased as the gap length increased. The principal effect of the increased gap length is a reduction of the average electric field gradient in the space between the electrodes. Consequently, a slight, but as yet unanalyzed, dependency of spectral intensity on electric field gradient is indicated by the data of Figures 4.3 and 4.4. Other data, however, (cf. Runs 23C and 25D in Section 4.2) show almost no dependence of spectral intensity on gap length. The conclusion is that gap length has

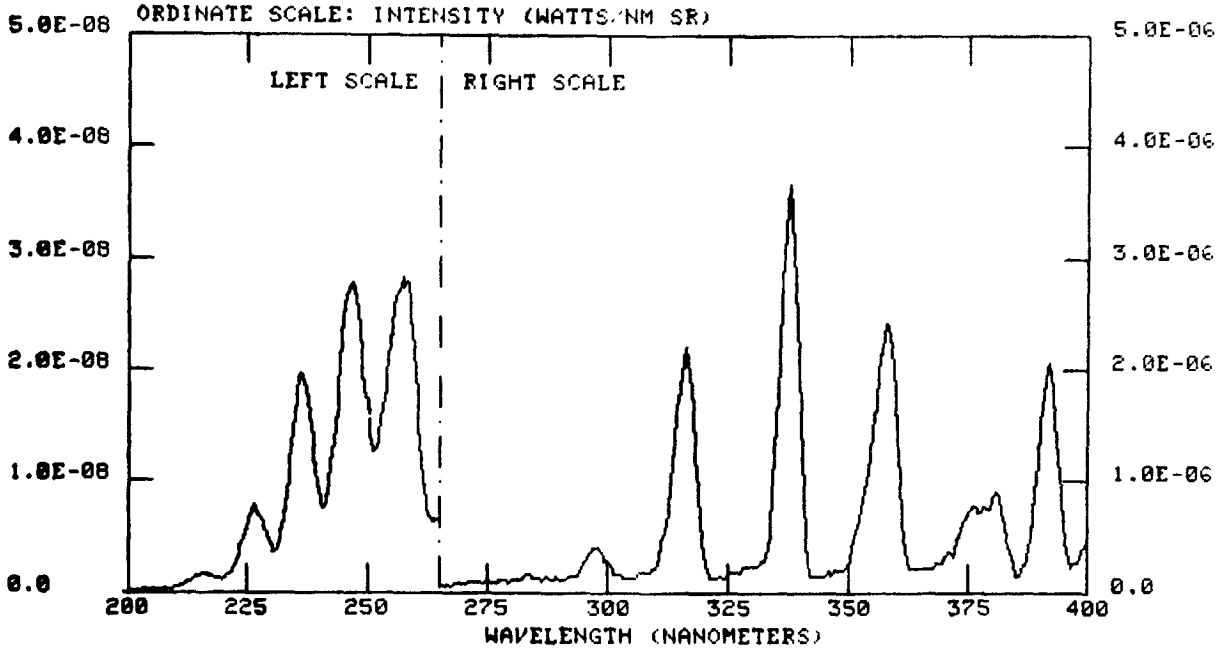

FIGURE 4-3 CORONA SPECTRAL INTENSITY - GAP = 2mm

little influence on the magnitude of corona spectral intensity, at least for the range of gap lengths employed in this study. Gaps greater than 6mm in length were not employed in this study to insure that the corona glow remained completely within the spectrometer field of view. Likewise, the small range of gap lengths used in this study effectively confined the corona glow to the region between the electrodes. Such localized corona glows represent UV emitting sources which likely present severe challenges to all feasible corona detection systems. Similarly, gaps less than 2mm in length gave rise to corona glows which were difficult to control due to the tendency for the glow to change unexpectedly into a spark discharge. The strong UV emissions from the spark discharge are expected to be relatively easy to detect, and, as such, present no real challenge to most candidate corona detection systems.

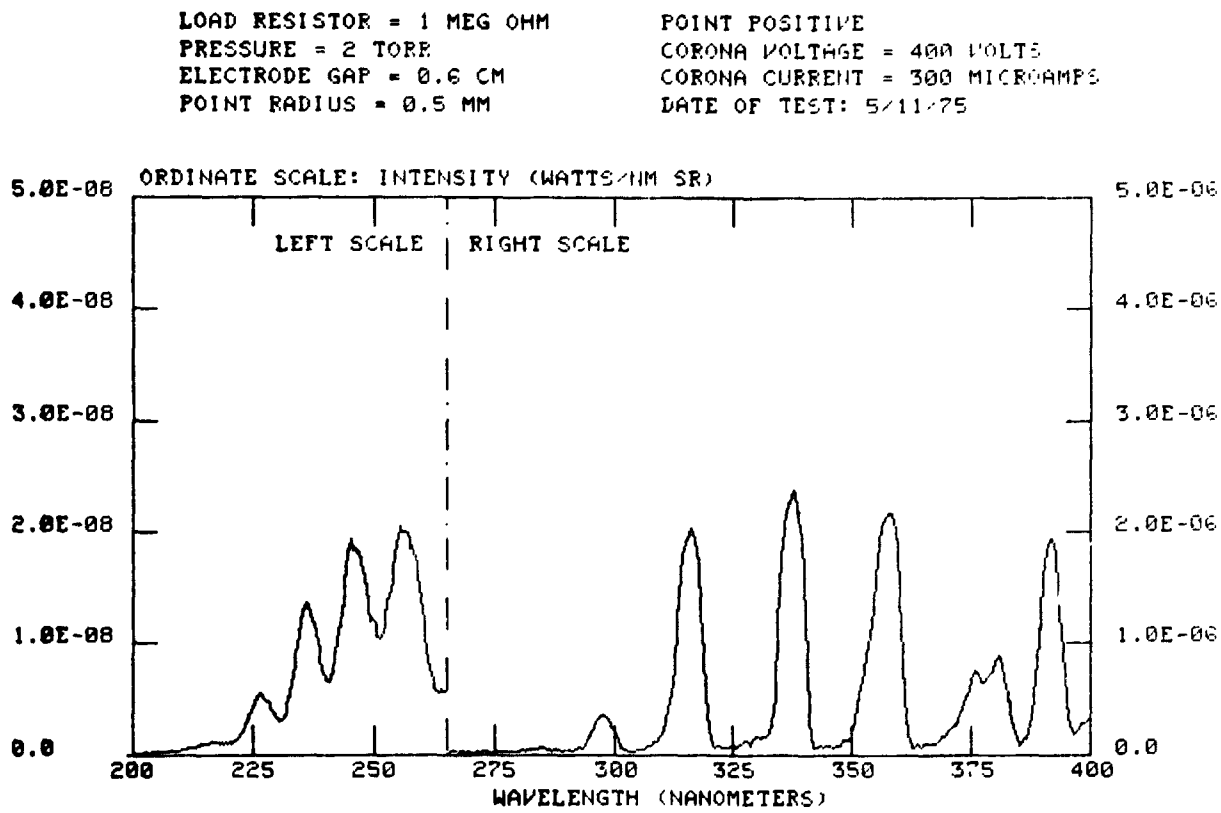

FIGURE 4-4 CORONA SPECTRAL INTENSITY - GAP 6mm

Figures 4.5 and 4.6 show spectral intensity data due to extremes in pressure, 2 torr and 20 torr, respectively. For these scans in which the corona current was 300μa, no significant difference in the intensity spectra was apparent. This behavior was generally observed throughout this program, viz, the intensity spectra at constant corona current was effectively independent of pressure in the 2 to 20 torr range.

The effects of the anode electrode radius are indicated in Figures 4-7 and 4-8 (radius equal to 0.5mm and 2.5mm, respectively). Again, for nearly constant corona current, the effect of anode radius on the intensity spectrum is minimal.

The principal conclusion of this spectroradiometer data summary is that the spectral intensity of the UV corona emissions is most nearly correlated with corona current.

LOAD RESISTOR = 1 MEG OHM
PRESSURE = 2 TORR
ELECTRODE GAP = 0.2 CM
POINT RADIUS = 0.5 MM

POINT POSITIVE
CORONA VOLTAGE = 420 VOLTS
CORONA CURRENT = 180 MICROAMPS
DATE OF TEST: 11/11/75

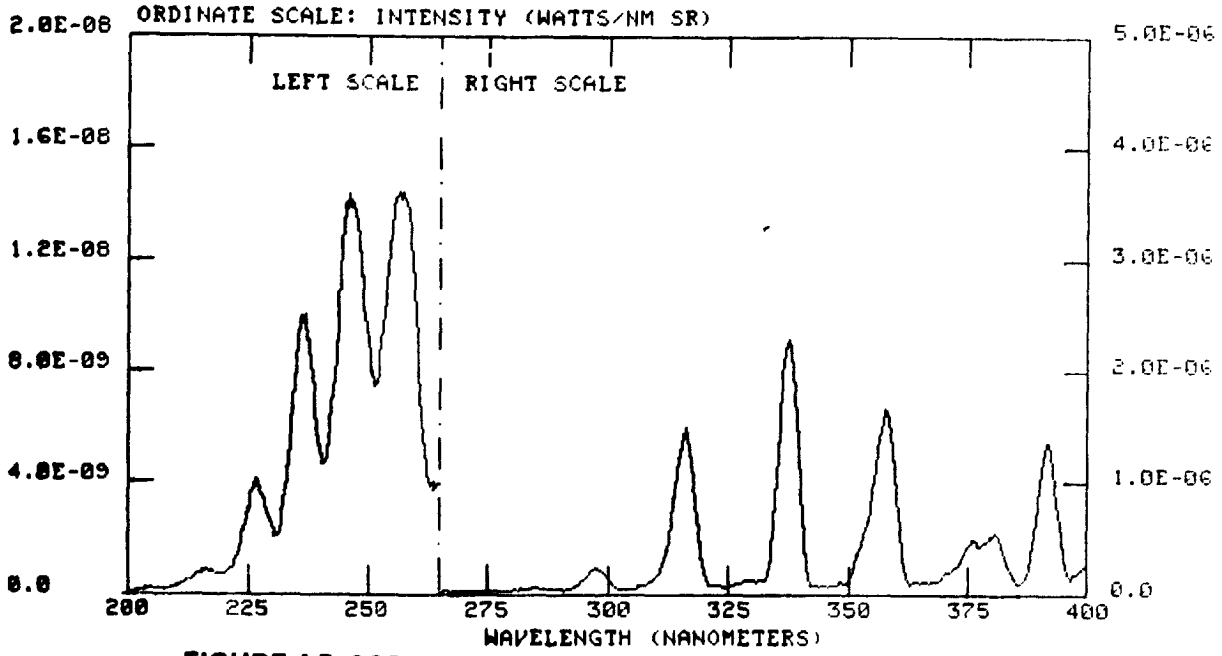

FIGURE 4-5 CORONA SPECTRAL INTENSITY - PRESSURE = 2 TORR

4.2 INTEGRATED CORONA INTENSITY DATA. Since the candidate UV corona detection systems discussed in the following sections are designed with relatively large spectral bandwidths (~50 nm to 100nm), the spectral intensity data were integrated over selected wavebands to provide the required input data for the system analyses. Integrated corona intensity data are presented in this section for two wavebands, 200 to 280 nm and 280 to 400 nm. The selection of λ=280 nm was based primarily on the fact that the background light due to ordinary incandescent and fluorescent sources effectively falls to zero at wavelengths shorter than 280 nm. This is due primarily to the transmission characteristics of the common soda lime glass envelopes found in these light sources. Consequently, for a UV corona detection system to function properly in an ordinarily lighted laboratory environment, the waveband should be limited to 200 to 280 nm by means of an optical band pass filter.

Other sources of background light, such as quartz heating lamps and solar

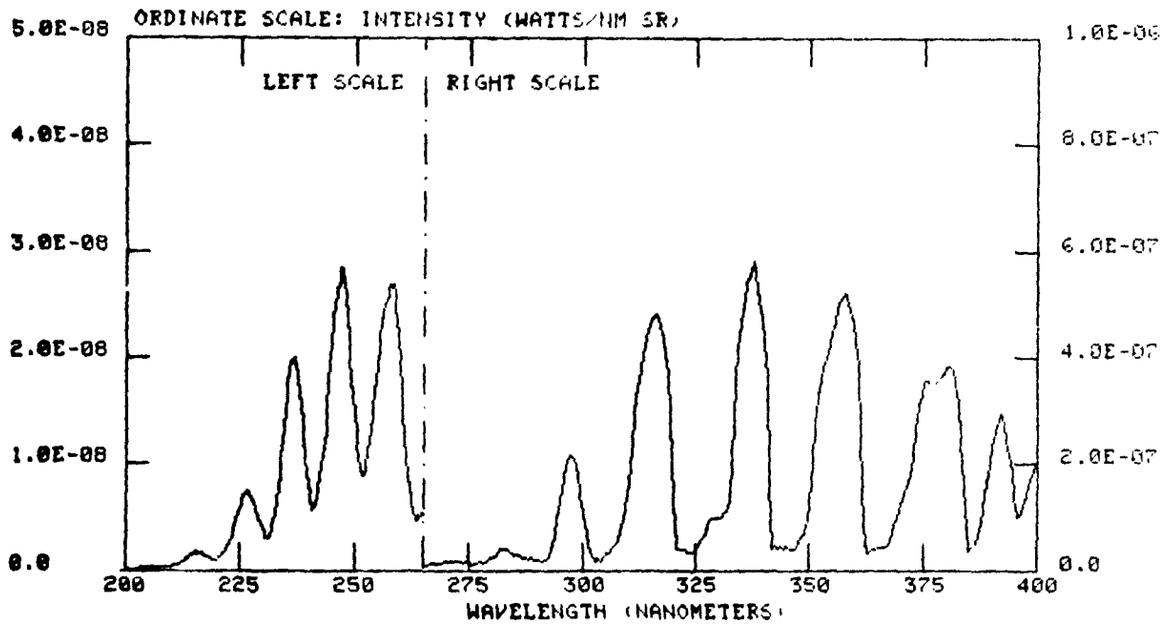

FIGURE 4-6 CORONA SPECTRAL INTENSITY - PRESSURE = 20 TORR

simulator lights, will generate background light in the 200 to 280nm waveband. The effects of this background on UV corona detection systems are discussed in Section 5-2.

Tables 4-1, 4-2, and 4-3 summarize the integrated intensity of corona glows for three anode radii, 0.5mm, 1.0mm and 2.5mm, respectively. Integrated intensity ranges from $5 \times 10^{-8} Wnm^{-1}$ to $10^{-5} Wnm^{-1}$ in the 200 to 280nm range or waveband for a span of corona currents from 4μa to approximately 800μa. Over this current range the corona phenomena range from nonsteady burst pulse, to steady glows to incipent spark breakdown conditions. Similarly, the range of corona voltage, 370 to 1158V, encompassed by these data corresponds roughly to the ordinary range of voltages found on most test articles commonly submitted for thermal vacuum testing.

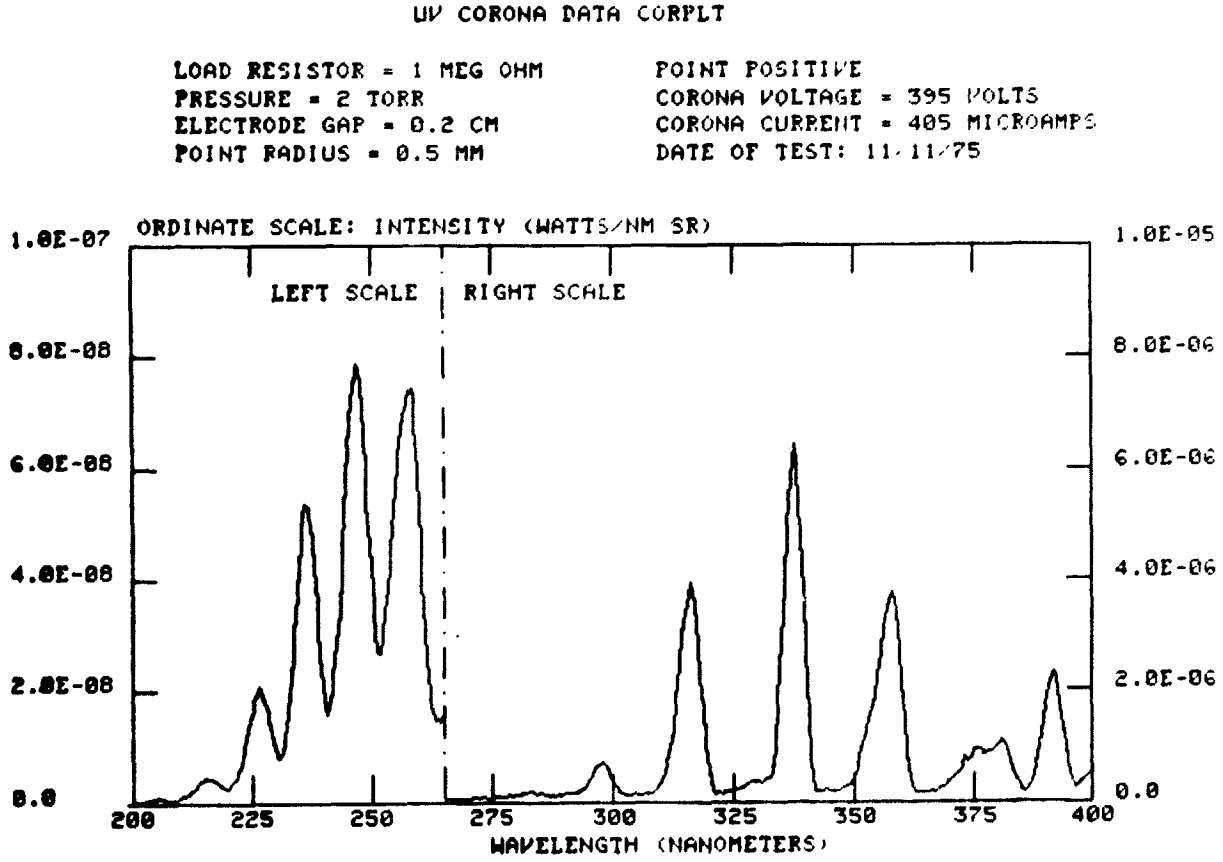

FIGURE 4-7 CORONA SPECTRAL INTENSITY - ELECTRODE RADIUS = 0.5mm

The integrated intensity in the 280 to 400 nm waveband is included in these tables for comparison to corresponding values in the lower waveband. The former values range from 1-1/2 to 2 orders of magnitude greater than the latter values.

Figures 4-9, 4-10 and 4-11 summarize the data of Tables 4-1 thru 4-3 for selected spectroradiometer runs. The solid curves are isobaric current-voltage (I-V) data for p=2 torr and 20 torr. The bracketed data are integrated intensity data for the 200 to 280 nm waveband. Included in these figures are two dashed curves at constant electric power (IV) levels of 10mW and 100mW.

In terms of the present study, these figures principally serve to establish a workable threshold for UV corona detection. For corona currents less than 50ua, the integrated UV intensity falls below $10^{-7}Wsr^{-1}$. This intensity level was used as an effective threshold value for the detection systems evaluations in

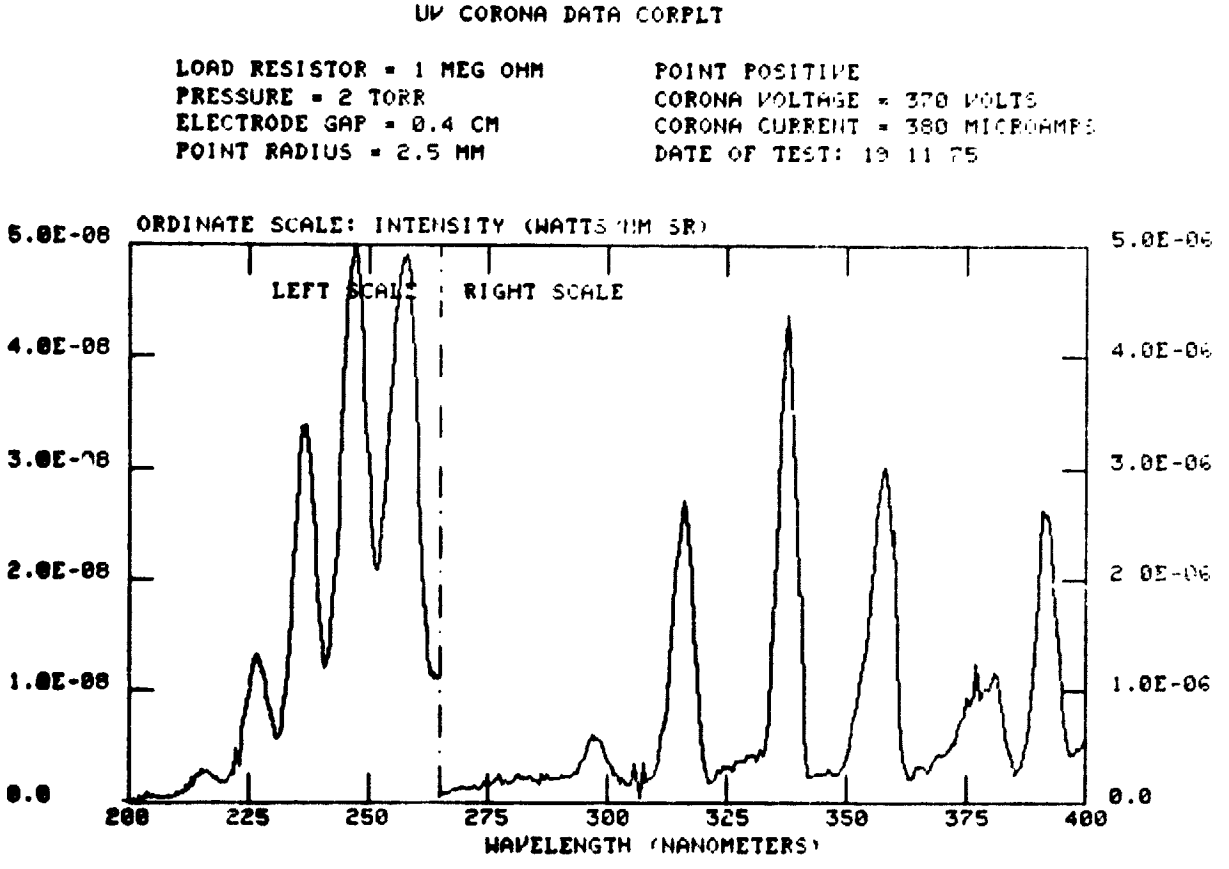

FIGURE 4-8 CORONA SPECTRAL INTENSITY - ELECTRODE RADIUS = 2.5mm

the following section.

4.3 ANALYSIS OF BREADBOARD SYSTEMS. Two types of systems evaluation procedures were applied to candidate UV corona detection systems. Several UV detectors were breadboarded and evaluated in the course of the spectroradiometer scans. Other systems were analyzed from manufacturer's specifications due to unavailability of detectors, mostly of the video type, for breadboard evaluation. The latter analyses are discussed in Section 5-1.

Table 4-4 summarizes the performance of a Honeywell UV gas discharge detector positioned 30 cm from the corona simulator pointed electrode. The detector viewed the corona glow through Suprasil window #2 (cf. Figure 3-1). Using the inverse square relation, the response of this detector for a 3 meter separation was computed. This distance is roughly typical of corona-detector separations expected in thermal vacuum tests conducted in large space simulation

TABLE 4-1 - POINT ELECTRODE - 0.5 mm RADIUS

Run	Pressure (torr)	Gap (mm)	Point Radius (mm)	Corona Voltage (V)	Corona Current (μa)	$\int_{200}^{280} W d\lambda$ (Wsr^{-1})	$\int_{280}^{400} W d\lambda$ (Wsr^{-1})
25A	2	2	0.5	450	100	2.82×10^{-7}	1.61×10^{-5}
25B	2	2	0.5	420	180	7.82×10^{-7}	4.72×10^{-5}
25C	2	2	0.5	400	300	1.95×10^{-6}	7.64×10^{-5}
25D	2	2	0.5	395	405	2.74×10^{-6}	1.14×10^{-4}
24A	20	2	0.5	670	180	7.83×10^{-7}	2.28×10^{-5}
24B	20	2	0.5	610	300	1.66×10^{-6}	5.88×10^{-5}
24C	20	2	0.5	565	485	2.79×10^{-6}	1.16×10^{-4}
24D	20	2	0.5	520	730	5.86×10^{-6}	1.69×10^{-4}
20A	2	4	0.5	460	130	5.39×10^{-7}	3.40×10^{-5}
20B	2	4	0.5	432	218	9.30×10^{-7}	5.85×10^{-5}
20C	2	4	0.5	420	330	1.82×10^{-6}	9.22×10^{-5}
20D	2	4	0.5	410	590	3.30×10^{-6}	1.89×10^{-4}
21A	20	4	0.5	875	125	3.05×10^{-7}	9.34×10^{-6}
21B	20	4	0.5	850	170	6.44×10^{-7}	2.07×10^{-5}
21C	20	4	0.5	780	280	1.73×10^{-6}	6.89×10^{-5}
21D	20	4	0.5	655	645	6.81×10^{-6}	2.62×10^{-4}
23A	2	6	0.5	540	90	4.13×10^{-7}	3.13×10^{-5}
23B	2	6	0.5	400	300	8.22×10^{-7}	6.63×10^{-5}
23C	2	6	0.5	390	410	2.54×10^{-6}	1.43×10^{-4}
22A	20	6	0.5	1110	54	3.58×10^{-7}	1.01×10^{-5}
22B	20	6	0.5	1078	120	8.06×10^{-7}	2.21×10^{-5}
22C	20	6	0.5	950	290	2.13×10^{-6}	8.19×10^{-5}
22D	20	6	0.5	820	680	8.02×10^{-6}	3.26×10^{-4}

TABLE 4-2 - POINT ELECTRODE - 1.0mm RADIUS

Run	Pressure (torr)	Gap (mm)	Point Radius (mm)	Corona Voltage (V)	Corona Current (ma)	$\int_{200}^{280} W_\lambda d\lambda$ (Wsr^{-1})	$\int_{280}^{400} W_\lambda d\lambda$ (Wsr^{-1})
17A	2	2	1.0	400	120	4.50×10^{-7}	2.54×10^{-5}
17B	2	2	1.0	390	160	5.76×10^{-7}	3.45×10^{-5}
17C	2	2	1.0	380	220	8.42×10^{-7}	4.84×10^{-5}
17D	2	2	1.0	380	420	2.99×10^{-6}	1.24×10^{-4}
18A	20	2	1.0	580	270	1.08×10^{-6}	4.52×10^{-5}
18B	20	2	1.0	560	340	1.63×10^{-6}	7.03×10^{-5}
18C	20	2	1.0	540	460	2.91×10^{-6}	1.13×10^{-4}
18D	20	2	1.0	510	690	4.50×10^{-6}	1.63×10^{-4}
15C	20	4	1.0	590	610	6.46×10^{-6}	1.88×10^{-4}
16A	2	6	1.0	440	160	7.72×10^{-7}	3.48×10^{-5}
16B	2	6	1.0	415	225	1.30×10^{-6}	5.78×10^{-5}
16C	2	6	1.0	390	460	4.20×10^{-6}	1.69×10^{-4}

TABLE 4-3 - POINT ELECTRODE - RADIUS 2.5 mm

Run	Pressure (torr)	Gap (mm)	Point Radius (mm)	Corona Voltage (V)	Corona Current (μa)	$\int_{200}^{280} W_\lambda d\lambda$ (Wsr^{-1})	$\int_{280}^{400} W_\lambda d\lambda$ (Wsr^{-1})
28A	2	2	2.5	446	4	3.72×10^{-7}	1.51×10^{-5}
28B	2	2	2.5	380	120	8.32×10^{-7}	3.32×10^{-5}
28C	2	2	2.5	375	225	1.81×10^{-6}	6.39×10^{-5}
28D	2	2	2.5	375	375	2.35×10^{-6}	9.19×10^{-5}
31A	20	2	2.5	680	80	6.93×10^{-8}	2.78×10^{-6}
31B	20	2	2.5	575	225	7.44×10^{-7}	2.89×10^{-5}
31C	20	2	2.5	510	490	3.60×10^{-6}	1.14×10^{-4}
31D	20	2	2.5	470	830	1.28×10^{-5}	3.57×10^{-4}
27A	2	4	2.5	418	6.2	6.14×10^{-7}	2.06×10^{-5}
27B	2	4	2.5	375	175	9.06×10^{-7}	4.80×10^{-5}
27C	2	4	2.5	370	380	3.27×10^{-6}	1.01×10^{-5}
26A	20	4	2.5	974	26	2.61×10^{-7}	7.00×10^{-6}
26B	20	4	2.5	885	135	1.12×10^{-6}	4.20×10^{-5}
26C	20	4	2.5	730	370	2.91×10^{-6}	1.34×10^{-4}
26D	20	4	2.5	650	600	5.19×10^{-6}	2.36×10^{-4}
29A	2	6	2.5	522	10	4.44×10^{-7}	2.19×10^{-5}
29B	2	6	2.5	425	125	7.75×10^{-7}	3.58×10^{-5}
29C	2	6	2.5	395	255	1.15×10^{-6}	6.22×10^{-5}
29D	2	6	2.5	400	500	5.73×10^{-6}	1.90×10^{-4}
30A	20	6	2.5	1158	17	2.26×10^{-8}	1.11×10^{-6}
30B	20	6	2.5	1080	150	1.76×10^{-7}	7.11×10^{-6}
30C	20	6	2.5	960	340	1.76×10^{-6}	6.84×10^{-5}
30D	20	6	2.5	800	700	7.56×10^{-6}	2.28×10^{-4}
32A	10	6	2.5	800	100	4.08×10^{-7}	1.19×10^{-5}
32B	10	6	2.5	716	200	3.77×10^{-6}	1.34×10^{-4}
32C	10	6	2.5	546	600	1.20×10^{-5}	3.10×10^{-4}
32D	10	6	2.5	534	800	1.54×10^{-5}	3.57×10^{-4}
33A	5	6	2.5	671	50	4.27×10^{-7}	6.50×10^{-6}
33B	5	6	2.5	530	200	1.48×10^{-6}	4.37×10^{-5}

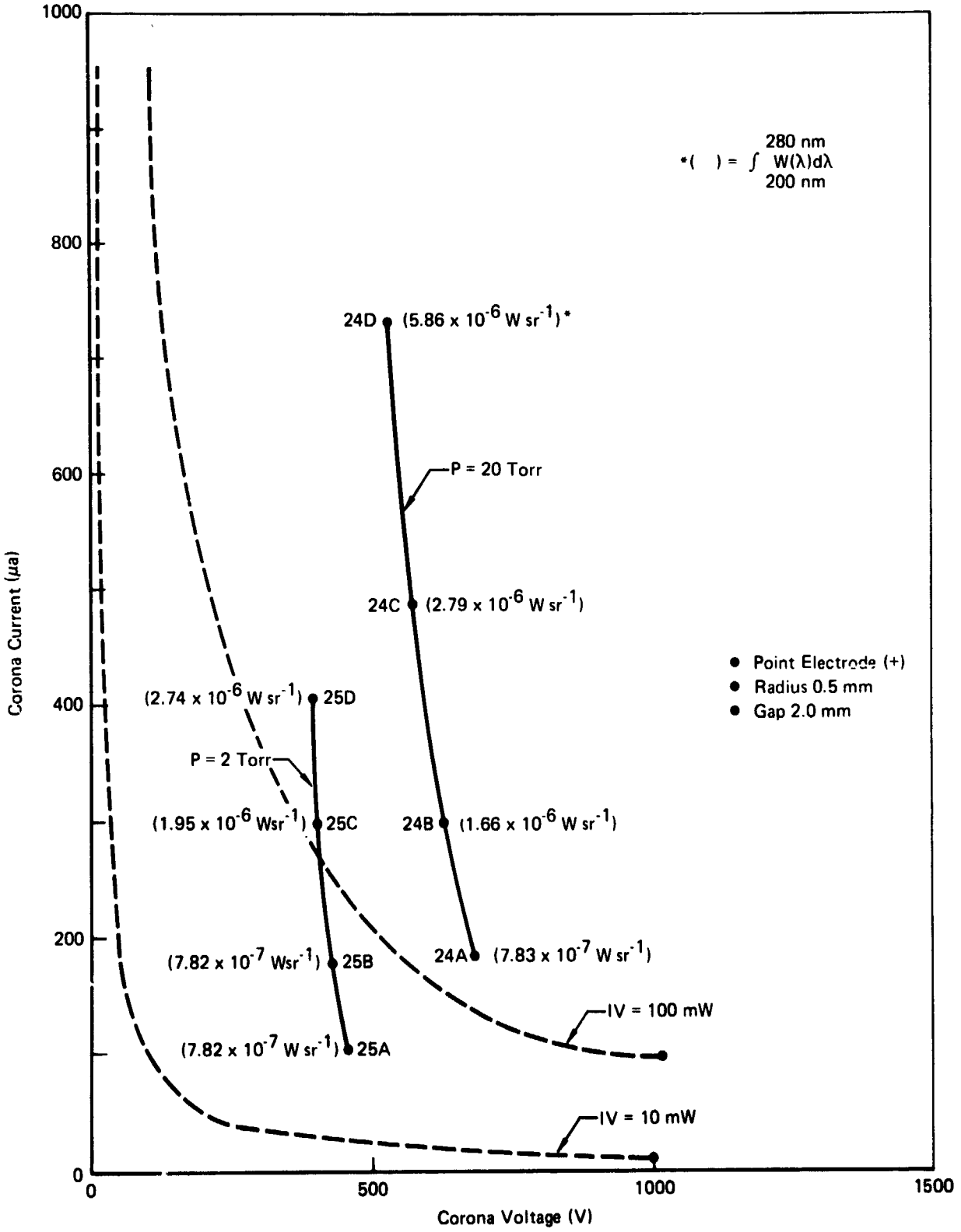

FIGURE 4-9 DATA SUMMARY FOR 0.5 mm RADIUS ELECTRODE

GP76-6183 19

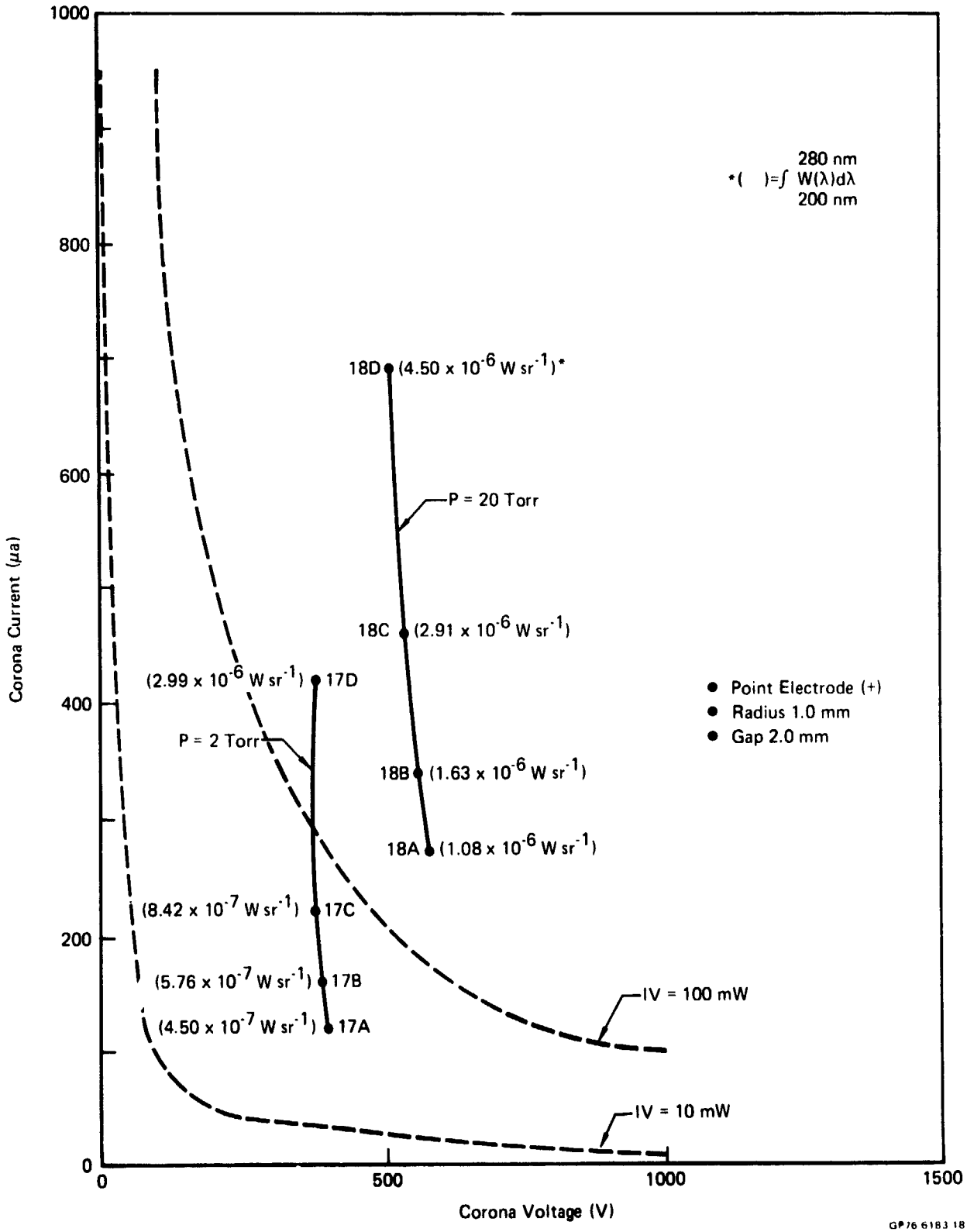

FIGURE 4-10 DATA SUMMARY FOR 1.0 mm RADIUS ELECTRODE

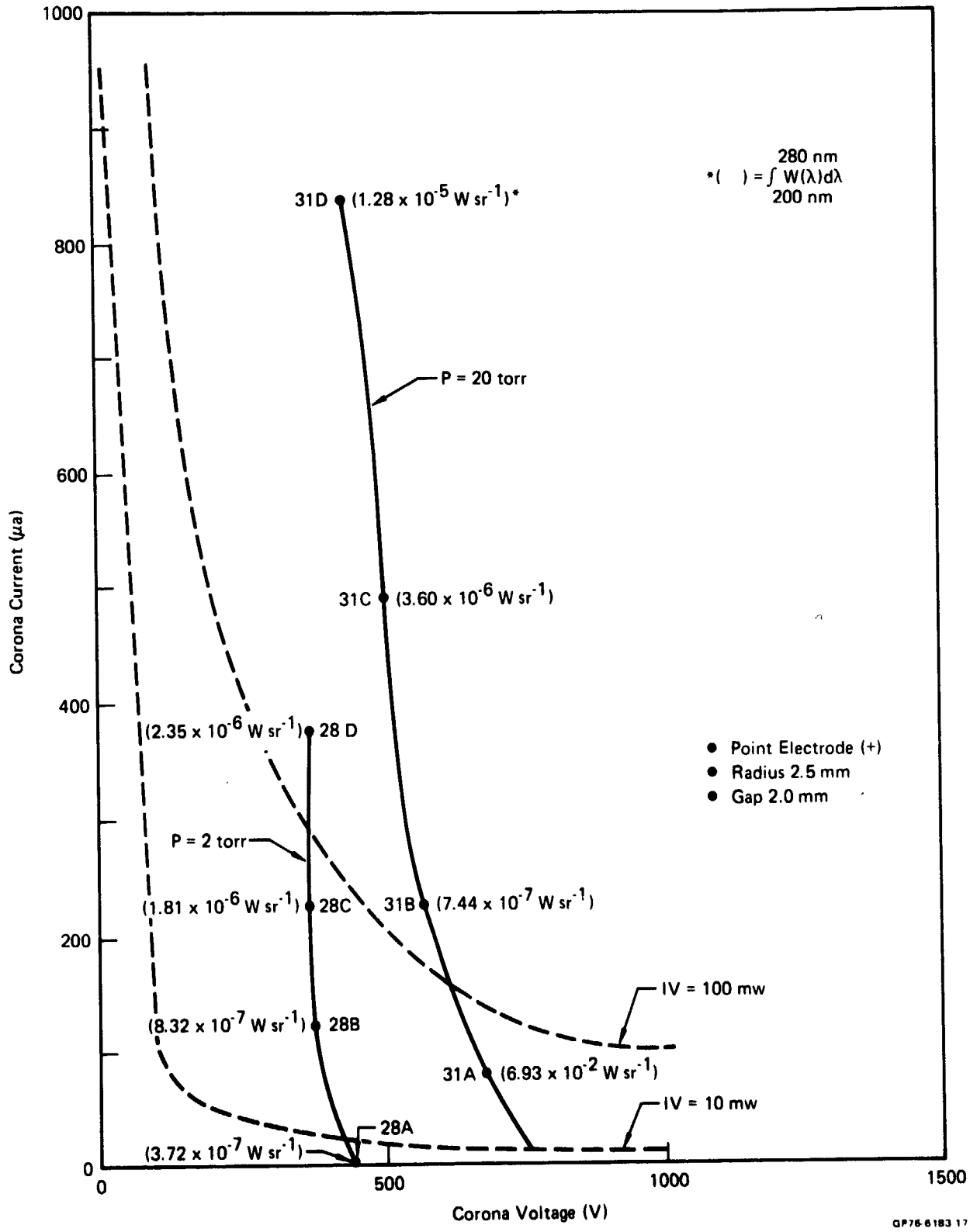

FIGURE 4-11 DATA SUMMARY FOR 2.5 mm RADIUS ELECTRODE

chambers. The gas discharge detector is "solar-blind", i.e. it has no measureable response to light at wavelengths greater than 280 nm. Consequently, this detector can be operated without filtering in the presence of normal incandescent and fluorescent background lighting.

Since detector response varies directly with corona source integrated intensity, the gas discharge detector will produce about 0.3 count/second at a range of 300 cm for $10^{-7} Wsr^{-1}$ integrated intensity, the design threshold intensity. The noise level, approximately one count/sec, entirely obscures this signal

TABLE 4-4 - PERFORMANCE SUMMARY -
HONEYWELL TYPE EP431-0-2A GAS DISCHARGE IN DETECTOR

Run	Integrated Intensity ($200 \leq \lambda \leq 280$ nm)	Counts/sec at 30 cm (measured)	Counts/sec at 300 cm (calculated)
19A	3.59×10^{-7} W/sr	110	1.1
19B	6.32×10^{-7}	235	2.4
19C	2.46×10^{-6}	450	4.5
19D	1.03×10^{-5}	653	6.5

due to the threshold corona. Consequently, to use this detector at 300 cm, auxiliary optics are required to increase the amount of UV light concentrated on the photocathode of the gas discharge detector. If a 7.5 cm dia. quartz lens is employed, the fractional increase in photocathode irradiance is approximately equal to ($A_L/A_{PC} = 45$) where A_L = area of the lens and A_{PC} = photocathode area ($1 cm^2$). At 10^{-7}W/sr intensity level, the detector output for 300 cm range with this lens is approximately (45) (0.3) = 13.5 counts/sec, which is well above the detector noise level.

Silicon photodiode detectors are attractive candidates for UV corona detector systems since they are compact and require very low bias voltages (~30V). A UDT-500 photodiode with enhanced UV spectral response was breadboarded and installed near Suprasil window #2 at 50 cm from the corona simulator electrodes. Since the response of this detector is appreciable over the 200 to 1100 nm range, a blocking filter is required to reduce the sensitivity to background light at wavelengths longer than 280 nm. Table 4-5 shows typical data obtained for the UDT-500 detector for the 200 to 280 nm waveband.

TABLE 4-5

UDT-500 SILICON PHOTODIODE DATA

Run	Integrated Intensity (Wsr^{-1})	Output Voltage (mV)	Photodiode Current (amps)
30A	2.26×10^{-8}	0.15	1.5×10^{-11}
30B	1.76×10^{-7}	0.7	7.0×10^{-11}
30C	1.76×10^{-6}	1.6	1.6×10^{-10}
30D	7.56×10^{-6}	3.5	3.5×10^{-10}

The output voltage refers to the signal measured at the output of a current-to-voltage converting preamplifier (UDT Model 505) with transfer function

$$V_{out} = 10^{7} i_e \qquad (4\text{-}1)$$

where i_e = corona current (amp)
V_{out} = output voltage (volts)

Figure 4-12, showing the output voltage produced by the UDT-500 UV detector during Run 30, indicates that a linear relation exists between corona current and detector output voltage. Since the response of this detector is a linear function of corona intensity, corona intensity is proportional to corona current for the conditions of this run.

The noise level of this detector is composed of two principal components. A DC component, called "dark current", amounting to approximately 10^{-9} amps, is present due to various charge leakage processes in the silicon wafer. The current-to-voltage converting preamplifier of the UDT-500 produces approximately 0.5mV output due to dark current. This noise component changes with detector temperature and bias voltage level in a predictable manner and can be compensated to zero volts by using offset nulling techniques. Such methods are more or less successful depending on the precision obtainable in control of detector operating temperature and bias voltage fluctuations. In a laboratory environment, dark current compensation presents no real problem. However, in a space chamber, control of detector temperature can be a problem requiring special precautions to minimize fluctuations.

The silicon photodiode detector also exhibits a random noise component due

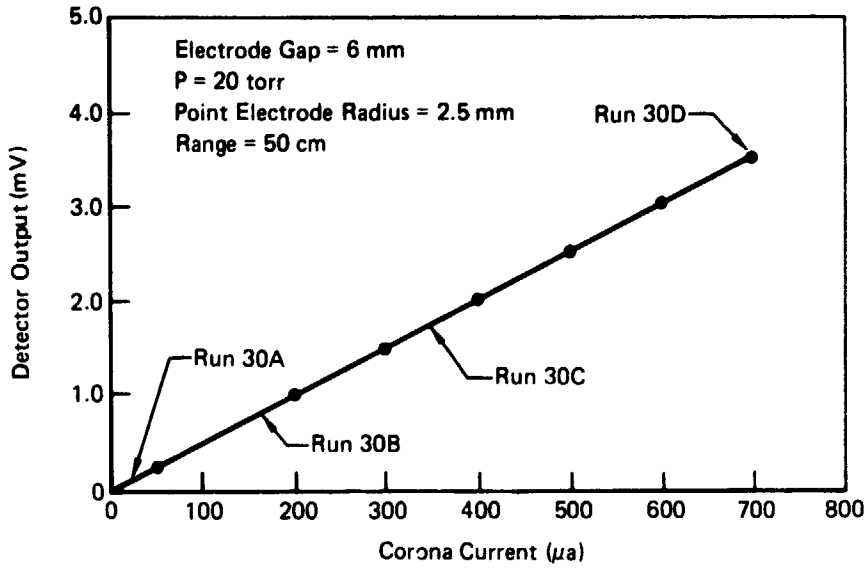

FIGURE 4-12 UDT 500 UV SILICON PHOTODIODE OUTPUT vs CORONA CURRENT

GP76-6183 16

mainly to the Johnson noise typical of the detector internal resistance. The rms noise voltage due to photodiode resistance is dependent on the electrical bandwidth, Δf, of the UDT-500 preamplifier. For a 10KHz bandwidth, V_{rms} = 0.15mV at the preamp output, indicating a noise current $i_{rms} \sim (0.15mV)\ (10^{-7}) = 1.5 \times 10^{-11}$ amp detector output.

From Figure 4-12, the output from the UDT-500 UV detector/preamp at $10^{-7} Wsr^{-1}$ and 50 cm range is 0.6 mV. Using the inverse square relation, the expected output at 300 cm range is $0.6mV \left(\frac{50}{300}\right)^2 = 17\mu V$. This result indicates the need for auxiliary collection optics if detection at 300 cm is to be accomplished. The use of 3 in. dia. quartz optics provide a factor of 45 increase in the power incident on the UDT-500 UV detector (sensitive area = $1cm^2$), yielding a preamp output voltage of $(17\mu V)\ 45 = 765\mu V$.

5.0 ANALYSIS OF CANDIDATE UV CORONA DETECTION SYSTEMS

The principal result of the experimental phase of this study was the measurement of spectral intensity for representative corona glows upon which to base realistic analyses of candidate UV corona detection systems. The data obtained for threshold corona indicated that one criterion required of a successful system is the capability to detect threshold corona emissions of $10^{-7} Wsr^{-1}$ or lower for wavelengths from 200 to 280 nm at a minimum 300 cm range. The two breadboard systems previously discussed met this criterion; however both required auxiliary optics to insure detection of the threshold corona.

In Section 5.1 video corona detection systems are considered. Due to program constraints, breadboarding of these systems was not possible, necessitating the analysis presented below. The principal reason for considering video systems is the desire to obtain directional information. The simple breadboard systems of Section 4 provide threshold corona detection capability, but are relatively useless for precisely locating the corona source. As such, these systems represent minimal solutions to the UV corona detection problem, with the advantages of simplicity and relatively low cost.

Section 5.2 contains a discussion of the effects of background light sources on the performance of candidate UV corona detection systems. The limitations due to the presence of background light were alluded to in Section 2.4. These considerations are extended in Section 5.2 to establish the magnitude of the background light interference expected for operating conditions typical of thermal vacuum testing and to assess the capabilities of candidate systems to operate satisfactorily in the presence of this background. Section 5.3 contains a selection of designs suitable for UV corona detection.

5.1 VIDEO UV CORONA DETECTION SYSTEMS ANALYSIS. The initial step in this analysis involved a survey of available video systems which operate in the 200 to 280 nm waveband. Recently RCA has developed a silicon target vidicon (Model C23231) with enhanced response in the 200 to 400 nm waveband. Figure 5-1 shows data obtained by RCA and by Princeton Applied Research Corporation (PAR). This detector is developmental and currently is in the process of evaluation prior to production for consumer use. The spectral response (amp/watt) of this vidicon approximates that for the UDT-500 UV photodiode detector. The C23231 vidicon

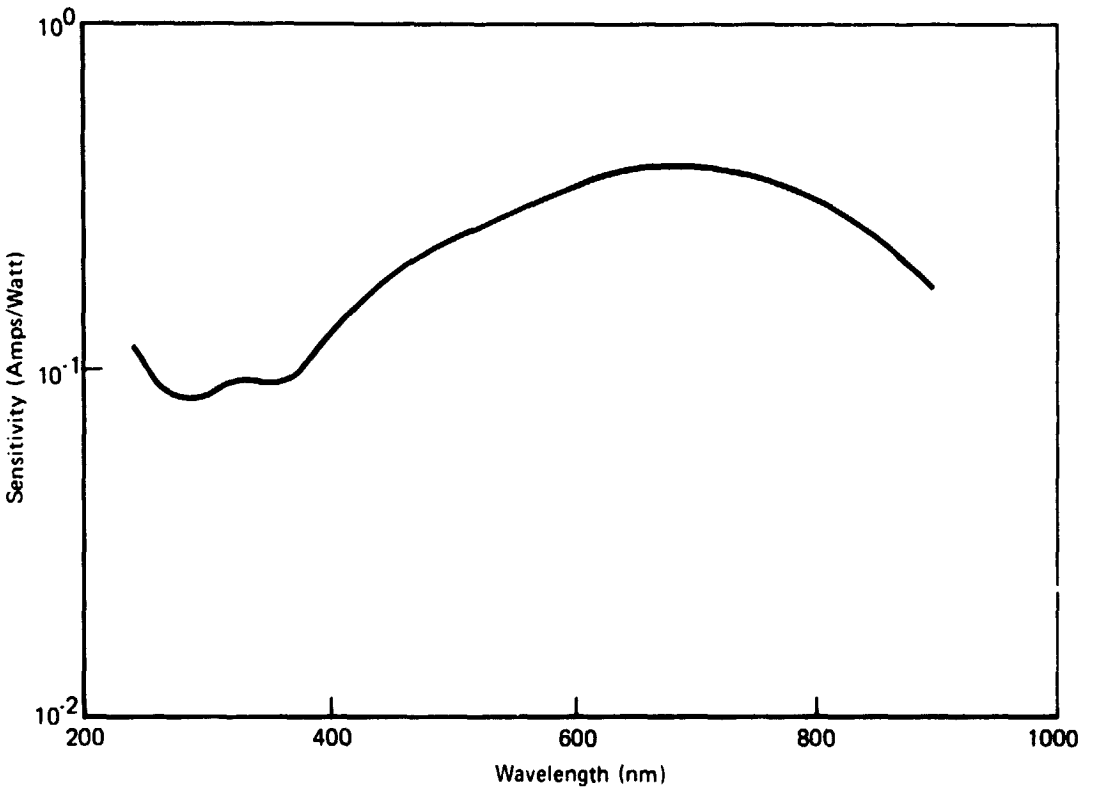

FIGURE 5-1 RCA C23231 S-T VIDICON SPECTRAL SENSITIVITY GP76 6183 4

is electrically and mechanically identical to the RCA Model 4532 silicon target (S-T) vidicon, a production model which operates in the 300 to 1100 nm waveband. The silicon target is composed of a rectangular array of small individual photodiode detectors located on 10 micron centers. The sensitive area, or target, is approximately square with sides 11.3mm in length. Consequently, there are about 12,800 individual photodiode detectors contained in the target area. Light photons incident on the photodiode array form charge pairs in the diodes. The target material, on which the diode array is deposited, is a thin silicon wafer. An electron beam scans the backside of the target area, much in the usual manner for a normal lead oxide or cesium oxide vidicon. Current flcws into the preamplifier input in proportion to the photon-generated charge on the individual photodiodes. This current is transformed into an equivalent amplified voltage proportional to the target charge. Conventional video circuitry is utilized to produce a television raster representation of the target charge pattern and, hence, of the optical image focussed on the target. S-T vidicons like the RCA 4532 family are pin-for-pin replacements for ordinary vidicon tubes found in T-V equipment. However, since the operating voltages are lower for the S-T

vidicon than for conventional vidicons, the self-induced corona problem is less severe.

To assess the threshold detection capabilities of the UDT-500 single silicon photodiode detector, it was sufficient to consider the effects of dark current and the random noise level per the discussion of Section 4.3. The corresponding analysis for the S-T vidicon requires additional considerations of spectral resolution and contrast since the purpose of the vidicon is to provide a usable two-dimensional representation of the scene focussed on the target of the S-T vidicon. In addition, the electrical bandwidth of the vidicon system necessarily is much larger than that of the single photodiode detector such as the UDT-500. This implies that the effects of the photodiode random noise level is significantly more severe for vidicons.

S-T vidicons typically show DC dark current noise levels from 10^{-9} to 10^{-8} amps, similar to that of a single silicon photodiode detector. Electronic methods for offsetting the effects of S-T vidicon dark current are more or less successful depending on the target array diode-to-diode variation of dark current. As the target is scanned by the electron beam, the dark current variations produce noise signals at video frequencies. Current manufacturing processes are capable of reducing the effects of dark current variations to less than ±5% of the average dark current level, i.e., to less than 10^{-9} amps.

The RCA 4532 S-T vidicon typically shows an rms random noise level of approximately 5na (5MHz bandwidth) which effectively constitutes the threshold limit for light detection. The signal-to-noise ratio (SNR) at the output of the S-T vidicon is related to the corona intensity, W, and the distance (range), d, between the vidicon and the corona glow according to

$$SNR = \frac{i_{signal}}{i_{noise}} = \frac{RWA_c}{i_{noise}\, d^2} \qquad (5\text{-}1)$$

where i_{signal} = vidicon signal current (amps)

i_{noise} = rms vidicon noise level = 5na

R = response of the vidicon (amps/watt)

W = integrated corona intensity in the 200-280nm waveband (watts/sr)

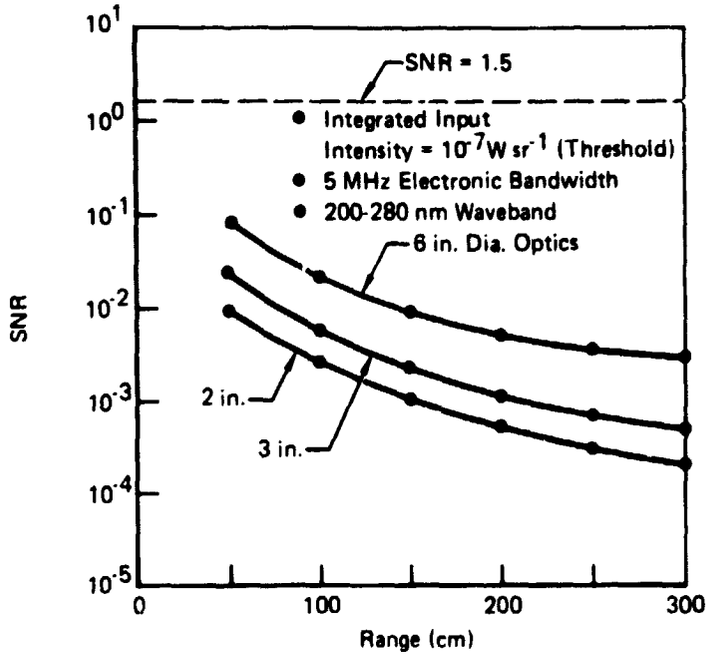

FIGURE 5-2 S-T VIDICON SIGNAL-TO-NOISE RATIO VERSUS RANGE FOR THE THRESHOLD CORONA INTENSITY GP76-6183-3

A_c = area of the vidicon collection optics (cm^2)
d = vidicon-to-corona range (cm).

The quantity $\Omega = A_c/d^2$ is the solid angle subtended by the vidicon collection optics at range d.

Figure 5-2 shows vidicon SNR versus range for several collection optics diameters. For unambigious detection of the corona glow, the SNR should be at least 1.5 or greater. The effects of the 5 MHz bandwidth of the S-T vidicon system are apparent: The threshold corona (10^{-7}Wm^{-1} integrated intensity) is impossible to detect at even 50 cm range using oversized 6 in. (15 cm) dia. collection optics. This system requires at least three orders of magnitude increase in the corona integrated intensity (~10^{-4}Wm^{-1}) for unambigious detection. Consequently, S-T vidicons such as the RCA C23231 are not sufficiently sensitive for use in a candidate UV corona detection system.

It should be noted that the noise current is proportional to Δf, where Δf is the electrical bandwidth of the corona detection system. Consequently, if Δf is reduced from 5 MHz to 1Hz, typical of the single silicon photodiode detectives discussed in Section 4-3, the SNR data of Figure 5-2 will be scaled upwards by a factor $(5\times10^6)^{1/2}$=2236. Of course, a video corona detection system requires the wide 5 MHz bandwidth.

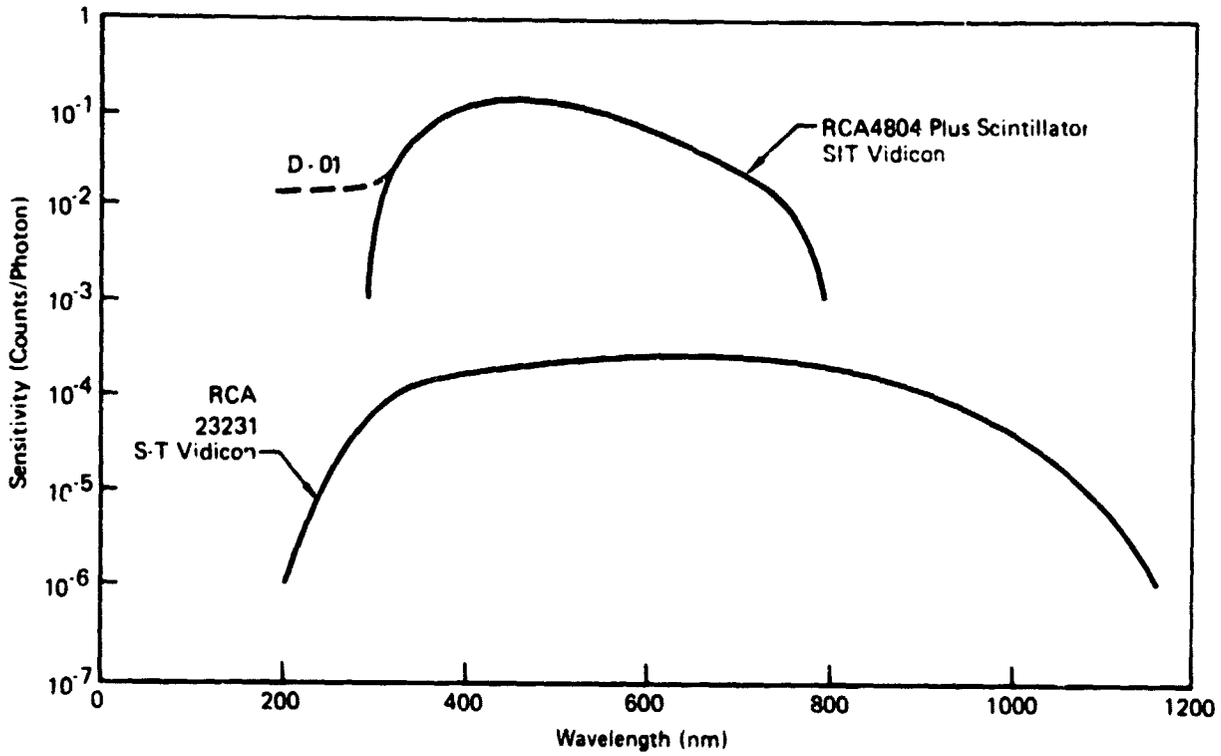

FIGURE 5-3 SIT AND S-T VIDICON SPECTRAL RESPONSE - PAR DATA

GP76-6181-2

RCA has developed an improved S-T vidicon detector for use in very low light level TV applications. These tubes, called silicon intensified target (SIT) vidicons, have an image-intensifier front end with a fiber optic faceplate over the photocathode. Photoelectrons released by the action of light incident on the photocathode are accelerated toward the silicon diode array target. The high energy photoelectrons produce large accumulations of charge on the individual target photodiodes, which are scanned by an electron beam in a manner similar to the S-T vidicon. A large increase in the intrinsic sensitivity of the silicon vidicon is obtained via the SIT design. Figure 5-3 shows comparative sensitivity data for S-T and SIT vidicons obtained by Dr. D. C. Baker of Princeton Applied Research (PAR) Corporation. Increases by two to three orders of magnitude in sensitivity are obtained via the SIT design.

The spectral response of the RCA 4804 SIT vidicon in the 200 to 300nm waveband can be increased by coating the fiber optic faceplate with a semi-transparent scintillator coating (dashed D-01 curve of Figure 5-3). With the scintillator, the RCA 4804 vidicon is approximately 10^3 times greater in sensitivity than the RCA 23231 S-T vidicon in the 200 to 280nm waveband. This translates into a 10^3 increase in the SNR data of Figure 5-2 for the SIT vidicon. Consequently,

a video UV corona detection system based on the RCA 4804 SIT vidicon will satisfy the criterion for detecting the threshold corona ($10^{-7}Wn^{-1}$) at 300 cm range with 3 in. dia. collection optics.

The SIT vidicon has one significant drawback which militates against its use in a candidate UV corona detection system. The accelerating voltages required by the intensifier section of the SIT vidicon fall in the -2500 to -9000 volt range. Thus, self-induced corona discharges are possible in the SIT vidicon system during operation in space simulation chambers. The most direct remedy is to install the SIT vidicon system in a heremetic enclosure which is maintained at atmospheric pressure during chamber pumpdown. This "fix" causes some problems in panning the vidicon detection system due to the bulk of the hermetic enclosure which must be moved.

The calculations leading to the results of Figure 5-2 rest on several tacit assumptions concerning the S-T and SIT vidicon system design. First, the transmission of the vidicon collection optics in the 200-280nm waveband was assumed to be unity. To approximate this performance, the real vidicon collection optics should be fabricated from high purity fused quartz rather than from the normal crown or flint glass typically used in commercial vidicon systems. In addition, anti-reflection coatings are required to maximize the transmission of the quartz optics in the 200-280nm waveband.

To limit the spectral response of the silicon vidicon to wavelengths less than 280nm, a suitable bandpass filter should be inserted into the optical system between the quartz collection optics and the silicon vidicon target. The results of Figure 5-2 presuppose that the bandpass filter operates perfectly by reducing the response of the vidicon detection system to zero at wavelengths longer than 280nm. In this way the effects of strong background light at $\lambda \geq 280$nm are reduced.

An approach to ideal filter performance is available via interference filter technology. In the design of bandpass interference filter, two somewhat competing considerations have to be balanced. First, the in-band transmission of the filter should be as high as possible to insure that an unacceptable insertion loss is not introduced into the system. Secondly, the out-of-band transmission should be sufficiently low to reduce the amount of stray light which passes through the filter. These considerations are especially important for a candidate

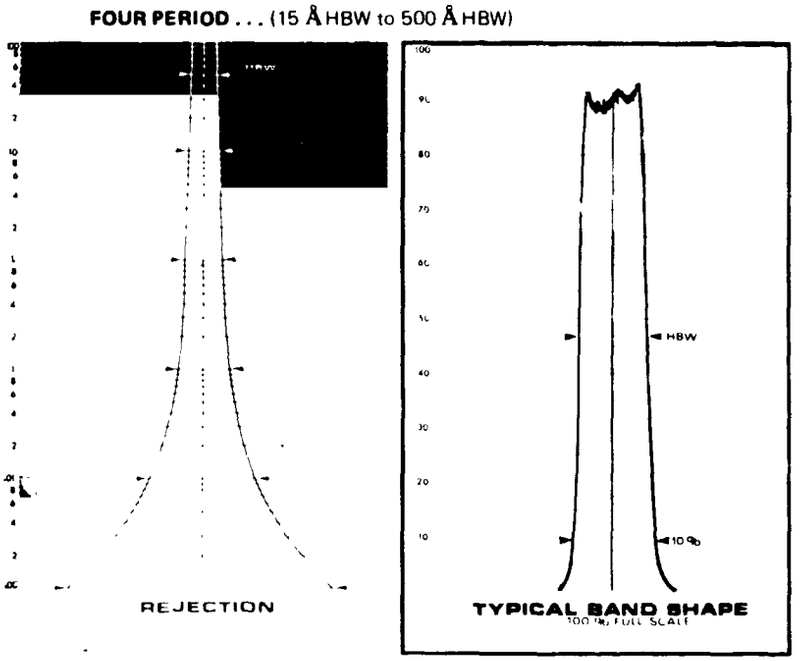

BANDWIDTH REJECTION or % BANDWIDTH POINT or DENSITY = BANDWIDTH AS SHOWN					
10^{-1}	or	10%	or	(D1)	= 1.1 - 1.25 x 50% B/W
10^{-2}		1%		(D2)	= 1.5 - 1.65 x 50% B/W
10^{-3}		.1%		(D3)	= 2.0 - 2.25 x 50% B/W
10^{-4}		.01%		(D4)	= 3.5 - 4.25 x 50% B/W
10^{-5}		.001%		(D5)	= 9 - 12 x 50% B/W

FIGURE 5-4 TRANSMISSION OF FOUR-PERIOD INTERFERENCE FILTER

GP7606183 7

UV corona detection system since the corona intensity in the filter bandpass region (nominally 200-280nm for the ideal filter) is significantly lower then the background light at wavelengths longer than 280nm.

Interference filters are constructed as layers or stacks of thin vacuum deposited films of proper thicknesses and refractive indices. Narrow bandpass filters (<10nm bandpass) can be simple "single period" filters which are made up of film stacks deposited on both sides of a suitably flat and transparent substrate (e.g. fused silica for UV filters). For broadband filters (>10nm bandpass), rejection of out-of-band straylight is accomplished by the use of multi-period designs. Figure 5-4, taken from product literature of Spectro-Film, Incorporated, Winchester, Massachusetts, shows the performance of a four-period interference filter currently available as custom manufactured items. The use of this data can be illustrated by considering a four-period filter suitable for use in the UV corona detection system with the following characteristics:

- Center wavelength: 250nm
- Half-peak bandwidth (HBW): 40nm
- In-band transmission: 20 percent

From Figure 5-4b, the 40nm HBW specification implies that this transmission of this filter is 10% (50% x 20%) at λ=230nm and λ=270nm and that the filter pass-band is more or less rectangular in shape. The out-of-band transmission for this filter can be estimated using Figure 5-2b as follows:

Wavelength	Transmission
290nm	1.0%
305nm	0.1%
320nm and up	<0.01%

It should be emphasized that this filter is typical of the present state-of-the-art in UV bandpass filter design and that the effectiveness of the filter in reducing the effects of background light requires an estimation of the typical background light levels in space simulation chambers.

5.2 BACKGROUND LIGHT EFFECTS. The effects of background light on the candidate UV corona detection systems detailed in Section 5-1 are considered in the following paragraphs. The bandpass filters discussed in the previous section provides out-of-band rejection ratios of 10^{-4} or more for wavelengths longer than 320nm. Figure 5-5 shows the spectral irradiance levels due to the two principal sources of background light, quartz heating lamps and high fidelity solar UV simulators and the irradiance at range 300 cm due to the threshold corona (approximated by the spectral intensity data obtained for Run 30B, c.f. Figure 5-6). The irradiance shown for the quartz heating lamp was estimated from the NBS calibration data for a 1KW halogen lamp spectral irradiance secondary standard light source at 300 cm range. Likewise, the solar data was taken from the NASA-Goddard extra-terrestrial solar spectrum(5).

Both background sources effectively swamp the emission from the threshold corona in the 230 to 270nm passband of the interference filter discussed in Section 5-1 if the UV corona detection system views these light sources directly. A more typical situation arises when the background light is reflected into the UV corona detection system by the test article and the space chamber walls. Each such case has to be evaluated individually. However, due to the relatively high background light level from the quartz lamps and the solar simulator, it is

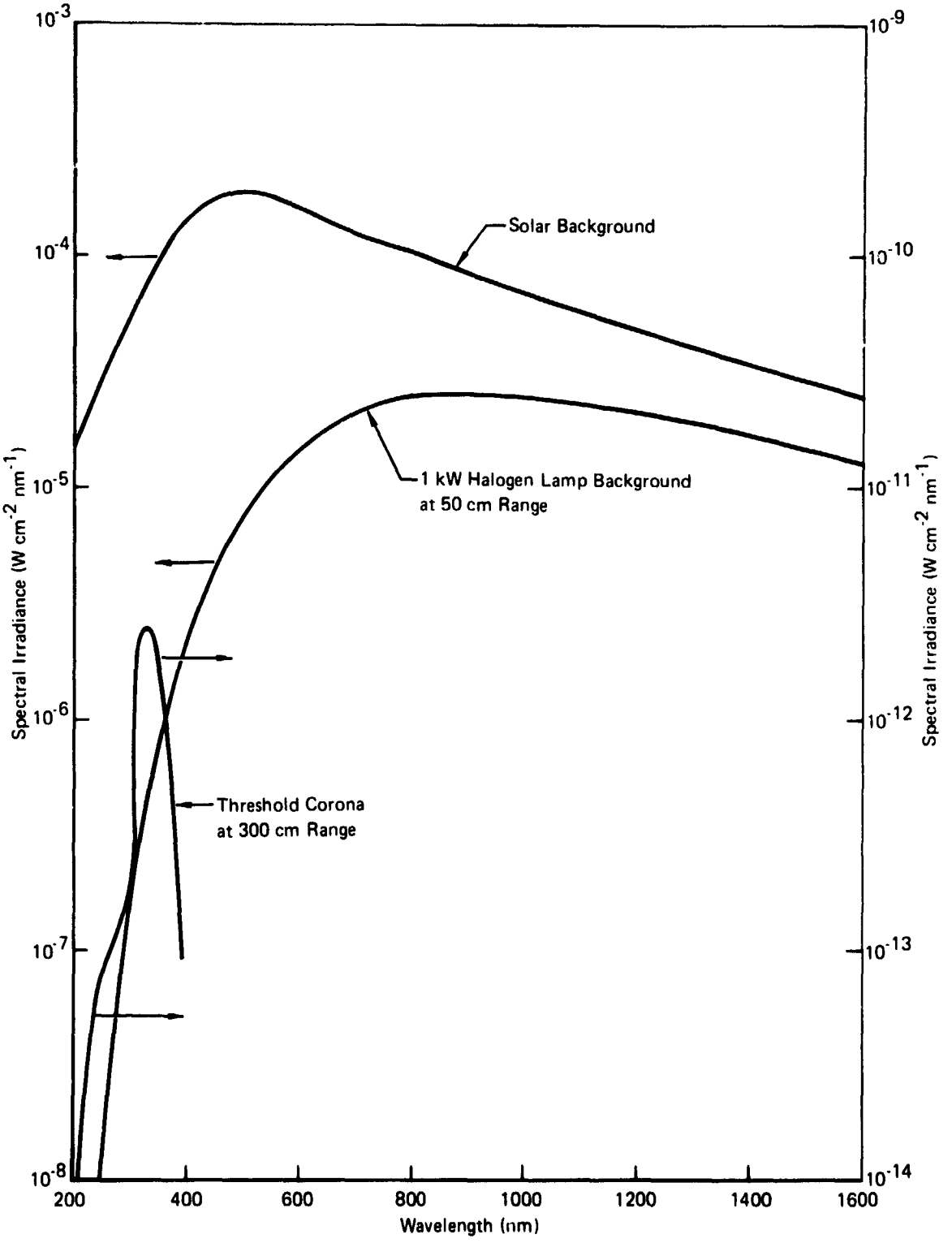

FIGURE 5-5 SPECTRAL IRRADIANCE OF THRESHOLD CORONA AND BACKGROUND LIGHT SOURCES

GP76-6183 1

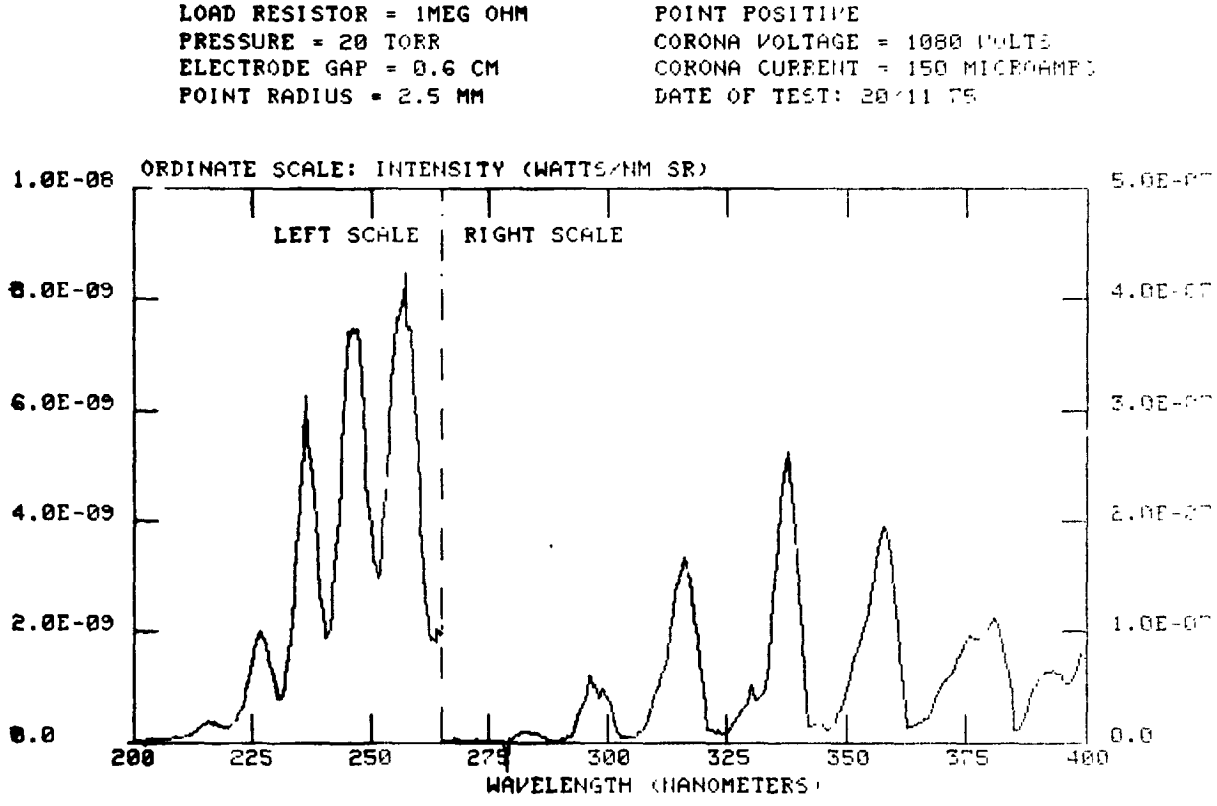

FIGURE 5-6 SPECTRAL INTENSITY DATA-RUN 30B

likely that the UV corona detector systems will be swamped by reflected background light as well as by directly incident background light. Consequently, the operation of the UV corona detection system will be limited to t e situations in which there is no background from quartz heating lamps and the olar simulator. This restriction may not be intolerable in the case of the solar simulator since most such systems can be "turned off" briefly by means of a shutter without the need to actually power down the solar simulator arc lamps. The case of the quartz heat lamps conceivably is more troublesome since these sources are used specifically to establish temperature levels on the test article. If these lamps are extinguished even for brief period to allow operation of the UV corona detection system, test article temperatures might change by unacceptable amounts. Here, again, each case has to be considered individually in order to estimate the effects both on the UV corona detection system and on the test article.

There remains one source of background light which might be tolerated by the UV corona detection system, viz that due to normal fluorescent and incandescent lightning. The low-grade glass envelopes typically found in these sources effectively reduce the emission to zero at wavelengths below λ=300nm. Because of the wide variety of lightning conditions which are possible in a space simulator chamber, an estimation of the effects of this source of background light on the UV corona detection system is difficult to generalize. Figure 5-4, however, and the data for the interference filter design discussed in Section 5.1 provide a basis for determining the maximum tolerable background light irradiance level at wavelengths greater than 300nm. The spectral irradiance at 300cm due to the threshold corona amounts to approximately 10^{-13}Wcm^{-2}nm^{-1} in the 230-270nm bandpass of the filter. The available out-of-band rejection of this filter is 10^{-4} for wavelengths greater than $\lambda \geq$320nm. Consequently, the maximum tolerable background light irradiance level at $\lambda \geq$320nm is roughly 10^{-13}Wcm^{-2}nm^{-1}x (10^{4}) = 10^{-9}Wcm^{-2}nm^{-1}. This level is sufficiently small, when compared to the irradiance of the 1KW halogen lamp at 50 cm range (cf. Figure 5-5), to cause serious concern that the performance of the UV corona detection system might be compromised even by normal fluorescent and incandescent lighting.

5.3 SELECTION OF UV CORONA DETECTION SYSTEMS. The considerations of the previous sections provide a basis for selecting a number of concepts for a UV corona detection system. The performance trade-offs are summarized in this section.

- "Solar-blind" Systems: Included are systems built around both the Honeywell gas discharge UV detector and various solar blind PMT's such as the EMI G-26H215, which has a cesium telluride photocathode (cf. Figure 5-7). These systems have the advantage of compactness, relatively low cost, and some capability for operating in the presence of normal incandescent and fluorescent background light without the need for UV bandpass filters. The disadvantages include minimal directional information for locating the corona discharge and the necessity for hermetically enclosing these detectors to prevent the generation of self-induced corona in the UV corona detection system. The gas discharge UV detector requires several hundred volts bias, while the PMT requires 1 to 2kV for operation. One strong factor favoring the gas discharge UV detector arises from its demonstrated usefulness as a UV fire detector in the recent NASA Skylab

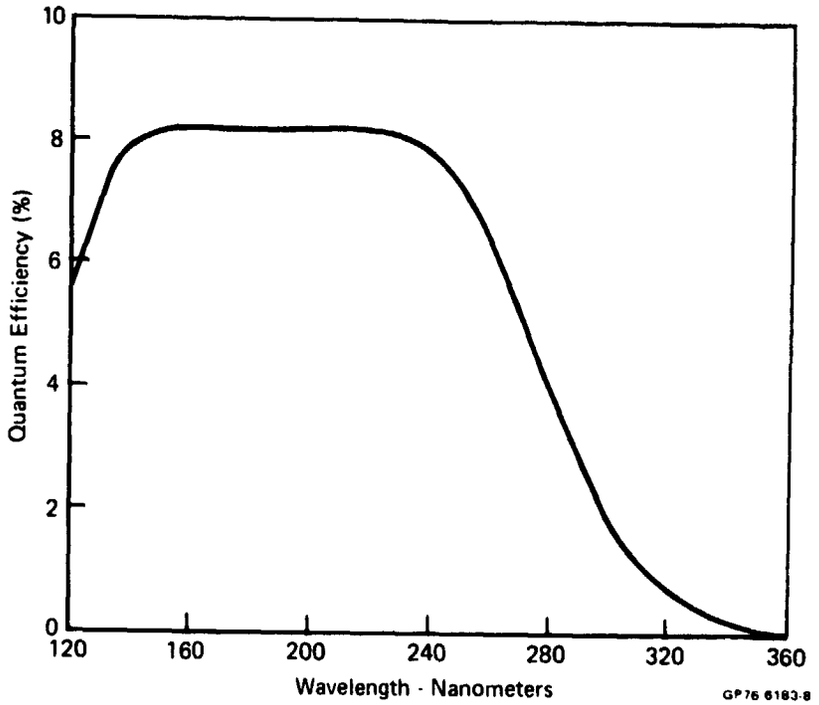

FIGURE 5-7 SPECTRAL RESPONSE OF CESIUM TELLURIDE PHOTOCATHODE BEHIND MAGNESIUM FLUORIDE WINDOW

mission.

° Silicon Photodiode Systems: Suitable UV-enhanced silicon photodiode detectors are available from United Detector Technology (UTD) and EG&G Electro-Optics Division. The specifications of the UDT-500 detector and the EG&G HUV-4000B are suitable for the proposed UV corona detection system. Since these detectors require very low bias voltages (~15v), the self-induced corona problem is non-existent and hence, hermetic enclosures are unnecessary for operation in a space simulation vacuum chamber. In addition, extremely compact designs can be realized for UV corona detection systems built around these detectors. The principal drawbacks include limited directional capability for locating corona discharges and the necessity to employ high quality UV bandpass interference filters to reduce system sensitivity to normal incandescent and fluorescent background lighting. Breadboard models employing the UDT-500 detector sucessfully demonstrated in this study the capability to detect UV corona emissions near the nominal threshold operating conditions of the corona simulator.

° Silicon Vidicon Systems: A suitable SIT vidicon/scintillator combination was identified in this study to enable video detection of UV corona emissions. The principal advantage of such a system derives from the directional capabilities of video systems, which permits the location of corona discharges. However, because of the high voltages required for operation of the SIT vidicon (~10kV), hermetic enclosures are required to eliminate self-induced corona problems. In addition, vidicon systems tend to be significantly more expensive than the simpler solar blind and silicon photodiode systems. As in the case of the silicon photodiodes, a bandpass UV interference filter is required to reduce the effects of background light. The capabilities of the SIT vidicon system for UV corona detection have been estimated from vendor specifications. Verification of the actual performance to date has not been achieved by a breadboard UV corona detection system based on the SIT vidicon.

This study has been successful in identifying three types of candidate UV corona detection systems which show high potential feasibility. Each system has one or more disadvantages which reduce its attractiveness. It is possible to rank these candidate systems in terms of the technological risks involved in each design. The solar blind gas discharge system presents the least developmental risk since existing designs have demonstrated the required UV corona detection capabilities. The silicon photodiode systems have risk factors similar to the gas discharge designs, due mainly to the fact that both types are extremely simple concepts, consisting of only a quartz lens and a detector. The SIT vidicon system represents a higher order developmental risk because of the increased complexity (and cost) of video designs.

In terms of unit cost, the silicon photodiode system is least expensive. The cost of the solar blind designs is higher due principally to the necessity for a hermetic enclosure. Likewise, the SIT vidicon design is the most expensive of the three candidate systems because of the need for a hermetic enclosure and because of the cost of the video electronics and the required TV monitors. The cost of developing "from scratch" the optical and electronics designs for a SIT vidicon system for UV corona detection is at least one order of magnitude more than the costs for the other two designs. The RCA Model TC1030 SIT CCTV camera is a compact unit specifically designed for very low light level appli-

cations. It appears feasible to adapt this existing SIT camera design for use as a UV corona detection system rather than starting from scratch on a completely new design. Specifically, the conventional glass lens in the TC1030 camera has to be replaced by a suitable quartz lens design. A UV bandpass interference filter should be incorporated into the optical system to reduce system sensitivity to background light. Finally, a suitable thin-film scintillator material has to be deposited on the input end of the fiber optic faceplate attached to the photocathode of the SIT vidicon. The scintillator is required since the fiber optic faceplace is fabricated from conventional glass (not quartz) fibers which have appreciable transmission only for wavelengths greater than 320nm.

The current costs of the principal hardware items required to implement each of the three candidate systems are summarized in Table 5-1. Not included in this listing are the costs of display/alarm hardware required for the solar-blind and the silicon photodiode systems. Since there are numerous conceivable designs for the display/alarm hardware, the costs are difficult to generalize Similarly, the costs of assembling a new design, or in the case of the SIT vidicon system the costs of modifying an existing system, have to be included in an estimate of the total cost of the UV corona detection system. Cost estimates for each of the three candidate systems, based on current MCAIR labor rates and the hardware costs listed in Table 5-1, have been forwarded to NASA-JSC under separate cover. These estimates included the costs for six complete UV corona detection systems.

TABLE 5-1 - CANDIDATE UV CORONA DETECTION SYSTEMS - HARDWARE COSTS

Solar Blind Systems	
° UV Gas Discharge Detector	$ 100
° EMI G-26H215 PMT	$ 950
° Quartz Lens (3" Dia. f/2)	$ 250
Silicon Photodiode Systems	
° UDT-500 Photodiode/UDT-505 Preamplifier	$ 210
° EG&G HUV-4000B	$ 125
° Quartz Lens (3" Dia. f/2)	$ 250
° UV Bandpass Interference Filter	$ 400
SIT Vidicon/Scintillater System	
° RCA TC1030 SIT CCTV System	$4,300
° CCTV Monitor (Single 9 Inch Unit)	$ 158
° Quartz Lens Assembly	$ 800
° UV Bandpass Interference Filter	$ 400

6.0 CONCLUSIONS AND RECOMMENDATIONS

The principal aim of this program was identification of promising methods for detecting corona discharge processes by means of the UV emissions produced by the corona glows. A systematic approach was used to measure the intensity characteristics of corona UV emission, to determine the response of several breadboarded candidate systems, to analyze the performance of other UV corona detection systems which could not be breadboarded due to programmatical constraints, and to estimate the costs for producing six copies of a UV corona detector system. The spectral intensity measurements accomplished in this study represent the most comprehensive absolute (NBS-traceable) UV intensity data accumulated to date for corona glows. It is anticipated that these data will be useful in contexts other than the present one.

Three types of candidate UV corona detection systems designs were successfully identified in this study: solar blind types, silicon photodiode types, and silicon-intensified-target (SIT) vidicon designs. For each type of system one or more commercially available designs were found which could be modified to function as a UV corona detection system. These include: the Honeywell design for the Skylab Solar-Blind Fire Detection System, modified to accept a quartz collection lens (7.5cm dia.); the EG&G Model 500 Lite-Mike modified to accept a quartz lens, a blocking interference filter and a UV sensitive photodiode detector; and the RCA Model TC1030 SIT Vidicon Camera modified to accept a scintillator plate, a quartz collection lens and a blocking interference filter. These systems constitute the recommended starting points for development of the UV corona detection system.

Background light from quartz heating lamps and high fidelity solar simulators was found to adversely affect the performance of all three designs. Consequently, suitable operational ground rules are recommended to reduce the interaction between the background light sources and the UV corona detection system. For thermal vacuum testing in the 0.1 to 50 torr pressure range in which corona processes are most likely, these ground rules may be troublesome, since the background light will have to be controlled from the space simulation chamber if the UV corona detection system is to function properly.

7.0 REFERENCES

1. Loeb, L. B.: Electrical Coronas: Their Basic Physical Mechanisms. Berkeley, 1965.

2. Grum, F. and Costa, L. F.: Spectral Emission of Corona Discharges. Applied Optics, 1970, pp. 76-79.

3. Nasser, E.: Fundamentals of Gaseous Ionization and Plasma Electronics. New York, 1971.

4. Bandel, H. W.: Point-to-Plane Corona in Dry Air. Physical Review, 1951, pp. 92-99.

5. Thekaekara, M. P.: Solar Energy Outside the Earth's Atmosphere. Solar Energy, 1973, pp. 109-127.

APPENDIX

A listing of the data reduction FORTRAN Program is contained in this appendix. The program was developed in the Digital Equipment Corporation (DEC) RT-11 FORTRAN IV language for use with a PDP 11/40 processor.

```
RT-11 FORTRAN IV        V01B-08     MON 16-FEB-76 08:14:30        PAGE 001

      C     FILE "CORDAR.FOR"
      C     UV CORONA DATA REDUCTION PROGRAM
      C
      C     VERSION     01B     30-OCT-75       BAB.
      C
0001        REAL*4 DAT(440),STD(440),CAL(440)
0002        REAL*4 DATA1(220),DATA2(220)
0003        REAL*4 SENS(440)
0004        REAL*4 PMTV(15),PMTF(15)
0005        REAL*4 POLY(4),COPPLT(2)
0006        REAL*4 WAVE(440),INTENS(440)
0007        LOGICAL*1 DAY(10),TIM(9),FILE1(7),FILE2(7),FILE3(7)
0008        EQUIVALENCE (DATA1(1),DAT(1)),(DATA2(1),DAT(221))
0009        COMMON FILE1,FILE2,FILE3
0010        DATA CORPLT/6RDK COR,6RPLTSAV/
0011        DATA POLY/-5658.01,5540.93,-2217.31,2747.36/
0012        DATA C1,C2/1.1909E-12,1.4380/        !CONSTANTS FOR MAX PLANCK
0013        DATA PMTV/800.,850.,900.,950.,1000.,1050.,1100.,1150.,
           1     1200.,1250.,1300.,1750.,1400.,1450.,1500./
0014        DATA PMTF/0.027,0.048,0.081,0.129,0.204,0.315,0.48,0.70,
           1     1.00,1.42,1.95,2.64,3.45,4.30,5.25/
      C
      C     PRINT HEADING, DATE AND TIME
      C
0015        CALL DATE(DAY)
0016        CALL TIME(TIM)
0017        DAY(10)=.FALSE.
0018        TIM(9)=.FALSE.
0019        TYPE 201,DAY,TIM
0020  201   FORMAT('0 UV CORONA DATA REDUCTION PROGRAM',2X,10A1,2X,9A1//)
      C
      C     GENERATE THE WAVELENGTH TABLE
      C
0021        WAVE(1)=400.0
0022        DO 10 I=2,220
0023  10    WAVE(I)=WAVE(I-1)-137.5/220.0
0024        WAVE(221)=265.0
0025        DO 15 I=222,440
0026  15    WAVE(I)=WAVE(I-1)-68.75/220.0
      C
      C     READ IN CALIBRATION LAMP CURVE
      C
0027        CALL OPENF(CAL,440,'CALDAT')
      C
      C     GENERATE STANDARD LAMP CURVE
      C
0028        DO 20 I=1,440
0029        XLAM=WAVE(I)*1.0E-3
0030        TEMP=XLAM+POLY(1)
0031        DO 25 J=2,4
0032  25    TEMP=TEMP*XLAM+POLY(J)
0033        XLAM=WAVE(I)*1.0E-7
0034        T1=C1/(XLAM**5)
0035  20    STD(I)=T1/(EXP(C2/(XLAM*TEMP))-1.0)*1.0E-7
      C
      C     INPUT DATA FILE NAMES FROM KEYBOARD
      C
```

```
RT-11 FORTRAN IV        V01B-0(     MON 16-FEB-76 08:14:30       PAGE 002

0036          TYPE 202
0037    202   FORMAT('$ ENTER NAME OF FILE CONTAINING 400-265 NM DATA:')
0038          CALL GETSTR(5,FILE1,6,901)
0039          CALL OPENF(DATA1,220,FILE1)
0040          TYPE 212
0041    212   FORMAT('$ ENTER FULL SCALE MICRO^OLTS:')
0042          ACCEPT 208,FS1
0043    32    TYPE 207
0044    207   FORMAT('$ ENTER PMT VOLTAGE FOR THIS RUN:')
0045          ACCEPT 208,PMT1
0046    208   FORMAT(F20.0)
0047          DO 30 I=1,15
0048          IF(PMT1.GT.PMTV(I)+0.5)GO TO 30
0050          IF(PMT1.LT.PMTV(I)-0.5)GO TO 30
0052          FACT1=PMTF(I)
0053          GO TO 35
0054    30    CONTINUE
0055          TYPE 209,PMT1
0056    209   FORMAT('0 ***** PMT VOLTS =',G10.4,' INVALID, TRY AGAIN.')
0057          GO TO 32
0058    35    TYPE 203
0059    203   FORMAT('$ ENTER NAME OF FILE CONTAINING 265-200 NM DATA:')
0060          CALL GETSTR(5,FILE2,6,901)
0061          CALL OPENF(DATA2,220,FILE2)
0062          TYPE 212
0063          ACCEPT 208,FS2
0064    42    TYPE 207
0065          ACCEPT 208,PMT2
0066          DO 40 I=1,15
0067          IF(PMT2.GT.PMTV(I)+0.5)GO TO 40
0069          IF(PMT2.LT.PMTV(I)-0.5)GO TO 40
0071          FACT2=PMTF(I)
0072          GO TO 45
0073    40    CONTINUE
0074          TYPE 209,PMT2
0075          GO TO 42
0076    45    TYPE 211,FACT1,FACT2
0077    211   FORMAT('0 1ST PMT FACTOR =',G10.4,'  2ND PMT FACTOR =',G10.4/)
0078          TYPE 213
0079    213   FORMAT('$ ENTER APERTURE AREA IN CM^2:')
0080          ACCEPT 208,AREA
0081          DO 50 I=1,220
0082          DAT(I)=DAT(I)/FACT1*FS1
0083          DAT(I+220)=DAT(I+220)/FACT2*FS2
0084    50    CONTINUE
              C
              C     COMPUTE SENSITIVITY AND INTENSITY
              C
              C     UNITS:      SENS-- W  NM^-1 SR^-1 MICROAMP^-1
              C     INTENS-- W NM^-1 SR^-1
              C
0085          DO 60 I=1,440
0086          SENS(I)=STD(I)/CAL(I)*AREA
0087          INTENS(I)=DAT(I)*SENS(I)
0088    60    CONTINUE
              C
              C     LIST ALL DATA ON LINE PRINTER
```

```
RT-11 FORTRAN IV        V01B-08     MON 16-FEB-76 08:14:30        PAGE 003

      C
0089          PRINT 206
0090  206     FORMAT('1',20X,'UV CORONA DATA REDUCTION LISTING'//)
0091          PRINT 204,FILE1,FILE2
0092  204     FORMAT('0',10X,'DATA FROM FILES: ',7A1,' & ',7A1//)
0093          PRINT 205
0094  205     FORMAT(6X,'WAVELENGTH',9X,'STANDARD LAMP',5X,'CALIBRATION',
     1 8X,'SENSITIVITY',8X,'CORRECTED',10X,'CORONA'/
     2 28X,'RADIANCE',6X,'DATA-AVERAGED',6X,'(WATTS/NM-SR',
     3 5X,'CORONA DATA',8X,'INTENSITY'/5X,'(NANOMETERS)',7X,
     4 '(WATTS/CM**3-SR)',4X,'(MICROAMPS)',8X,'PER MICROAMP)',5X,
     5 '(MICROAMPS)',6X,'(WATTS/NM-SR)'/)
0095          PRINT 220,(WAVE(I),STD(I),CAL(I),SENS(I),DAT(I),INTENS(I),
     1 I=1,440)
0096  220     FORMAT(1X,6G18.6)
0097          PRINT 210
0098  210     FORMAT('1')
      C
      C       WRITE THE DATA ON DISK FOR PLOTTING
      C
0099          CALL SENDF(WAVE,440,'WAVECR')
0100          TYPE 214
0101  214     FORMAT('0 ENTER AN OUTPUT FILE NAME FOR THE REDUCED DATA'/
     1 ' $ (DEFAULT NAME = "CORPLT.DAT") : ')
0102          CALL GETSTR(5,FILE3,6)
0103          CALL SCOMP('',FILE3,IFLAG)
0104          IF(IFLAG.NE.0)GO TO 70
0106          CALL SCOPY('CORPLT',FILE3)
0107  70      CALL SENDF(INTENS,440,FILE3)
      C
      C       CHAIN TO PLOTTING PROGRAM 'CORPLT'
      C
0108          CALL CHAIN(CORPLT,FILE1,11)
0109          END
```